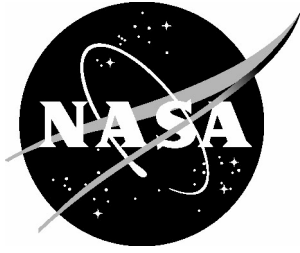# Development of an Actuator for Flow Control Utilizing Detonation

Patrick J. Lonneman and Andrew D. Cutler
The George Washington University
Joint Institute for Advancement of Flight Sciences
Langley Research Center, Hampton, Virginia

Since its founding, NASA has been dedicated to the advancement of aeronautics and space science. The NASA Scientific and Technical Information (STI) Program Office plays a key part in helping NASA maintain this important role.

The NASA STI Program Office is operated by Langley Research Center, the lead center for NASA's scientific and technical information. The NASA STI Program Office provides access to the NASA STI Database, the largest collection of aeronautical and space science STI in the world. The Program Office is also NASA's institutional mechanism for disseminating the results of its research and development activities. These results are published by NASA in the NASA STI Report Series, which includes the following report types:

- TECHNICAL PUBLICATION. Reports of completed research or a major significant phase of research that present the results of NASA programs and include extensive data or theoretical analysis. Includes compilations of significant scientific and technical data and information deemed to be of continuing reference value. NASA counterpart of peer-reviewed formal professional papers, but having less stringent limitations on manuscript length and extent of graphic presentations.

- TECHNICAL MEMORANDUM. Scientific and technical findings that are preliminary or of specialized interest, e.g., quick release reports, working papers, and bibliographies that contain minimal annotation. Does not contain extensive analysis.

- CONTRACTOR REPORT. Scientific and technical findings by NASA-sponsored contractors and grantees.

- CONFERENCE PUBLICATION. Collected papers from scientific and technical conferences, symposia, seminars, or other meetings sponsored or co-sponsored by NASA.

- SPECIAL PUBLICATION. Scientific, technical, or historical information from NASA programs, projects, and missions, often concerned with subjects having substantial public interest.

- TECHNICAL TRANSLATION. English-language translations of foreign scientific and technical material pertinent to NASA's mission.

Specialized services that complement the STI Program Office's diverse offerings include creating custom thesauri, building customized databases, organizing and publishing research results ... even providing videos.

For more information about the NASA STI Program Office, see the following:

- Access the NASA STI Program Home Page at *http://www.sti.nasa.gov*

- E-mail your question via the Internet to help@sti.nasa.gov

- Fax your question to the NASA STI Help Desk at (301) 621-0134

- Phone the NASA STI Help Desk at (301) 621-0390

- Write to:
  NASA STI Help Desk
  NASA Center for AeroSpace Information
  7121 Standard Drive
  Hanover, MD 21076-1320

NASA/CR-2004-213508
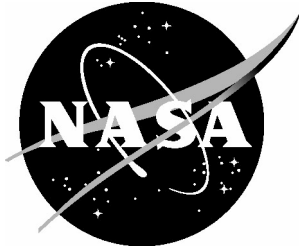
Development of an Actuator for Flow Control Utilizing Detonation

Patrick J. Lonneman and Andrew D. Cutler
The George Washington University
Joint Institute for Advancement of Flight Sciences
Langley Research Center, Hampton, Virginia

National Aeronautics and
Space Administration

Langley Research Center
Hampton, Virginia 23681-2199

December 2004

ABSTRACT

The control of flow separation has been demonstrated using both passive and active methods in multiple computational and experimental studies. Active flow control devices including mass injection systems and zero-net-mass flux actuators (synthetic jets) have been employed to delay flow separation. These devices are capable of interacting with low-speed, subsonic flows, but situations exist where a stronger crossflow interaction is needed. Small actuators that utilize detonation of premixed fuel and oxidizer should be capable of producing supersonic exit jet velocities. An actuator producing exit velocities of this magnitude should provide a more significant interaction with transonic and supersonic crossflows. This concept would be applicable to airfoils on high-speed aircraft as well as inlet and diffuser flow control.

The present work consists of the development of a detonation actuator capable of producing a detonation in a single shot (one cycle). Multiple actuator configurations, initial fill pressures, oxidizers, equivalence ratios, ignition energies, and the addition of a turbulence generating device were considered experimentally and computationally.

It was found that increased initial fill pressures and the addition of a turbulence generator aided in the detonation process. The actuators successfully produced Chapman-Jouguet detonations and wave speeds on the order of 3000 m/s.

TABLE OF CONTENTS

LIST OF FIGURES

LIST OF TABLES

LIST OF ACRONYMS AND SYMBOLS

AIAA	American Institute of Aeronautics and Astronautics
CJ	Chapman-Jouguet
DDT	Deflagration to Detonation Transition
psia	Pounds per square inch absolute
psig	Pounds per square inch gage
c	Speed of sound.
γ	Gamma, Ratio of specific heats
ϕ	Phi, Equivalence Ratio
J	Joules
u	Velocity
P	Pressure
q	Heat added per unit mass
ρ	Rho, Density
T	Temperature
V_D	Detonation Velocity
H_2	Gaseous hydrogen
O_2	Gaseous oxygen
N_2	Gaseous nitrogen
H_2O	Water vapor

CHAPTER 1

INTRODUCTION

Large performance gains can be achieved through the control of the flow associated with aircraft, automobiles, sea vehicles, turbomachines, and other flow systems. In most cases, these gains are achieved through the postponement of boundary layer separation which leads to reduced drag, delayed stall, enhanced lift, and improved pressure recovery. Future applications in thrust vectoring may even require the intentional separation of a boundary layer [1]. Separation control has been demonstrated through both passive and active methods. Passive methods such as micro-vortex generators give improvements in efficiency without the need for complex mechanical systems. However, in low angle of attack configurations, performance drops significantly. Active flow control devices include mechanical deflection actuators, mass injection systems, and zero-net-mass flux actuators (synthetic jets). Synthetic jets have shown promise in manipulating flow over airfoils and other bluff bodies [2]. These micro actuators use an oscillating diaphragm to add momentum to a flow without net mass transfer. Studies have shown exit jet velocities up to 50 m/s. Mass injection systems include steady blowing jets, pulsed jets [3], and combustion driven jet actuators [4]. The combustion driven jet actuators utilize low-speed or deflagration combustion to produce a pulsed exit jet. However, they have been shown to penetrate a crossflow only up to Mach 0.7. These types of actuators and the others listed above all suffer the same limitations, namely the ability to manipulate a crossflow in the transonic and supersonic flow regime. The SparkJet, a solid state device which rapidly heats gas within a chamber

by means of an electrical discharge to obtain a high velocity jet, has been proven capable of penetrating supersonic flows [5]. This paper will describe research on another device, which utilizes detonation combustion, and holds the promise of controlling high-speed flows.

1.1 Detonation Actuator Overview

The detonation actuators are small convergent nozzles that utilize localized detonation combustion to produce a pulsed supersonic exit jet. A premixed fuel-oxidant (hydrogen-oxygen) mixture is injected into the combustion chamber before being ignited by a spark. Once ignited, a deflagration will propagate downstream, ideally transitioning to a strong detonation before exiting the nozzle. A simplified schematic of the detonation actuator is shown in Figure 1.

Detonations are highly energetic combustion waves coupled with shock waves capable of flame speeds up to 3000 m/s in premixed hydrogen-oxygen mixtures. An actuator with exit velocities of this magnitude should be capable of extending the effectiveness of actuator jet interaction for separation control well into the supersonic flow regime [6]. This paper will present the results from experimental parametric studies completed to determine the capability of this device. Numerical calculations were also completed to help understand and validate the flow processes seen in the laboratory experiments. All results are for a single cycle (inject fuel, ignite mixture, purge products). Work is concurrently in progress to develop resonant detonation actuators that these results may guide [6].

Numerous applications besides active flow control have been envisioned for the actuators. Pulse Detonation Engines (PDEs) rely on detonation combustion for the

pressures needed for thrust generation. A small actuator like the one researched for this thesis could be used to start the detonation process in a shorter distance or initiate a detonation in a less reactive fuel. High-speed military rockets could use them as thrusters for lateral control. A detonation actuator would improve the effectiveness by providing a more substantial crossflow interaction.

1.2 Detonation Theory

There are two types of combustion phenomena: deflagration and detonation. Deflagration combustion is characterized by subsonic flame speeds and negligible pressure rises. For this reason, deflagrations can be modeled as an isobaric (constant pressure) process. Detonations on the other hand are characterized by supersonic flame speeds and very high-pressure differentials [8]. A constant volume process is often used to model detonations because of the high flame speed. The differences in velocity, pressure, temperature, and density of deflagrations and detonations are shown in Table 1.1. The subscripts u and b used in Table 1.1 stand for unburned and burned gases, respectively.

It is helpful to look at a development of the different types of combustion through the use of the Hugoniot Curve. Starting with the integrated conservation equations and the state equations, the Hugoniot curve (Equation 1.1) is obtained after some manipulation [9].

$$\frac{\gamma}{\gamma-1}(\frac{P_2}{\rho_2} - \frac{P_1}{\rho_1}) - \frac{1}{2}(P_2 - P_1)(\frac{1}{\rho_1} + \frac{1}{\rho_2}) = q \tag{1.1}$$

The Hugoniot is essentially a plot of all the possible values of $(1/\rho_2, P_2)$ for a given value of $(1/\rho_1, P_1)$ at the given heat added per unit mass, q. The regions of possible

solutions are constructed by drawing tangents to the curve that go through $[(1/\rho_1), P_1]$. Since the form of the Hugoniot equation obtained is a hyperbola, there are two tangents to the curve through A as shown in Figure 2. The tangents and the horizontal and vertical lines through the initial condition A divide the Hugoniot into five regions, as specified by Roman numerals.

Ratio	Usual magnitude of ratio	
	Detonation	Deflagration
$u_u/c_u{}^a$	5-10	0.0001-0.03
u_b/u_u	0.4-0.7	4-16
P_b/P_u	13-55	0.978-0.9776
T_b/T_u	8-21	4-16
ρ_b/ρ_u	1.4-2.6	0.06-0.25

^{a} c_u is the acoustic velocity in the unburned gases. u_u/c_u is the Mach number of the wave.

Table 1.1. Qualitative differences between detonations and deflagrations in gases [9].

In regions I and II solutions give compression waves, high velocities, and are regions of detonations. Solutions in regions III and IV give expansion waves, which are low velocity subsonic waves already classified as deflagrations. Solutions in regions II, IV, and V are said to not exist since the solutions are physically unrealizable. The only experimentally possible results along the Hugoniot curve are the point J and region III. It can be shown that the velocity of sound in the burned gases is greater than the velocity of the detonation wave relative to the burned gases. Consequently, if a rarefaction wave due to any reason whatsoever starts behind the wave, it will catch up with the detonation front. The rarefaction will then reduce the pressure and cause the final value of P_2 and $1/\rho_2$ to drop and move down the curve toward J. Thus points above J are not stable and are referred to as overdriven detonations. Heat losses, turbulence, friction, etc., can start the rarefaction. At point J, the velocity of the detonation wave is equal to the velocity of

sound in the burned gases plus the mass velocity of the gases, so that the rarefaction will not overtake it. The point and conditions at J are referred to as the Chapman-Jouguet results. Therefore, solutions in region I are possible, however they are transient and the solution will converge on the point J. For a more thorough development see Glassman [9].

Glassman offers an explanation to how a deflagration can be transitioned into a detonation, known as deflagration to detonation transition (DDT) [9]. If a mixture is ignited at the closed end of a long horizontal tube, a combustion wave is formed. The burned gas products of this wave have a specific volume of the order of 5-15 times the unburned mixture and act as a piston. This piston generates compression waves that impart a velocity down the tube to the unburned gases ahead of the flame. Each compression wave tends to heat the unburned gas mixture somewhat, causing the sound velocity to increase and the succeeding waves to catch up with the initial one. The preheating tends to increase the flame speed, which then accelerates the unburned gas mixture further to a point where turbulence is developed in the unburned gas. Then, a greater flame velocity is obtained, accelerating the unburned gases, and creating compression waves. Therefore, a shock strong enough to ignite the gas mixture is formed. The reaction zone behind this shock sends forward a continuous compression wave that keeps the shock front from decaying and a stable detonation is obtained.

The characteristic pressure distribution of a detonation wave propagating downstream that has been initiated at the closed end of a tube is shown in Figure 3 [10]. The detonation wave can be modeled as a 1-D strong shock, which triggers combustion, and a thin flame front in which heat addition occurs just behind the shock. The shock

front moves at the detonation velocity, V_D, relative to the gas and increases the pressure and temperature of the gas from its previous values of P_1 and T_1.

Just behind the shock front is an area of high pressure known as the von Neumann pressure spike. This area consists of the ignition delay and its thickness is governed by chemical kinetics. The duration of the spike is on the order of one microsecond. Once the chemical kinetics are initiated, heat addition occurs, and consequently the pressure is lowered and the temperature increases. The thickness of this region is determined by the time required for the combustion processes to complete. Finally, in a tube where the detonation is initiated at the closed end, an expansion region is developed to ensure that zero velocity is realized at State 3.

1.3 Acceleration of DDT

The transition of a deflagration to a detonation requires a certain distance downstream of the ignition point. The detonation actuators are less than 0.125 m (5 in) long and accelerating the DDT process is of the utmost importance. DDT acceleration methods such as varying the initial fill pressure and equivalence ratio will be discussed in this paper along with results from the addition of a turbulence generating device. These devices include orifice plates, centerbodies, concentric rings, and Shchelkin spirals in addition to the use of additives. The use of these devices has been shown to help promote the transition to a detonation [11,12,13,14]. Of these methods, the one most commonly used is the Shchelkin spiral [15], which is a wire coil of certain diameter and pitch.

The success of the Shchelkin spiral over other methods may be due to an important feature of the transition process as visualized by Urtiew and Oppenheim [16]. They observed a phenomenon known as an 'explosion-in-the-explosion' in smooth tubes

that produces a bow-shaped shock which reflects off the side walls and intensifies the flame-shock interaction. Unlike axisymmetric obstacles, the Shchelkin spiral can support additional helical modes that can propagate upstream as they grow and interact with the side walls. This increases the probability of coupling between the shock structure and turbulent flame propagation, thereby increasing the likelihood of DDT [14]. For this reason, the Shchelkin spirals were utilized in this experimental study. A detailed discussion of the dimensions and installation of the spiral will be presented in the next chapter.

1.4 Objectives of Research

As stated above, the need exists for an actuator with a strong exit jet capable of interacting with transonic and supersonic crossflows. Research was undertaken to extend the effectiveness of flow control actuators to meet this need. This thesis describes the work completed on a single shot actuator installed in a detonation tube. The experimental study was broken into two parts. The first consists of understanding the detonation process and how to obtain a CJ detonation experimentally in a constant area tube. Second, actuator concepts were tested experimentally applying the lessons learned from the constant area tube studies. In addition, the actuators were studied computationally to help validate and understand the experimental results.

In both cases a number of parameters were studied to determine their significance to the detonation phenomena. Since the detonation tube was airtight, various initial fill pressures above atmospheric were studied. In addition, the effect of fuel-oxidizer ratios was studied to determine if certain values accelerate the detonation process. Other factors evaluated included varying the oxidizer from pure oxygen to air and varying the

ignition energy released by the spark. Finally, the effect of adding turbulence was tested by installing a spiral of wire inside the actuators. It was the purpose of this thesis to understand the detonation process and apply that knowledge to the development of a better flow control actuator.

CHAPTER 2

EXPERIMENTAL DESCRIPTION

The experiment consisted of four main components: the detonation tube, injection system, ignition system, and the instrumentation. The majority of the components were located in the test cell of NASA Langley's Direct Connect Supersonic Combustion Test Facility, a 4.8 by 4.8 by 15.8 m (16 by 16 by 52 ft) test cell with 0.61m (2 ft) steel-reinforced concrete walls. The room was equipped with a forced air ventilation system that yielded a ventilation rate of 225 room exchanges of air per hour. These features guarded against any potential problems associated with a hydrogen gas leak. The control software and data acquisition equipment was located outside the test cell allowing the operator to start the tests from a remote location.

2.1 Detonation Tube

The detonation tube and its components were designed to allow tests with fill pressures up to 689 kPa (100 psia). As shown in Figure 4, the 316 stainless steel schedule XXS pipe was 1.22 m (48 in) long with a 11.1 kN (2500 lb) 316 stainless steel flange welded to the ignition end and a 6.67 kN (1500 lb) flange welded to the opposite end. It had a 0.051 m (2.0 in) outer diameter and a 0.038 m (1.5 in) inner diameter. The blind flanges enclosing it on either end, together with a gasket, formed an airtight seal. The flange on the ignition end had three holes for tungsten electrodes. Seven ports are tapped at 0.152 m (6 in) intervals along the tube for the PCB pressure transducers (see Section 2.6). Fuel and oxidizer were injected into the tube through a valve rated at 69000 kPa (10000 psia). The tube was vented directly into the test cell through another valve rated at the same pressure located at the opposite end. A picture of the tube with an actuator

installed is shown in Figure 5. A detailed engineering drawing of the tube is given in Figure A1 in Appendix A. A detailed drawing of the modifications to the blind flange on the ignition end for the electrode installation is given in Figure A2.

2.2 Detonation Actuators

Three actuators were fabricated for the study that differ in the size and type of the throat. The actuators were convergent-divergent nozzles with one version having a constant area throat extension. A picture of the actuators is shown in Figure 6. The first nozzle, actuator A, diagrammed in Figure 7(a), had an inlet to throat area ratio of 25. Figure 7(b) shows the second nozzle, actuator B, which had a throat radius of 0.25 cm (0.098 in) and an inlet to throat area ratio of 100. Finally, in Figure 7(c), the third nozzle, actuator C, had the same throat radius, however, it had a constant area throat extension of 1 cm (0.394 in). It was designed with this feature to help sustain and possibly strengthen a detonation formed in the convergent section of the nozzle. From this point on the actuators will be referenced based on their letter, as designated by Figure 7.

The actuators were installed between the end flange and the tube on the ignition end. The setup is shown in Figure 4. In this setup, the detonation tube was used as a dump tank for the actuators.

2.3 Injection System

The system was designed to supply a combination of gaseous hydrogen, oxygen, and air to the detonation tube. A schematic of the injection system is supplied in Appendix A in Figure A3. A simplified schematic of the injection system is shown in Figure 8. A series of piping and valves connected the fuel and oxidizer bottles to the detonation tube components. The hydrogen, oxygen, and nitrogen gas is located in k-

bottles outside of the test cell. The air was supplied from 689 kPa (100 psig) service air.

Flow of these gases was regulated with needle valves and a Mensor digital pressure

gauge for accurate injection into the tube. The Mensor gauge was accurate to 68.9 Pa

(0.01 psia) and could measure pressures from 0-1030 kPa (0-150 psia). Because of this

pressure limitation, a series of valves isolated it from the tube during tests. The tube was

evacuated before fuel and oxidizer injection by use of a Cenco Hyvac vacuum pump. The

pump was capable of evacuating the tube down to approximately 6.89 Pa (0.001 psia),

which allowed for very near stoichiometric mixtures in the tube for tests. During the fill

process and after a test nitrogen was used to purge the supply lines and the tube of any

reactive gases.

2.4 Ignition System

The ignition system consisted of a high-voltage power supply, flash lamp power

supply, 5 μF capacitor and two or three tungsten electrodes, depending on the energy

required. A detailed drawing of the electrodes is included in Figure A4 in Appendix A.

Initially, only two electrodes were used to form a spark gap. They were connected to the

Spectralite 919 flash lamp power supply, which housed a bank of capacitors and was

capable of discharging up to 2.5J into the gap. A simplified schematic showing this

system is shown in Figure 9(a). It was later determined that more energy was needed to

obtain CJ detonations within the actuators. A third electrode, 5 μF capacitor, high-voltage

power supply, and required circuitry were added to boost the maximum energy to 15J.

The gas between the electrodes was ionized by a high-voltage pulse from the flash lamp

power supply and upon creation of the plasma in the gap, the capacitor connected to the

third electrode discharged in the same gap creating a spark of the stated energy. A

simplified schematic of the circuit is shown in Figure 9(b). A detailed schematic of this

ignition system is given in Figure A5 in Appendix A.

Due to the large currents and voltages imposed by the ignition system, shielding

was required to keep the noise created by electrical interference at a minimum. The

cables running from the electrodes to the capacitors were kept as short as possible and

were shielded with an aluminum mesh. Gaps between the cables and the electrodes were

filled with putty and wrapped in aluminum foil so that the entire component was

shielded. A filtering technique was used to remove the remainder of the noise and will be

discussed in Chapter 4.

2.5 Shchelkin Spiral

As discussed in Chapter 1, a turbulence generator known as a Shchelkin spiral

was installed in the actuators and tube for evaluation. Two spirals made from copper

wire that had approximately five turns and were 0.076 m (3 in) long were tested in the

actuators and are shown in Figure 10(a). The two spirals differed in the diameter of the

copper wire: one was 1.6 mm (0.0625 in) and the other was 4.8 mm (0.1875 in) The

smaller diameter spiral reduced the entrance area of the actuator by ~12% and the larger

spiral by ~35%. This constriction was greater as the spiral approached the throat. The

spiral with the diameter of 1.6 mm (0.0625 in) was used in the majority of the testing and

the 4.8 mm (0.1875 in) version was evaluated as a comparison. Since these spirals were

conical, a constant area version was made for testing in the straight tube, shown in Figure

10(b). It was made from the 1.6 mm (0.0625 in) diameter copper wire and was 0.076 m

(3 in) long with approximately 5 turns.

The dimensions of the spirals were based loosely on the references given in Chapter 1. Schauer, et al [13] placed a 0.305 m (12 in) spiral made from wire with a 4.8 mm (.1875 in) diameter in a tube with an inner diameter of 0.051 m (2 in). Meyer, et al [14] also used two 4.8 mm (0.1875 in) wire diameter spirals which were 0.457 m (18 in) and 1.37 m (54 in) long. The spirals used in the current study were only 0.076 m (3 in) long so that the throat of the actuators was not blocked. The spiral used in the tube was made the same length for comparison purposes.

The spirals were installed immediately downstream of the ignition end wall and were secured with aluminum tape. The tape was used so that the spirals were flush with the side walls and so that they could be removed with ease during the various tests of the tube and actuators. A picture of the smaller spiral installed in an actuator is shown in Figure 11.

2.6 Instrumentation and Data Acquisition

The instrumentation consisted primarily of six piezoresistive pressure transducers, manufactured by PCB Piezotronics, Inc. Four of the PCB transducers were model 113A22 with a full-scale range of 0-34500 kPa (0-5000 psi), rise time of 1.0 μsec, and a resonant frequency of 500 kHz. The other two PCB transducers were model 113A21 and had a full-scale range of 0-6900 kPa (0-1000 psi), rise time of 1.0 μsec, and a resonant frequency of 500kHz. These two probes were placed in strategic locations to help see the DDT process while the four model 113A22 transducers were used to capture the higher pressures of the detonation waves. The PCB transducers could withstand a maximum flash temperature of 1922 °K (3000 °F). Since detonation waves typically have temperatures greater than this value, the faceplates of the PCB transducers were coated

with approximately 0.36 mm (0.014 in) of high temperature silicon RTV compound, as recommended by PCB.

The PCB pressure transducers were connected to a PCB Amplifier model 4B3803. LeCroy model 9314 and 9314A oscilloscopes acquired the data from the transducers. Model 9314 had a 300 MHz bandwidth and four channels each with 10 Kpts of acquisition memory. Model 9314A had a 400 MHz bandwidth and four channels each with 50 Kpts of acquisition memory. Both models were capable of 100 MHz simultaneous sampling rate on all channels. A LabVIEW program was written to setup and calibrate the oscilloscopes and PCB transducers and ignite the mixture. Since the PCB transducers were dynamic probes, and not capable of measuring mean pressures, the Mensor model 2101 digital pressure probe was used to monitor the filling and evacuation of the tube.

2.7 Test Procedures

The first step in running the experiments was to determine the configuration that was to be tested. This was recorded in the log book and the tube was setup accordingly. The next step was to shutdown the AC power inside the test cell and turn on the explosion proof lights and ventilation fan. Once this was complete the fuel and oxidizer bottles, located outside of the test cell, were opened. The service air was then turned on by opening the valve located in the test cell and all the test equipment located in the test cell was then turned on. Next, the tube was purged using inert nitrogen gas to ensure no reactive chemicals remained. Once this was complete, the tube was evacuated using the vacuum pump. When the pressure in the tube was at or below 68.8 Pa (0.01 psia), the vacuum pump was turned off and the oxidizer was injected into the tube. To prevent a

premature ignition caused by the transient start-up voltages and currents of the ignition

system components, they were turned on and set to the correct voltages before the

injection of the fuel. Once they were powered up the fuel was injected and allowed to

mix with the oxidizer. When the tube was filled to the desired pressure it was sealed off

and the injection system piping was then purged using nitrogen. This was done to prevent

damage to equipment from an explosion traveling back through the injection system. All

test personnel were then evacuated and the test cell was sealed off.

While waiting for the fuel and oxidizer to properly mix, the oscilloscopes and

computer were powered up. Next, the LabVIEW program was setup with the proper

values for the LeCroy scopes and PCB transducers. When the mixing time, discussed in

Section 2.8, was complete, the 5 µF capacitor was charged and the contents in the

detonation tube were then immediately ignited. Once the combustion was complete and

the data was saved, the ignition system was turned off and the tube was purged of any

product and unreacted fuel mixture. Additional tests were completed by evacuating the

detonation tube. If the last run of the day had been completed the fuel and oxidizer bottles

were closed and all the test equipment was powered off.

2.8 Fuel-Oxidizer Mixing

The fuel and oxidizer were not premixed before they were injected into the

detonation tube. To understand and compare various tests it was important to have

consistent, repeatable results. Therefore, time was devoted to understanding the mixing

process and its effect on deflagration to detonation transition. Two methods were

evaluated on their ability to produce repeatable results. These tests were completed using

actuator C. The number of transducers and their spacing in this actuator will be discussed

in Chapter 5. One method used to mix the fuel and oxidizer was to inject them in layers.

For example, the fills would be layered by putting fuel, oxidant, fuel, oxidant, etc. into

the tube. A mixture of 103 kPa (15 psia) H_2/O_2 with four layers would be obtained by

injecting 17.2 kPa (2.5 psia) of O_2, 34.5 kPa (5 psia) of H_2, 17.2 kPa (2.5 psia) of O_2, and

34.5 kPa (5 psia) of H_2. Tests using 2, 4, and 5 layers were studied to understand the

methods effect on mixing. Approximately thirty seconds passed while the injection

piping was purged and the test cell was secured before the mixture was ignited. The

wave speeds for each run are shown in Figure 12. The method for calculating the wave

speed will be discussed in Chapter 4. The wave speeds compare nicely at the first three

locations, however, at the fourth location large variations exist. The next method simply

allowed the fuel and oxidizer to mix over increasing longer periods. For these cases, the

oxidizer was injected before the fuel with no layering. As the mixing wait time

increased, the fuel and oxidizer should approach a premixed mixture. Three mix times

were tested: 5, 10, and 20 minutes. The wave speeds for these runs are also shown in

Figure 12. As the data in the figure shows, all three cases compare very well at each of

the transducer locations. Since the 5 minute data agrees well with the 10 and 20 minute

cases, it was decided that all subsequent tests would be completed with this mix time. It

should be noted that the data points shown in Figure 12 are the average wave speeds from

multiple tests at each test condition.

CHAPTER 3

TEST PROGRAM

The research undertaken consisted of experimental parametric studies. The parameters that were investigated can be put into three different categories. The first consists of parameters associated with the fuel and oxidizer mixtures. Variables studied included initial fill pressure, equivalence ratio, and different oxidizers. The second category contains the geometric parameters such as tube or actuator and the subsequent variations on the actuator dimensions. Thirdly, methods to initiate a detonation were evaluated. The ignition energy was varied and a spiral of wire was added to develop turbulence and enhance mixing. A summary of all the tests discussed in this thesis is shown in Table 3.1.

3.1 Initial Fill Pressure

As mentioned before, the detonation tube was designed to handle conditions from a vacuum to the pressure associated with detonations without leaking significant reactants or products to the test cell. The leak rates are discussed in Chapter 7. Therefore, tests were completed with fill pressures ranging from 103 kPa (15 psia) to 483 kPa (70 psia). From these results, the effect of higher fill pressures could be determined. This effect was studied in the constant area tube and all the actuator configurations.

3.2 Equivalence Ratio

Mixtures of varying equivalence ratio were studied to determine the effect of added fuel or oxidizer to the initiation of a detonation. Fuel-lean mixtures down to an equivalence ratio of 0.3 were investigated in addition to fuel-rich mixtures up to a ratio of 1.3. It was important to understand the effect of equivalence ratio because of its impact

on fuel consumption. If the actuators could perform well at a lean mixture, less fuel would be needed on board the vehicle.

3.3 Oxidizer Composition Fraction

The composition of the oxidant was varied to discover how changing the oxidizer from pure oxygen to air affected the performance. The composition fraction was defined as follows

$$Composition\ Fraction = \frac{a}{a+b} \tag{3.1}$$

where a and b are coefficients in the following chemical reaction

$$H_2 + aO_2 + b(0.21O_2 + 0.79N_2) = H_2O + 0.79bN_2 \tag{3.2}$$
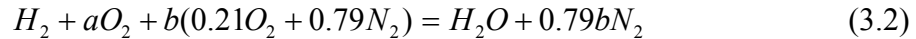
The coefficients can be solved once the value of the composition fraction is chosen since there are two equations and two unknowns. A composition fraction of one corresponded to all oxygen, while a fraction of zero meant the oxidizer was air. Between these limits, fractions of 0.25, 0.50 and 0.75 were studied. A vehicle that used an actuator using only air as an oxidizer would require no onboard oxygen storage.

3.4 Geometric Configuration

To get an understanding of how detonations are initiated and the properties of their propagation, tests were completed using the constant area detonation tube. Once this understanding was obtained the various actuator concepts were evaluated. The actuators were developed as convergent-divergent nozzles in an attempt to create high pressures through compression to help the DDT process. Numerical calculations done prior to this study showed that the actuators were capable of accelerating the DDT process. The three configurations vary in the value of their throat diameter. As shown before, two had a throat diameter of 0.25 cm (0.098 in) and one had a diameter of 0.50

cm (0.197 in). In addition, one of the smaller diameter nozzles had a constant area throat extension of 1 cm (0.394 in) before the small diffuser.

3.5 Ignition Energy

CJ detonations can be initiated directly or through a deflagration to detonation transition. To obtain direct initiation large amounts of energy must be deposited into the combustible mixture to immediately create the shock-coupled combustion wave. Using the Spectralite 919 power supply and a 5 μF capacitor at 3kV, energies from 0.025 Joules up to 15 Joules were tested in an attempt to directly initiate a CJ detonation. The advantage of direct initiation is that smaller actuators can be designed, however, at the disadvantage of higher electrical power consumption and higher weight.

3.6 Turbulence Generator

Finally, in an attempt to develop a detonation in the convergent section of the actuators, coils of wire were added to create turbulence in the flow. The motivation behind the spirals and a physical description is given in Chapters 1 and 2, respectively. As previously discussed, two different spirals were tested. The spirals were tested at various initial fill pressures in both the tube and the actuators to determine their effect on the detonation process.

Configuration	Initial Fill Pressure, kPa (psia)	Test Description	Figure #
Tube	103 (15)	Varied fill pressure	13
Tube	207 (30)	Varied fill pressure	14
Tube	345 (50)	Varied fill pressure	15
Tube	483 (70)	Varied fill pressure	16
Tube	103 (15)	Equivalence Ratio = 0.3	20
Tube	103 (15)	Equivalence Ratio = 0.5	21
Tube	103 (15)	Equivalence Ratio = 0.7	22
Tube	103 (15)	Equivalence Ratio = 0.9	23
Tube	103 (15)	Equivalence Ratio = 1.1	24
Tube	103 (15)	Equivalence Ratio = 1.3	25
Tube	103 (15)	Ignition Energy = 0.025 J	28
Tube	103 (15)	Ignition Energy = 0.25 J	29
Tube	103 (15)	Ignition Energy = 2.50 J	30
Tube	103 (15)	Ignition Energy = 5.00 J	31
Tube	103 (15)	Ignition Energy = 10.0 J	32
Tube	103 (15)	Ignition Energy = 15.0 J	33
Tube	345 (50)	Composition Fraction = 0.25	35
Tube	345 (50)	Composition Fraction = 0.50	36
Tube	345 (50)	Composition Fraction = 0.75	37
Tube	103 (15)	Shchelkin Spiral	41
Tube	207 (30)	Shchelkin Spiral	42
Tube	345 (50)	Shchelkin Spiral	43
A	103 (15)	Varied fill pressure	45
A	207 (30)	Varied fill pressure	46
A	345 (50)	Varied fill pressure	47
A	483 (70)	Varied fill pressure	48
B	103 (15)	Varied fill pressure	50
B	207 (30)	Varied fill pressure	51
B	345 (50)	Varied fill pressure	52
B	483 (70)	Varied fill pressure	53
C	103 (15)	Varied fill pressure	55
C	207 (30)	Varied fill pressure	56
C	345 (50)	Varied fill pressure	57
C	483 (70)	Varied fill pressure	58

Table 3.1. Summary of completed experimental tests.

Configuration	Initial Fill Pressure, kPa (psia)	Test Description	Figure #
A	103 (15)	Equivalence Ratio = 0.7	61
A	103 (15)	Equivalence Ratio = 0.9	62
A	103 (15)	Equivalence Ratio = 1.1	63
A	103 (15)	Equivalence Ratio = 1.3	64
B	103 (15)	Equivalence Ratio = 0.7	66
B	103 (15)	Equivalence Ratio = 1.3	67
C	103 (15)	Equivalence Ratio = 0.7	69
C	103 (15)	Equivalence Ratio = 1.3	70
A	103 (15)	Shchelkin Spiral	72
A	207 (30)	Shchelkin Spiral	73
A	345 (50)	Shchelkin Spiral	74
A	483 (70)	Shchelkin Spiral	75
B	103 (15)	Shchelkin Spiral	77
B	207 (30)	Shchelkin Spiral	78
B	345 (50)	Shchelkin Spiral	79
B	483 (70)	Shchelkin Spiral	80
C	103 (15)	Shchelkin Spiral	82
C	207 (30)	Shchelkin Spiral	83
C	345 (50)	Shchelkin Spiral	84
C	483 (70)	Shchelkin Spiral	85
B	103 (15)	3/16" Shchelkin Spiral	87
B	207 (30)	3/16" Shchelkin Spiral	88
B	345 (50)	3/16" Shchelkin Spiral	89

Table 3.1. Summary of completed experimental tests, cont.

CHAPTER 4

EXPERIMENTAL DATA ANALYSIS

Pressure signals acquired from PCB transducers were transferred from the LeCroy oscilloscopes and stored on a PC by means of a LabVIEW control program. This data could then be analyzed without the need for any additional manipulation. However, because of the rapid nature of the detonation combustion process, much of the data from the probes carried noise. This noise was created when the shock wave passed the transducer, causing it to resonate. To combat this problem, the data was sent through a program written in MathWork's® MATLAB software which filtered the data, removing the majority of the high frequency noise. The program implemented a Butterworth low-pass filter, allowing only frequencies below 300kHz to pass through. The resonant frequency of the probes was 500kHz; however, this lower cutoff frequency was determined by achieving a balance between the level of noise reduction and amplitude attenuation. Once the data was filtered, it was output into a text file for analysis in a plotting software package.

Since the only measurement obtainable from the experiments was pressure, then analysis must be from it alone. If the pressure is plotted versus time, the profiles that arise show the pressure history for each individual probe throughout the combustion process. From these plots, wavespeed can be calculated in addition to location of DDT and the time required for it to occur. The wavespeed, *V*, was calculated from a simple time of flight equation,

$$V = \frac{Length\ between\ transducers}{Time\ of\ travel\ of\ combustion\ wave} \qquad (4.1)$$

Values obtained from this equation could be compared to the theoretical values obtained from the Gordon and McBride CEA$^{©}$ code [17]. The CEA$^{©}$ code calculates the theoretical detonation wavespeed for any reaction at any initial condition (temperature, pressure, equivalence ratio, etc…). The CEA$^{©}$ code was also used to find the speeds of sound of the unburned mixtures for the various initial conditions above. This value was helpful in determining whether the wave could be considered a weak detonation or deflagration.

Much can be learned from studying the pressure histories. When a detonation is fully formed, it consists of a shockwave coupled to a combustion zone. Because the shockwave is moving at or above sonic speeds, no information about its arrival is propagated downstream. Therefore, a fully formed CJ detonation should appear in the pressure plots as a sharp pressure rise followed by an expansion wave of decreasing pressure. Because of this property, the time required for DDT to occur and the distance needed can be found from the pressure history plots. This information allows for the detonability of mixtures to be determined.

Experimental and theoretical pressure ratios associated with the detonation process for a number of mixtures have been calculated. However, the magnitudes of the pressure rises were not trusted due to the filtering of the data. For this reason, only wavespeed and pressure histories were used to determine whether a detonation had formed.

CHAPTER 5

DISCUSSION OF EXPERIMENTAL RESULTS

As mentioned previously, parametric studies of selected initial conditions were conducted using two different configurations. A 1.22 m (48 in) long constant area tube was used to observe the detonation process and understand how certain variables affect it. Next, three actuator concepts were tested using the ideas learned from the constant-area tube studies with the primary objective of obtaining a Chapman-Jouguet (CJ) detonation. Table 3.1 summarizes all the experimental tests to be discussed.

5.1 Constant-Area Tube

Parametric studies using the constant area tube are presented first. Using gaseous hydrogen as the fuel, both oxygen and air were used as potential oxidizers. Attempts were made using the hydrogen/air mixture; however, CJ detonation never occurred before the combustion wave reflected from end of the tube. Fill pressures up to 689 kPa (100 psia) were attempted with no success. Therefore, hydrogen/oxygen mixtures will be the focus of the following results. It is a much more reactive mixture and, as the results will show, proved excellent at developing CJ detonations.

5.1.1 Variation of Initial Fill Pressure

The first variable evaluated was the initial fill pressure, using stoichiometric mixtures ranging from 103 (15) to 483 kPa (70 psia). The pressure plots for the 103 (15), 207 (30), 345 (50), and 483 kPa (70 psia) cases are shown in Figures 13-16, respectively. A comparison of these four cases shows that varying the pressure had a significant effect on the detonation process. Figure 13 shows the pressure histories from a run using a 103 kPa (15 psia) fill pressure. A phenomena known as precompression is apparent in the

first two plots. Since the flame speed is lower than the Chapman-Jouguet (CJ) velocity,

the flame accelerates in areas where the combustion rate increases such as the boundary

layer caused by the shockwave [18]. This acceleration in the boundary layer causes the

shock front to take on a concave "bowl-like" shape. As the flame front continues to

accelerate the shock front takes on a 1-D planar shape and the precompression mentioned

before diminishes. No precompression exists in the third plot of Figure 13 and a strong

detonation is assumed to have formed. A wave speed plot is given in Figure 17 that

shows the time of flight velocities between the transducers located in the tube. The 103

kPa (15 psia) curve shows that the wave accelerates to near CJ velocity. However, it is

not possible to determine if this velocity is maintained since no measurements exist

beyond this point. Table 5.1 shows the speed of sound and theoretical CJ velocities for

the four initial fill pressure cases to be discussed.

Initial Fill Pressure, kPa (psia)	Speed of Sound, m/s	Theoretical Wave Speed, m/s
103 (15)	537.9	2837.5
207 (30)	537.9	2875.0
345 (50)	537.9	2902.5
483 (70)	537.9	2920.5

 Table 5.1. Speeds of sound and CJ detonation velocities for various initial fill pressures.

        The 207 kPa (30 psia) case is shown in Figure 14. Comparisons with the 103 kPa

(15 psia) histories show that the DDT process occurs much faster in the higher fill

pressure case. A detonation has formed by the third transducer located 0.457 m (18 in)

downstream of the ignition end wall. The third plot in Figure 14 was created from data

collected using one of the pressure transducers with a maximum range of 3447 kPa (500

psia). As mentioned earlier, wave speed and DDT location and time could still be found

if the exact pressure was not known. Therefore, saturated probe data were often accepted.

Figure 15 shows the pressure histories from a 345 kPa (50 psia) case. The increase in fill pressure allows a detonation to form between the first and second transducers. The wave speed plot shows a velocity of 4200 m/s at the second transducer. The theoretical wave speed was calculated as 2902.5 m/s from the CEA code, confirming that an overdriven CJ detonation had formed in the tube. This situation was described earlier as a transient state with conditions that will converge on the stable Chapman-Jouguet point. Figure 17 shows that the wave speed has lowered to the CJ velocity by the second transducer and oscillates slightly as the wave propagates downstream. Nettleton [19] describes this oscillating velocity as a "galloping-front" and that the peak velocities of the leading front can exceed the CJ velocity. This occurs in mixtures that are too close to the limits of detonability and are not capable of supporting a continuous detonation front [19].

Pressure histories from a 483 kPa (70 psia) case are shown in Figure 16. Although the data is saturated in the first two plots, a detonation can be assumed to have formed by the first transducer due to the shape of the curve. The wave speeds were calculated as slightly higher than the CJ velocity throughout the tube. The pressure peak that occurs after the shock wave passes the transducer in the third plot of Figure 16 is most likely due to instabilities in the pressure transducer caused by the large accelerations from the detonation wave passing. Subsequent pressure rises downstream are from the wave reflecting off the end walls of the tube.

The location of DDT versus the fill pressure is shown in Figure 18. This location is the average of the location of the pressure transducer that first shows a CJ detonation profile and the one immediately upstream. Error bars are plotted to show that the CJ detonation could have been developed anywhere between these two transducers. It should be noted that the fill pressure plays an important role in the DDT process. As the fill pressure increases, the distance required for a CJ detonation to develop decreases.

The time required for a CJ detonation to develop versus the initial fill pressure is shown in Figure 19. Similar to Figure 18, the points plotted show the average between the time of arrival of the CJ detonation wave at the transducer first indicating a detonation and the time that the wave passes the transducer immediately upstream. The error bars for the 448 (65) and 483 kPa (70 psia) cases are much wider due to the fact that a detonation has setup by the first transducer. Therefore, a CJ detonation could have formed instantly or just before it passed the first transducer. Similar to the DDT distance trend, increasing the initial fill pressure decreases the time required to develop a CJ detonation.

5.1.2 Variation of Equivalence Ratio

The equivalence ratio was the second variable studied using the detonation tube. For the fill pressure tests, all mixtures were stoichiometric with an equivalence ratio of one. To understand the effect that fuel-lean and fuel-rich mixtures have on the combustion process, the equivalence ratio was varied between 0.3 and 1.3. Values less than unity denote a fuel-lean mixture, while values greater are fuel-rich. The tests were completed using 103 kPa (15 psia) H_2/O_2 mixture. Plotted in Figures 20-25 are the pressure plots for equivalence ratios of 0.3, 0.5, 0.7, 0.9, 1.1, and 1.3, respectively. Wave

speeds for each case plotted against distance from the ignition end wall are shown in Figure 26. The speeds of sound and CJ detonation velocities are shown below in Table 5.2.

Equivalence Ratio, ϕ	Speed of Sound, m/s	CJ Detonation Velocity, m/s
0.3	408.7	2023.0
0.5	451.7	2319.4
0.7	489.2	2554.2
0.9	522.5	2750.8
1.1	552.5	2917.0
1.3	579.7	3057.6

Table 5.2. Speeds of sound and CJ detonation velocities for various equivalence ratios. Figure 20 shows the pressure histories from a run with an equivalence ratio of 0.3.

DDT does not occur before the combustion wave reflects from the end wall. Pressure data from the first three transducers are plotted, showing a weakening combustion wave that is decelerating as it propagates down the tube. The wave speed plot shows that the velocity is slightly below the speed of sound. When the mixture is increased to an equivalence ratio of 0.5, shown in Figure 21, DDT occurs by 1.4 ms. The peak pressure in this case is around 3447 kPa (500 psia), similar to the peak pressure of the stoichiometric case discussed earlier. The wave speed plot shows that the velocity over shoots the CJ detonation speed before decelerating toward it. Figure 22 shows that a mixture with an equivalence ratio of 0.7 develops a CJ detonation by 1.2 ms at the same location in the tube. The velocity of the main front also overshoots the CJ value for this case. It appears to be converging on the CJ speed as it continues to propagate down the tube.

As the equivalence ratio nears unity, the time for a CJ detonation to develop increases. Figure 23 shows that a mixture with an equivalence ratio of 0.9 becomes CJ in

nature around 1.4 ms. The wave speed plot for this case looks very similar to the $\phi = 0.7$ case. It overshoots the CJ value and then converges back to it as it continues to propagate. Figure 24 shows that no CJ detonation develops by the last transducer in the tube, however, the wave speed plot for this case shows that the velocity is above the CJ value, indicating an overdriven detonation. If the wave behaved similar to the previous cases it would have tried to converge on the CJ velocity as it attempted to become more stable. The $\phi = 1.3$ case shows that no CJ detonation occurred by the last transducer.

The time required for the DDT process is shown in Figure 27. In order to show the spread of the data, included in this plot are results from all the tests completed. As was shown above, a mixture with an equivalence ratio of 0.7 gave the minimum time required to obtain a detonation, around 1.2 ms. Error bars are included to show that the detonation could have been formed earlier except the pressure probes are only located in a few discrete locations, every 0.152 m (6 in). This result is good in that fuel-lean mixtures can be used to obtain a detonation, thus lowering fuel and weight requirements.

5.1.3 Variation of Ignition Energy

The ignition energy could be varied from 0.025J to 15J, allowing its effect on detonation initiation to be evaluated. The fill pressure was held constant at 103 kPa (15 psia) using stoichiometric H_2/O_2 throughout all the tests. Pressure transducers were installed in the first six locations leaving the seventh empty. The pressure plots are shown in Figures 28-33, for ignition energies of 0.025, 0.25, 2.5, 5, 10, and 15J, respectively. The pressure histories from the first probe in addition to the last three are plotted. This was done to show how varying the energy changed the time at which the combustion wave passed the first transducer as well as changes in the DDT process.

The wave speeds for each ignition energy case are shown in Figure 34. The wave speeds are all initially right above the speed of sound and increase as the wave propagates downstream in tube. At the second transducer, the wave speeds are higher for increasing ignition energy; however, this trend is not held as the wave propagates downstream. The velocity of the wave at the final transducer has no dependence on the energy and the results behave randomly. The lack of dependence on energy could be due to the fact the ignition energy is possibly below a threshold where varying its value has no effect. The randomness could then be associated with experimental uncertainties discussed in Chapter 7.

Some important results from the plots are shown below in Table 5.3. The case that used 10J of energy was the only case in which DDT occurred by the last transducer. Therefore, the only difference that the ignition energy had was to decrease the amount of time before the combustion wave passed the first transducer, essentially decreasing the amount of time before the start of combustion. This was not a significant enough result to justify using higher energies. As described in a previous section, more equipment was required to create a higher energy spark. Hence, a decrease in the amount of energy required will lower the cost and weight requirements of the system.

E, J	Time to first transducer, ms	DDT?
0.025	6.1	No
0.25	5.4	No
2.5	5.2	No
5	4.7	No
10	4.8	Yes
15	4.5	No

Table 5.3. Summary of ignition energy tests.

5.1.4 Variation of Oxidizer Composition Fraction

The next variable that was studied using the tube configuration was the oxidizer composition fraction, which is the volume fraction of oxygen in a mixture of oxygen and air. One represents pure oxygen while zero denotes air. The fractions tested were completed using a more energetic 345 kPa (50 psia) fill pressure instead of 103 kPa (15 psia) since moving toward air as an oxidizer will increase the amount of time and distance required for a detonation to develop. It was shown in Section 5.1.1 that increasing pressure decreases the time and distance to detonation. The pressure plots are shown in Figures 35-37 for composition fractions of 0.25, 0.50, and 0.75, respectively. Figure 15 shows the results from the 345 kPa (50 psia) fill pressure case using pure oxygen as the oxidizer. The wave speeds for each case are shown in Figure 38 and the speeds of sound and CJ detonation velocities from the CEA code are shown below in Table 5.4.

Fraction, %	Speed of Sound, m/s	CJ Detonation Velocity, m/s
0	406.7	1965.5
25	455.5	2264.5
50	479.7	2484.1
75	510.3	2669.5

Table 5.4. Speeds of sound and CJ detonation velocities for various fractions.

Figure 35 shows the pressure plots from the case with a fraction of 0.25. No CJ detonation is developed before the wave reaches the end wall of the tube. A weak detonation appears to have developed since the wave speeds are above the speed of sound, however, they are still below the CJ value for this case. The results for the 0.50 case are shown in Figure 36. The pressure histories show that a strong detonation has developed by the transducer located 0.610 m (24 in) downstream of the ignition end wall.

Based on the wave speed plot, the detonation enters an overdriven state before it converges to the CJ velocity around 2500 m/s. Finally, the pressure histories for the fraction of 0.75 are shown in Figure 37, which show CJ profiles by the second transducer. Similar to the previous case, the detonation is overdriven and decelerates to the CJ velocity as it propagates downstream. As a comparison, the wave speed data from a 345 kPa (50 psia) case with a fraction of 1.0 is given in Figure 38. The CJ velocity and speed of sound are higher in this case, apparent from the greater wave speeds through out the tube.

From Figures 35-37, it can be noted that decreasing the fraction toward zero will lessen the likelihood that a detonation will develop. The time that is required for a detonation to develop is shown in Figure 39. A trend that should be noted is that as the fraction tends toward one the time for a CJ detonation to develop decreases. This is also apparent from the pressure plots above. A similar trend can be noted from Figure 40, which shows the distance required for a detonation to occur for varying composition fraction. A mixture with a fraction of 0.75 is still capable of developing a CJ detonation in approximately the same time and distance, but at lower velocities than the pure oxygen case.

5.1.5 Addition of a Turbulence Generator

A turbulence generator device as described in Section 2, in the form of a wire spiral, was installed in the tube immediately downstream of the ignition end wall. The goal of the spiral was to accelerate the transition to a CJ detonation as compared to the tube with no device added. Tests were completed using three initial fill pressures: 103 (15), 207 (30), and 345 kPa (50 psia). The 483 kPa (70 psia) case was not attempted

since a CJ detonation was initiated by the first transducer downstream of the ignition end wall without a spiral. The pressure time histories are shown in Figures 41-43. A comparison of the wave speeds with those measured with no spiral is shown in Figure 44.

In the 103 kPa (15 psia) fill pressure case, the wave speeds measured after the first transducer are greater than the no spiral case. A comparison of the pressure histories in Figures 13 and 41 show that DDT distance is shortened when the spiral is installed. The wave transitions 0.152 m (6 in) upstream compared to the case with no spiral. The results from the 207 kPa (30 psia) case show an even greater improvement. The case without the spiral reaches CJ velocities 0.914 m (36 in) downstream of the ignition end wall. The addition of the spiral accelerates this transition to just 0.457 m (18 in) downstream. Figure 43 shows the pressure histories from the 345 kPa (50 psia) case. Comparing this to the case with no spiral, shown in Figure 15, shows that both transition 0.305 m (12 in) from the ignition end wall. The only difference is in the wave speed plot, where the no spiral case shows overdriven velocities before it converges to the CJ speed.

5.1.6 Summary of Detonation Tube Experiments.

Results from the 483 kPa (70 psia) initial fill pressure case showed the fastest transition to a CJ detonation. Detonations were formed by the first transducer, which is located 0.152 m (6 in) from the ignition end of the tube. The second variable studied was the equivalence ratio, which showed the time to develop a detonation could be minimized by using a fuel-lean mixture of $\phi=0.7$. Ignition energy was then varied and it was learned that no significant gains came from increasing the energy to 15J. The flame front passed the first transducer quicker; however, the DDT did not occur at an earlier location as compared to lower ignition energies. The final variable evaluated was the composition

fraction. As expected, the detonation process was delayed or did not occur at all as the fraction tended toward zero. Mixtures with fractions of 0.75 and 0.50 developed CJ detonations at a location further downstream of the ignition end wall as compared with O_2 as an oxidizer. A spiral was added in an attempt to accelerate the transition to a CJ detonation. The addition of the spiral shortened the distance for DDT, except at 345 kPa (50 psia) where in both cases transition occurred very close to the ignition end wall.

.

5.2 Detonation Actuators

Three different configurations of the detonation actuators were installed in the detonation tube and tested at various initial conditions. Figure 4 shows an actuator installed between the flange and the tube on the ignition end. Parametric studies were again carried out toward the goal of developing a CJ detonation in the convergent section of the actuator. The initial conditions evaluated included varying the initial fill pressure, equivalence ratio, and the addition of a Shchelkin spiral turbulence generator. Ignition energy and composition fraction were not studied since they did not accelerate the DDT process in the constant area tube tests.

5.2.1 Variation of Initial Fill Pressure

The fill pressure was again varied between 103 (15) and 483 kPa (70 psia) for each actuator concept. Actuator A was the first evaluated, which had a 1 cm (0.394 in) throat diameter. The pressure histories for 103 (15), 207 (30), 345 (50), and 483 kPa (70 psia) initial fill pressure cases are shown in Figures 45-48, respectively. A plot of the wave speeds through the actuator for all four cases is shown in Figure 49. This actuator had five pressure taps available, however, only the last four were utilized since the first one was directly above the ignition point and was subject to a large amount of electrical noise from the spark.

For the 103 kPa (15 psia) case, shown in Figure 45, the first pressure rise occurs in 3.6 ms, 0.034 m (1.34 in) downstream of the ignition end wall. It has a peak pressure of around 1380 kPa (200 psia) and does not exhibit the sharp rise that is common for detonation waves [20]. An increase in pressure occurs by the second transducer with a wave speed of 1000 m/s. This is above the sonic velocity of the unburned gas, indicating

that a weak detonation had formed, although not of CJ strength. By the third and fourth transducers, the detonation could not be sustained as indicated by the subsonic wave speed, shown in Figure 49. The next case used a 207 kPa (30 psia) mixture. As shown in Figure 46, the pressure rises to a maximum of 11000 kPa (1600 psia) at the third transducer. The wave accelerates to a maximum wave speed of 700 m/s with the pressure increasing suddenly after a gradual rise, indicating that the shock is becoming more planar. Similar to the case above, the detonation can not be sustained as the wave speed decreases to 450 m/s and the pressure drops to about 6900 kPa (1000 psia) by the last transducer.

The increased initial pressure of 345 kPa (50 psia) in Figure 47 leads to higher pressure rises, with the maximum of 13800 kPa (2000 psia) occurring at the third transducer. This peak pressure is maintained through the fourth transducer and the wave speed remains supersonic after a slight deceleration from an initial value calculated at 1200 m/s. This decrease in wavespeed indicates that the detonation is weakening as it approaches the throat of the actuator, similar to the previous two cases. The final fill pressure attempted in this actuator was 483 kPa (70 psia), shown in Figure 48. As the pressure plots show the pressure increases and the spacing between the rises decreases as the wave propagates through the actuator. This is also apparent from the velocity plot, where the wave speed continues to increase to a maximum of 2350 m/s by the last transducer. This value is still below the 2920 m/s CJ velocity. However, it is interesting to note the strengthening of the wave in this case, as compared to the previous three results.

Actuator B, with a throat diameter of 0.5 cm (0.197 in), was installed in the detonation tube next. The pressure histories are shown in Figures 50-53 for each fill pressure case. The pressure transducers were located in the same locations as the previous actuator. A plot of the wave speeds is shown in Figure 54.

The pressure rises in the 103 kPa (15 psia) case appear to increase in amplitude, up to a maximum of around 4800 kPa (700 psia) by the third transducer. The fourth transducer records a peak pressure of only 2800 kPa (400 psia), indicating a weakening of the wave. From the velocity plot it should be noted that the wave speed is subsonic throughout the actuator and only deflagration combustion is present. The same can be said of the combustion process in the 207 kPa (30 psia) case, except a higher maximum pressure of 8300 kPa (1200 psia) is recorded. The wave speed decreases from a value close to the speed of sound and then increases again as the wave propagates through the throat, although never going above the sonic line. It should be noted in Figures 50-53 that the pressure readings are less than zero at the beginning of the run. This is from the oscillations that occurred when the ignition system was not shielded properly. It was determined that this did not affect the readings adversely since the pressure rises back to a normal value by 0.2 ms.

A 345 kPa (50 psia) initial fill pressure was attempted next and the results are shown in Figure 52. A peak pressure of almost 17240 kPa (2500 psia) was recorded by the third transducer and it appears as though the wave is strengthening. However, the velocity plot shows that this is not the case as the wave speed decreases from a supersonic to subsonic velocity by the last transducer. Results of the 483 kPa (70 psia) initial pressure case are shown in Figure 53. The pressure rises to 24800 kPa (3600 psia),

but the wave speed never rises above the sonic line. The sharp pressure rise at 0.0039 sec is due to a loose cable connecting the transducer to the signal conditioner and is not flow related. The problem was identified and fixed in later tests.

Every initial pressure attempted using actuator B produced only deflagrations at the throat. The wave speed and pressure for each case decreases by the last transducer. It is a possibility that the smaller throat diameter is constricting the flow to a large degree, creating unfavorable conditions for a transition to a detonation.

The next actuator, actuator C, had the same throat diameter, but had a 1 cm (0.394 in) throat extension. It was designed in this manner with the hope of sustaining or strengthening a detonation in the constant-area section. Pressure histories are shown in Figures 55-58. A plot of the wave speed at each location in the actuator is provided in Figure 59. Actuator C also had one extra pressure port located in the throat extension. This is now the final transducer before the exit of the actuator located 0.108 m (4.25 in) downstream of the ignition end wall.

The 103 kPa (15 psia) case, shown in Figure 55, has relatively low pressure rises with a maximum of around 4150 kPa (600 psia) in the constant area section. The pressure increases and decreases before reaching the throat. Velocity behaves in an opposite fashion by decreasing then increasing as the wave passes through the throat and constant area extension. The wave speed remains subsonic throughout the actuator. When the pressure and velocity plots are compared to those of the previous actuator, it should be noted that the constant area section helps to increase both velocity and pressure. It is also interesting to note that the pressure history in the throat extension exhibits a sudden rise typical of a CJ detonation. However, since only one transducer is

located in the section it is impossible to tell whether the wave speed and the pressure increase by the exit, possibly producing a detonation.

The pressure histories in Figure 56 look very similar to those in the 103 kPa (15 psia) case. However, the maximum pressure obtained is approximately 12400 kPa (1800 psia) at the third transducer. The pressure drops slightly by the constant area section, however, the wave speed increases to almost the speed of sound. This indicates that deflagration combustion is the driving process in the actuator.

It should be noted that only four transducers are used for the 345 kPa (50 psia) and 483 kPa (70 psia) runs due to a malfunction in the first transducer. The maximum peak pressure obtained in the 345 kPa (50 psia) case was around 12400 kPa (1800 psia). Similar to the previous two runs, the wave speed decreases to well below the sonic line before an increase caused by the deflagration propagating through the constant area section of the actuator.

An initial pressure of 483 kPa (70 psia) was the final variation used to study the effect on fill pressure in the three actuator configurations. Besides a maximum pressure of 20000 kPa (2900 psia) occurring at the second transducer, the actuator performed the same as in the other cases. The wave speed was subsonic throughout, decreasing until a slight acceleration when the wave propagated through the constant area section.

In summary, only the actuator with the largest throat diameter gave results that showed waves approaching CJ strength. Figure 60 shows the exit wave speeds for each nozzle at the various fill pressures. Only actuator A showed supersonic wave speeds at the throat. The 483 kPa (70 psia) case showed a strong acceleration up to a wave speed of 2350 m/s before the exit. Actuators B and C both constricted the flow to a point where

detonations could not be sustained or were not initiated at all. The constant area throat extension helped to increase both the pressure and the velocity of the wave propagating through it. However, it was impossible to determine if a detonation had developed due to only one pressure port in this location.

5.2.2 Variation of Equivalence Ratio

When fuel-lean mixtures were used in the constant area tube configuration, the detonations transitioned into CJ detonations over a shorter distance. For this reason, the same tests will be carried out using the detonation actuators. Four equivalence ratios were used: 0.7, 0.9, 1.1, and 1.3 at a 103 kPa (15 psia) initial fill pressure. Actuator A was tested first and its pressure histories for the four cases are shown in Figures 61-64, respectively. A plot of the wave speeds is included in Figure 65 showing the change in velocity as the wave propagates downstream from the ignition source. In addition, included in Figure 65 are curves indicating the speed of sound in the unburned mixture for each of the equivalence ratios. The speed of sound is a function of equivalence ratio causing it to change for each value.

A fuel-lean mixture with $\phi = 0.7$ was tested first in the actuator. Similar to the stoichiometric runs above, the pressure increases as the wave propagates passed the first three transducers and then decreases by the throat. A maximum of 4150 kPa (600 psia) was recorded by the third transducer. From the wave speed plot, the velocity decreases from supersonic to subsonic as the wave propagates through the actuator. The weak detonation that was formed by the second transducer was not sustained and a deflagration exited the actuator throat.

Similar results are obtained for the runs that used equivalence ratios of 0.9, 1.1, and 1.3, shown in Figures 62-64, respectively. Mixtures with ϕ=0.9 and 1.1 were initially supersonic, but weakened to subsonic deflagration by the throat. The ϕ=1.3 case is subsonic throughout. The equivalence ratio benefit seen in the constant area tube results was not enough to overcome the much shorter lengths used in the actuators.

Actuator B was tested next and based on the results from the previous actuator, only the more extreme equivalence ratios were tested. The pressure plots are shown in Figure 66 and 67 and the wave speed plot is given in Figure 68. Similar pressure rises are seen in Figure 66 as compared with the same case using the previous actuator. It may be seen that the wave speeds have dropped below the previous values plotted in Figure 65. However there is one difference in that they reach a minimum at the third transducer and then increase by the throat transducer. This value is still below the value obtained from the previous configuration.

The most significant difference in the results for the $\phi = 1.3$ case is the slightly higher wave speeds, as seen in Figure 68. This is due to the difference in the speed of sound between two mixtures. The fuel-rich case has a higher hydrogen content which has a lower molecular weight. This lowers the density and increases the speed of sound. The pressure histories are almost identical in both amplitude and profile.

The actuator with the constant area throat extension was installed in the detonation tube and tested with mixtures of $\phi = 0.7$ and 1.3. The pressure histories are shown in Figures 69 and 70 and the wave speeds plotted against x location in the actuator are shown in 71. As stated before, actuator C had a pressure tap located in the constant area section of the throat, making a total of five transducers. Looking at the $\phi = 0.7$ case

41

shows that the first four pressure transducers record very similar pressure curves as compared to actuator B. The additional transducer in the throat recorded a pressure of around 3447 kPa (500 psia), slightly lower than the peak pressure recorded at the second transducer.

The velocities of the wave are shown in the wave speeds plot shown in Figure 71. The first three wave speeds compare well against their counterparts in the previous actuator run. The velocity decreases at the third transducer and then increases slightly as the wave propagates toward the fourth probe. Then, similar to the fill pressure cases discussed earlier, the wave accelerates as it passes through the constant area section.

The fuel-rich case, $\phi = 1.3$, has very similar pressure curves when compared to the fuel-lean case. However, the pressure rise associated with the propagating wave occurs earlier and the overall wave speeds are slightly higher. Both of these changes are due to the increase in speed of sound. The constant area section manages to increase the velocity again, however, both waves remain below the speed of sound and no detonation is developed.

In summary, the variation of the equivalence ratio fails to assist in developing a strong CJ detonation in the actuators. In all cases, the wave is only a deflagration or possibly a very weak detonation. Actuators B and C showed promise by accelerating the wave as it approached the exit, contrary to the deceleration that occurred in actuator A.

5.2.3 Addition of a Turbulence Generator

The spiral made from the 1.6 mm (0.0625 in) diameter wire was installed in each actuator and tested with varying initial pressure. The actuators were evaluated using 103 (15), 207 (30), 345 (50), and 483 kPa (70 psia) mixtures. The results of the actuator A

tests are shown in Figures 72-75. A velocity plot is shown in Figure 76 with wave speeds plotted against location for this actuator. The first test completed used a mixture with a fill pressure of 103 kPa (15 psia). The results in Figure 72 show pressures similar to the case without the spiral, however the pressure rises appear to be spaced closer. Figure 76 shows that the velocity of the wave propagating from the first to the second transducer was around 1750 m/s, which is well above the sonic velocity. Even though the pressure rise increases by the third transducer the velocity drops below the speed of sound and a detonation can not be sustained. The initial pressure was then increased to 207 kPa (30 psia), shown in Figure 73. These plots show tightly spaced, sudden rises of pressure with little precompression. This type of profile is indicative of strong CJ detonations and the wave speed plot shows that the velocity increases from an initial value of about 1500 m/s to around 2600 m/s. This value is much closer to the CJ wave speed of 2875 m/s. It is not a CJ detonation, but it is an improvement over the runs with no added turbulence device.

The 345 kPa (50 psia) initial pressure case is shown next in Figure 74. Peak pressure is around 8300 kPa (1200 psia) with the precompression diminishing as the wave propagates toward the throat. The wave speed plot in Figure 76 shows a velocity of 3850 m/s, higher than the CJ detonation wave speed. The velocity drops to around 2400m/s and then increases to the CJ velocity by the fourth transducer. This "galloping-front" phenomena was described earlier and was attributed to regions where the detonation front could not be sustained, such as in area where the fuel-oxidizer mixing was poor. In addition, the combustion front accelerates in regions of greater turbulence. As the wave passes over the localized regions of enhanced mixing created by the spiral, an acceleration of the combustion wave occurs. The "galloping-front" can also be seen in

the 483 kPa (70 psia) fill pressure case. Figure 76 shows a wave speed of almost 4500 m/s at the third transducer before a deceleration brings the velocity of the wave to 3650 m/s at the actuator throat. These results show that overdriven and CJ detonations can be created in the actuators by the addition of a turbulence generator.

The results from the testing of the spiral in the actuator B are discussed next. Plots for initial pressures of 103 (15), 207 (30), 345 (50), and 483 kPa (70 psia) are shown in Figures 77-80, respectively. The wave speed plot is shown in Figure 81. From the plot of the 103 kPa (15 psia) case, it is apparent that a strong detonation is not initiated. The peak pressure is around 4800 kPa (700 psia) with a maximum velocity of 1200 m/s obtained at the throat. The 207 kPa (30 psia) case shows a peak pressure of 7200 kPa (1040 psia) with an accelerating wave reaching a velocity of 3900m/s by the throat. Figure 79 shows the 345 kPa (50 psia) case with a peak pressure around 10340 kPa (1500 psia). The pressure histories are detonation-like in nature and show almost no sign of precompression by the fourth transducer. The wave speed plot in Figure 81 shows that after an initial acceleration the velocity levels off slightly higher than the CJ velocity of 2900 m/s. Figure 80 shows the pressure histories from the 483 kPa (70 psia) initial fill pressure case. The wave quickly accelerates to the overdriven detonation regime before it begins to converge to the CJ velocity. This type of behavior is very similar to the previous runs and the large velocities that were measured are a result of the regions of localized mixing created by the coils of the spiral. In the third plot of Figures 77-79 some very large pressure spikes are recorded. As mentioned earlier these are due to a loose cable connecting the transducer to the signal conditioner.

The same set of tests was repeated using actuator C, with the 1 cm (0.394 in) constant area throat extension with a 0.5 cm (0.197 in) diameter. The pressure histories are shown in Figures 82-85 and the wave speeds are shown in Figure 86. Comparison of the pressure histories from this actuator to the previous one shows few differences. The addition of the constant area section appears to lower the pressure in all four cases. From Figure 86, it is apparent that it also lowered the velocity when the wave was already supersonic. The 103 kPa (15 psia) case shows an increase in velocity, however, the wave is still well below the CJ velocity. The 483 kPa (70 psia) case follows the same trends as the previous three cases; however, it is right above CJ velocity when it exits the actuator after being overdriven before the throat.

As a comparison, a spiral made from copper wire with a diameter of 4.8 mm (0.1875 in) was installed in actuator B and tested at various fill pressures. The pressure history plots are shown in Figures 87-89 and the wave speed plot is shown in Figure 90. The spiral was tested at initial pressures of 103 (15), 207 (30), and 345 kPa (50 psia). From the wave speed plot it can be noted that the larger diameter does not provide an advantage over the thinner version, shown in Figure 81. In both cases, the 103 kPa (15 psia) initial fill pressure mixture is not capable of producing a CJ detonation. In addition, the 207 (30) and 345 kPa (50 psia) cases develop into CJ detonations by the throat of the actuator. From these results, it was concluded that the thinner spiral worked equally well at accelerating the DDT process and no further testing of the thicker diameter was completed. The large pressure spikes in the third plot of Figures 87-89 are again due to the loose cable.

5.2.4 Summary of Detonation Actuator Tests

Of all the detonation actuator tests, the cases where the Shchelkin spiral was used proved the most capable of developing a CJ detonation before the exit of the actuator. Overdriven detonations were present in all three actuators at initial fill pressures 207 kPa (30 psia) or greater. The tests varying the initial fill pressure with no spiral failed to develop a CJ detonation and in only one case was the velocity approaching the CJ value. Actuator B and C appeared to constrict the flow to the point where the wave speeds decreased as the wave propagated downstream. The results from the variation of the equivalence ratio showed no development of a CJ detonation. In almost every case, only deflagration combustion was present.

5.3 Comparison of the Constant Area Tube and Actuators

The time to detonation, distance to detonation and the amplitude of the wave were considered when comparing the results from the constant area tube and the actuators. As mentioned in a previous section, the pressure histories recorded in the tube and various actuators for an initial pressure of 103 kPa (15 psia) are shown in Figures 13, 45, 50, and 55, respectively. As discussed earlier, no CJ detonations are formed in the actuators before the wave exits, however the pressure amplitude of ~4800 kPa (700 psia) is obtained in actuator B by 0.078 m (3.07 in) downstream of the ignition end wall. This amplitude is not reached until 0.762 m(30.0 in) downstream in the tube. Pressure histories of the 207 kPa (30 psia) case are shown in Figures 14, 46, 51, and 56, respectively. As the pressure histories show, the actuators do not accelerate the transition to detonation as well as the constant area tube. A CJ detonation has formed by the first transducer located 0.457 m (18 in) downstream of the ignition end wall in the tube. No CJ detonations are

even formed in the actuators. In addition, the peak pressures seen in the constant area tube are greater than the amplitudes recorded in the actuators.

The results from the addition of the Shchelkin spiral are discussed next. A vast improvement in the performance of the actuators can be noted from these plots. Figures 41, 72, 77, and 82 show the cases with an initial pressure of 103 kPa (15 psia) for both the actuators and the constant area tube, respectively. No CJ detonation is present in this case and the actuator's only advantage appears to be in the large increase in pressure that results from the wave being compressed in the convergent section of the actuator. The pressure amplitudes reach levels not seen in the constant area tube until a CJ detonation has almost formed toward the end of the tube. The 207 kPa (30 psia) fill pressure cases are presented Figures 42, 73, 78, and 83. CJ detonations have formed in each actuator by the throat located approximately 0.102 m (4 in) downstream of the ignition end wall. A detonation is not formed until 0.305 m (12 in) downstream in the tube case. In addition to the improvement in the DDT location, the DDT time is also decreased in the actuator runs. Pressure histories from the 345 kPa (50 psia) cases are shown in Figures 43, 74, 79, and 84. The same can be said about these plots as the previous one. CJ detonation occurs in each case in less distance and time for each of the actuators as compared to the constant area tube. In the 483 kPa (70 psia) fill pressure cases, shown in Figures 16, 75, 80, and 85, the deflagration in the constant area tube with out a spiral transitions to a detonation occurs faster than in the actuators with spirals. A CJ detonation is formed in less time and possibly less distance, although it is impossible to say due to pressure transducers only being located every 0.152 m (6 in) in the tube.

In summary, DDT occurs in a shorter distance in the constant area tube than in the actuators, when no spiral is installed. Without the spiral, CJ detonations do not occur in the actuators at all fill pressures; however, in some cases the pressure amplitudes are greater than in the tube. When a spiral is added to the actuators, their performance surpasses that of the tube for certain initial fill pressures. The 207 (30) and 345 kPa (50 psia) cases both produced CJ detonations in less distance and time than required by the constant area tube. Therefore, which configuration helps produce the quickest detonation depends on the initial conditions.

CHAPTER 6

DISCUSSION OF NUMERICAL RESULTS

Computational fluid dynamic (CFD) analysis was conducted to help understand and validate the flow processes observed in the laboratory experiments. The 2-dimensional, time-accurate SPARK code was chosen for the numerical study of the detonation actuators. It solves the elliptic Navier Stokes and energy equations as well as the species continuity equations. SPARK was developed by Drummond [21] to study supersonic reacting flowfields, which lends itself directly to the development of the actuators.

The constant area tube and the three actuator concepts were all evaluated using the SPARK code. An axisymmetric grid was used to model the actuators. An ignition spark was simulated by adding a specified spark energy to the source terms in a region near the centerline at the wall. The size of the region and the amount of energy were varied to understand their effect. It was found that above a certain spark energy for a given region size, all cases, including both H_2/O_2 and H_2/Air mixtures, a Chapman-Jouguet detonation was formed immediately. Below this energy value no ignition occurred. This being the case, a good comparison between the experimental and computational results could not be made. There are a few possibilities to the reason why the SPARK code predicted immediate initiation of CJ detonations. The first was the size of the grid that was used to study the various cases. Shapiro [22] states the width of the leading shock wave to be 1.4×10^{-7} m. A grid of this spacing would be needed to resolve the detailed structure of the shock wave coupled to the reaction zone. Resolving this structure is imperative to observing the DDT process, which is not seen in the coarser

grids. A grid of the spacing recommended by Shapiro would result in almost 800,000

nodes in the x-direction of the detonation actuators. The computer resources allotted for

this study only allowed spacing on the order of 1×10^{-4} m. A method of adaptive grid

refinement would have to be implemented in SPARK to ensure the grid was adequately

spaced in the vicinity of the shock/flame front. In addition, the system of equations being

solved is numerically stiff and as the grid became finer, the computational times

increased dramatically.

Due to the number of grid points required to resolve the detonation front and the

lack of adequate computer resources, the results of computations performed on much

coarser grids will not be discussed.

CHAPTER 7

EXPERIMENTAL UNCERTAINTIES

The experimental studies were not error-free and some uncertainties did exist. The first group of uncertainties deals with the injection of the fuel-oxidizer mixtures. Before each run, the tube and actuators were evacuated of any air and/or combustion products from previous runs. Ideally, the vacuum pump would evacuate the entire contents of the chamber; however, the pump was only able to evacuate the chamber to 103-207 Pa (0.015-0.030 psia). Although this amount was very small, it contaminated the fuel and oxidizer that was injected into the chamber. In addition, the tube and actuator assembly would ideally be airtight but some small leaks did develop at times. The leak rate could be reduced to approximately 2.06 Pa/sec (0.018 psia/min). Therefore, during mix times the initial fill pressure was not maintained. A third source of uncertainty deals with the injection of the fuel and oxidizer. It was controlled by turning valves and then monitoring the pressure on the Mensor pressure gauge. Since this was not automated, the partial pressures were not exact every time. This error was not significant since the actual partial pressures achieved varied by much less than 1% from the stated values. In addition, the fuel and oxidizer were not premixed before they were injected in the tube. As discussed in Chapter 2, the fuel and oxidizer were allowed to mix by waiting five minutes before they were ignited. Based on the mixing study results, it was assumed that each run was repeatable.

The PCB pressure transducers added more uncertainty to the experiments. Due to the sensitive nature of the transducers, they were susceptible to errors due to large accelerations caused by the violent explosions with in the chamber. These errors caused

overshoots in the pressure readings as well as noise to occur in the signals that was later removed with filtering. The filtering itself added more uncertainties because the low-pass filter did not allow anything over 300kHz to pass through. Any part of the signal above this cutoff frequency was eliminated whether it was noise or not. Therefore, the pressure histories that were obtained may not replicate the combustion process in the detonation chamber. The time of flight velocities should still be accurate since they do not depend on the pressure magnitude, only on the time of arrival.

Finally, the ignition energy stated may not exactly match with the value actually achieved. The Spectralite 919 flash lamp power supply was calibrated by technicians at Wyle Laboratories before and during the experimental studies and should have provided accurate energies. The components that were added to boost the maximum energy were not monitored and it was assumed that the stated energy was achieved if the 5 μF capacitor was completely discharged after each firing. This was checked when the equipment was installed, but was discontinued during the actual runs, therefore, actual energies may have varied.

CHAPTER 8

CONCLUSIONS AND RECOMMENDATIONS

An experimental investigation was performed in support of the development of actuators utilizing detonation for flow control. These actuators hold the promise of controlling high speed flows, including the transonic and supersonic flow regimes.

Parametric studies were completed using a 1.22 m (48 in) long constant area tube and three actuator concepts. From the tube tests, initial fill pressure was found to have a large effect on the detonation process, as higher fill pressures decreased the time and the distance required to transition to a CJ detonation. The equivalence ratio of the fuel and oxidizer mixture was varied between 0.3 and 1.3 and it was found that the DDT time could be minimized by a fuel-lean mixture with $\phi = 0.7$. The energy used to ignite the mixture in the tube was varied from 0.025J to 15J in an attempt to accelerate the DDT process. It was found that increasing energy increased the initial wave speeds; however, the wave could not maintain the velocities and the final values behave randomly with spark energy. It was concluded that the ignition energy within the range tested did not significantly improve the detonation process. The composition of the oxidizer was varied from pure oxygen to air. As the oxidizer composition approached air, the wave speeds decrease and the likelihood of DDT decreases. A composition fraction of 0.75 still allowed a CJ detonation to develop but the wave speeds were lower than in the pure oxygen case. In the final attempt to accelerate the DDT process, a Shchelkin spiral was added to the tube. It was tested at initial fill pressures ranging from 103 (15) to 345 kPa (50 psia). The presence of the spiral helped to decrease the DDT distance from 1.07 m (42 in) to 0.914 m (36 in) in the 103 kPa (15 psia) case and from 0.914 m (36 in) to 0.457

m (18 in) in the 207 kPa (30 psia) case. The 345 kPa (50 psia) case transitioned at the same point in both cases.

Of the variable values tested in the constant are tube, those that helped to transition deflagrations to detonations were also studied in the evaluation of the three detonation actuators. The initial fill pressure was varied from 103 (15) to 483 kPa (70 psia) using each of the actuators. Actuator A was the only one to produce supersonic wave speeds. No CJ detonations were developed and in most cases, only deflagration combustion was present. The equivalence ratio was varied to understand its effect on the flow processes in the actuators. The values tested ranged from 0.7 to 1.3, however, no CJ detonations developed in any of the runs attempted. A Shchelkin spiral was then installed in the actuators and initial fill pressures of 103 (15) to 483 kPa (70 psia) were used to evaluate its performance. Only the 103 kPa (15 psia) cases did not produce strong detonations. Most of the other three fill pressure cases had at least overdriven detonations from the throat of the actuator on downstream. Of the three actuators, only actuator B helped to transition waves to just below the CJ point. Overdriven detonations were present at the exit for fill pressures 207 kPa (30 psia) and greater. Actuator A had CJ or overdriven wave speeds for fill pressures of 345 kPa (50 psia) and greater. Actuator C had strong detonations present at the throat, but the constant area throat extension weakened the wave by lowering its wave speed.

When the constant area tube and the actuators are compared, the tube generates CJ detonations quicker than the actuators when no spiral is installed. The actuators are not capable of creating CJ detonations at any of the fill pressures tested; however, in some cases the pressure amplitudes are greater than in the tube. When a spiral is added to

the actuators, they are capable of developing CJ detonations faster than the tube for certain initial fill pressures. The 207 (30) and 345 kPa (50 psia) cases both produced CJ detonations in less distance and time than required by the constant area tube. Therefore, the initial conditions must be considered when deciding whether the actuators perform better than the constant area tube.

It should be noted that the actuator shape was not optimized in this study. The three geometries that were found to work well in simulations were studied experimentally. The results show that actuators with increasing throat diameters may be more favorable. More studies will have to be completed to optimize the design of the actuator.

The goal of this study was to obtain CJ detonations in the actuators and this was achieved with the help of the Shchelkin spiral. The results from the single shot experiments prove that the actuators are capable of producing CJ detonations or in some cases overdriven detonations. A multicycle version needs to be developed so that the actuator can be tested in a high speed cross flow to determine its effectiveness in flow control.

REFERENCES

[1] Gad-el-Hak, E., Bushnell, D., "Status and Outlook of Flow Separation Control," AIAA Paper 91-0037, Jan 1991.

[2] Jacobs, J.W., James, R.D., Ratliff, C.T., and Glezer, A., "Turbulent Jets Induced by Surface Actuators," AIAA Paper 93-3243, AIAA Shear Flow Conference, 1993.

[3] McManus, K., Ducharme, A., Goldey, C., and Magill, J., "Pulsed Jet Actuators for Suppressing Flow Separation," AIAA Paper 96-0442, Jan. 1996.

[4] Funk, R., Parekh, D., Glezer, A., and Crittenden, T., "Transient Separation Control Using Pulse Combustion Actuation," AIAA Paper 02-3166, June 2002.

[5] Grossman, K.R., Cybyk, B.Z., and VanWie, D.M., "Sparkjet Actuators for Flow Control," AIAA Paper 03-0057, Jan. 2003.

[6] Beck, B.T., Cutler, A.D., Drummond, J.P., and Jones, S.B., "A Resonant Pulse Detonation Actuator for High-Speed Boundary Layer Separation Control," Proceedings of the 11th International Symposium on Flow Visualization, August 9-12, 2004.

[7] Miller, D.N., Yagle, P.J., Bender, E.E., Smith, B.R., and Vermeulan, P.J., "A Computational Investigation of Pulsed Injection into a Confined Expanding Crossflow," AIAA Paper 01-3026, June 2001.

[8] Kanury, A.M., *Introduction to Combustion Phenomena,* Vol. 2, Gordan and Breach, New York, 1982.

[9] Glassman, I., *Combustion*, Academic Press, Inc., New York, 1977.

[10] Bussing, T.R.A., and Pappas, G., "An Introduction to Pulse Detonation Engines," AIAA Paper 94-0263, Jan. 1994.

[11] Hinkey, J.B., Bussing, T.R.A., and Kaye, L., "Shock-Tube Experiments for the Development of a Hydrogen-Fueled Pulse Detonation Engine," AIAA Paper 95-2578, July 1995.

[12] Li, C., and Kailasanath, K., "Detonation Initiation in Pulse Detonation Engines," AIAA Paper 03-1170, Jan. 2003.

[13] Schauer, F., Stuturd, J., and Bradley, R., "Detonation Initiation Studies and Performance Results for Pulsed Detonation Engine Applications," AIAA Paper 01-1129, Jan. 2001.

[14] Meyer, T.R., Hoke, J.L., and Brown, M.S., " Experimental Study of Deflagration-To-Detonation Enhancement Techniques in a H_2/Air Pulsed-Detonation Engine," AIAA Paper 02-3720, July 2002.

[15] Shchelkin, K.L., Soviet Journal of Technical Physics, Vol. 10, pp. 823-827, 1940.

[16] Urtiew, P.A., and Oppenheim, A.K., "Experimental Observations of the Transition to Detonation in an Explosive Gas," Proc. Royal Society London, A291:13.

[17] Gordon, S., and McBride, B.J., "Computer Program for Calculation of Complex Chemical Equilibrium Compositions, Rocket Performance, Incident and Reflecting Shocks, and Chapman-Jouguet Detonations," NASA SP 273, 1971.

[18] Lee, J.H., Knystautas, R., and Chan, C.K., "Turbulent Flame Propagation in Obstacle-Filled Tubes," 20th International Symposium on Combustion, The Combustion Institute, Pittsburg, 1984, pp. 1663-1672.

[19] Nettleton, M.A., *Gaseous Detonations: Their Nature, Effects, and Control*, Chapman and Hall, NY, NY, 1987.

[20] Ting, J.M., Bussing, T.R.A., and Hinkey, J.B., "Experimental Characterization of the Detonation Properties of Hydrocarbon Fuels for the Development of a Pulse Detonation Engine," AIAA Paper 95-3154, July 1995.

[21] Drummond, J.P., "A Two-Dimensional Numerical Simulation of a Supersonic, Chemically reacting Mixing Layer," NASA TM-4055, 1988.

[22] Shapiro, A.H., *The Dynamics and Thermodynamics of Compressible Fluid Flow*, Ronald Press Company, New York, 1953.
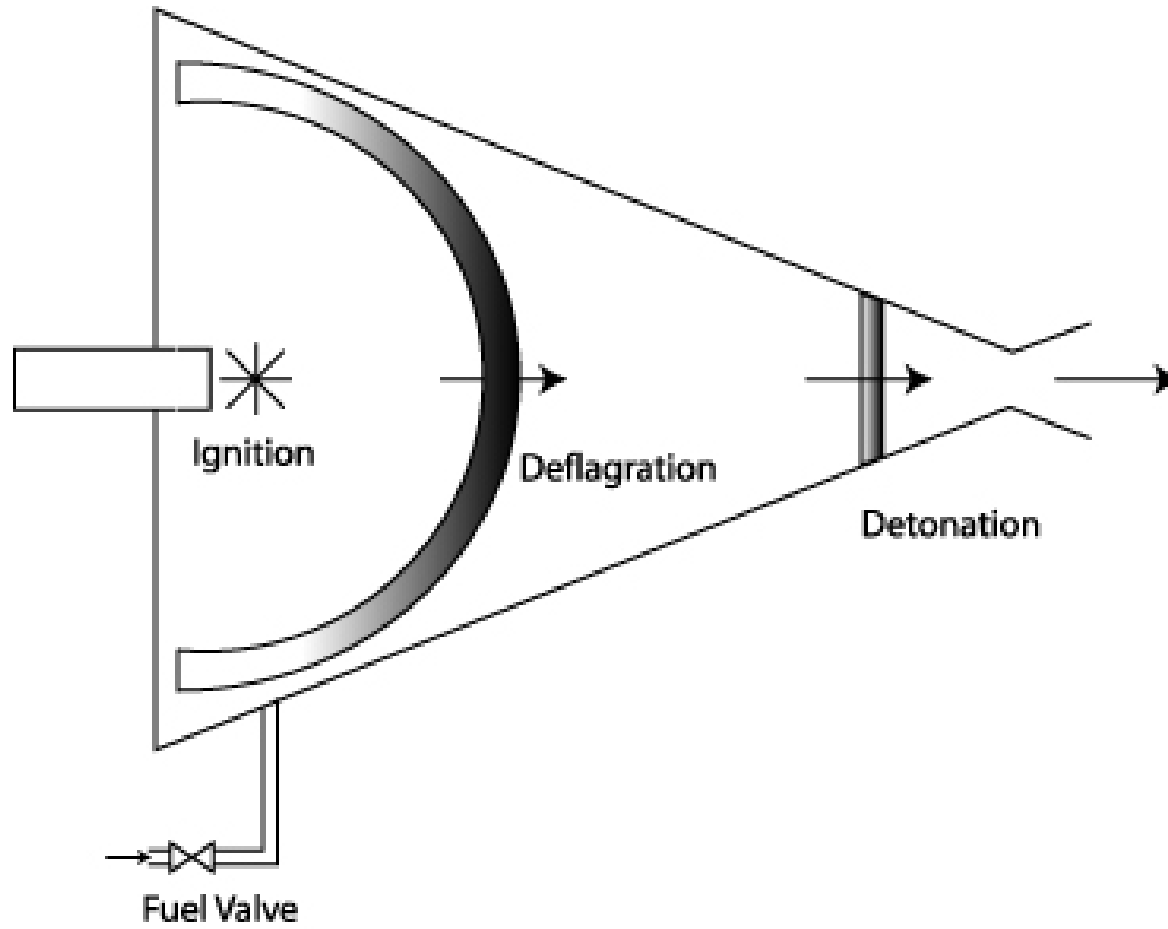
Figure 1. Simplified detonation actuator.
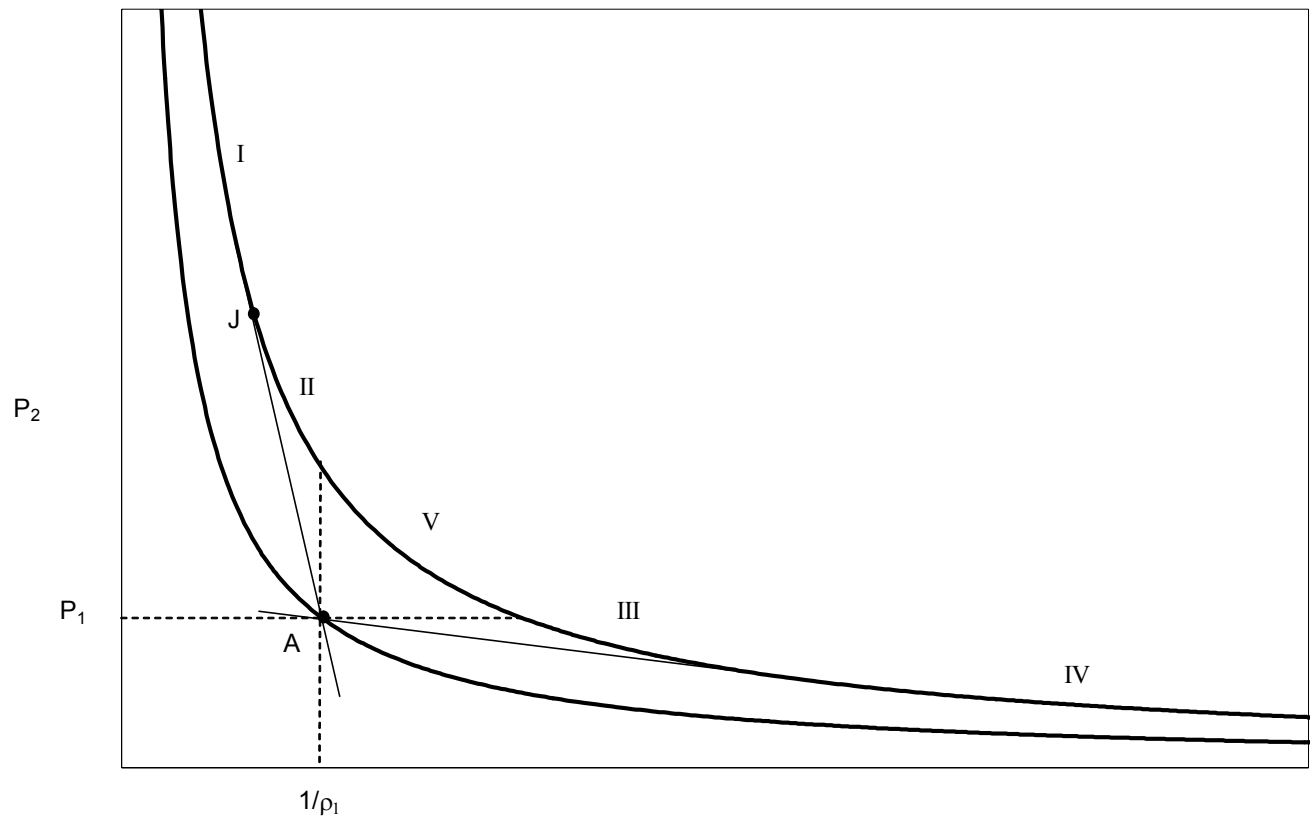
Figure 2. The Hugoniot plot divided into five regions.
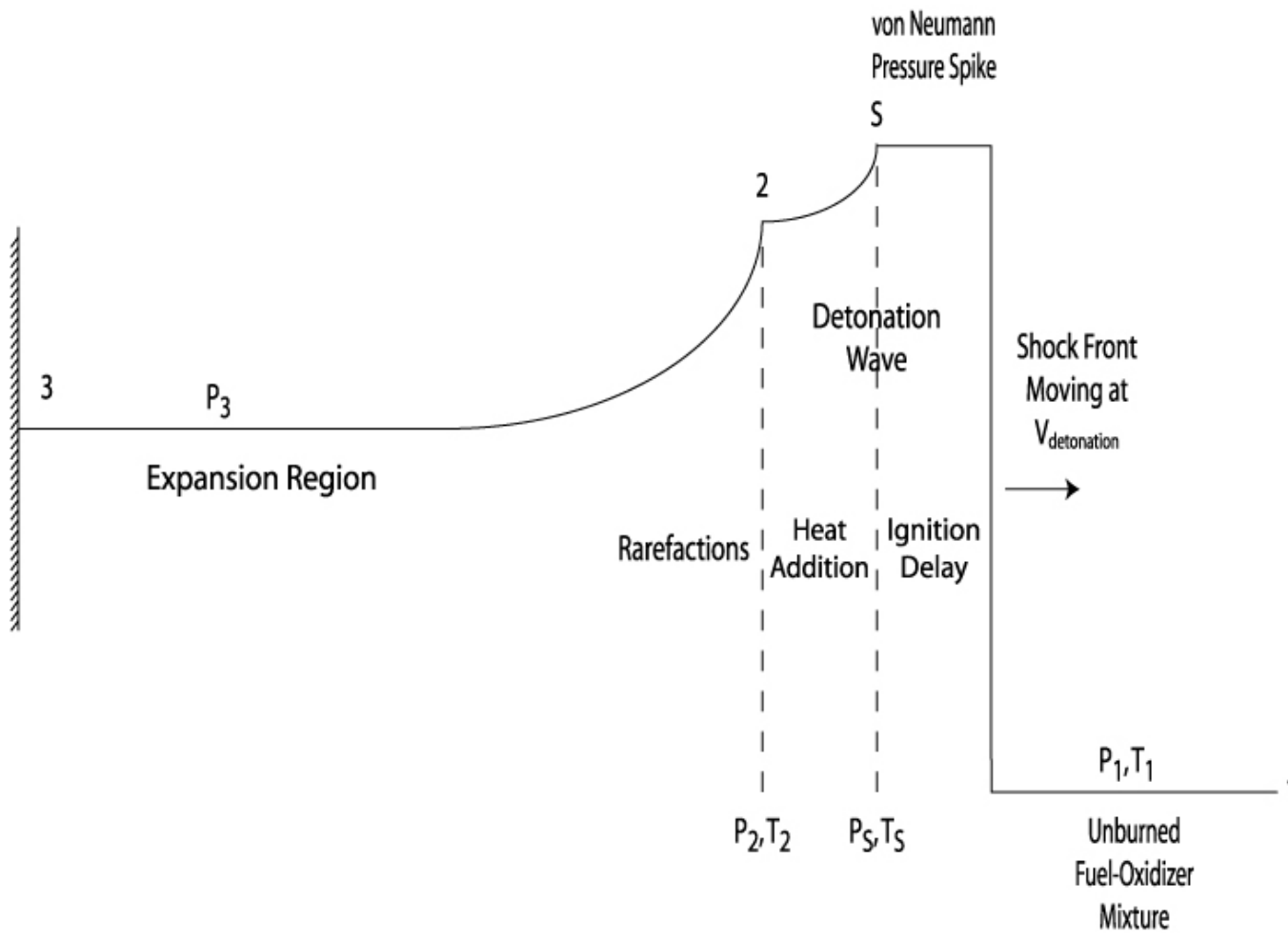
Figure 3. Characteristic detonation profile in a constant area tube [10].
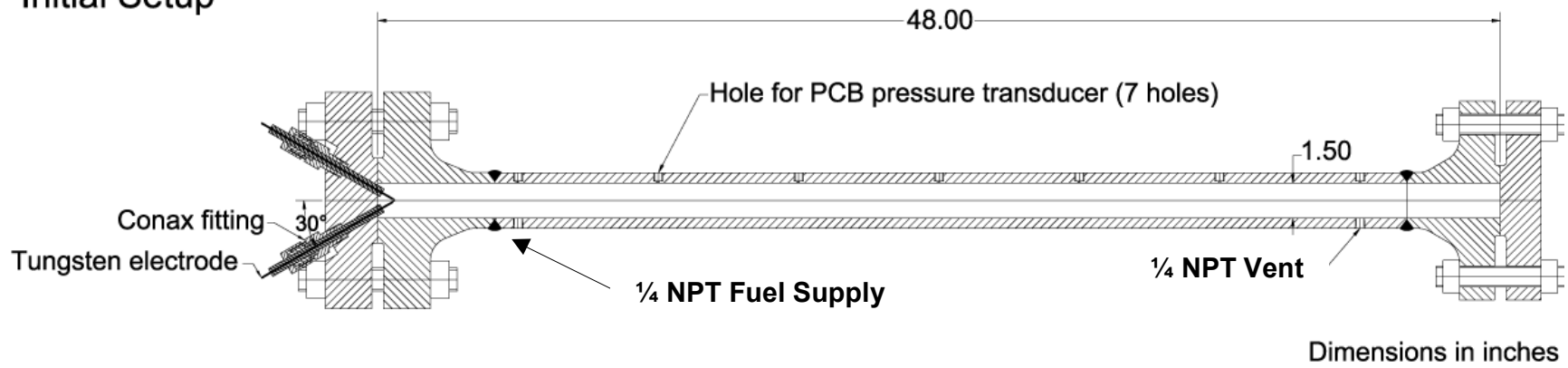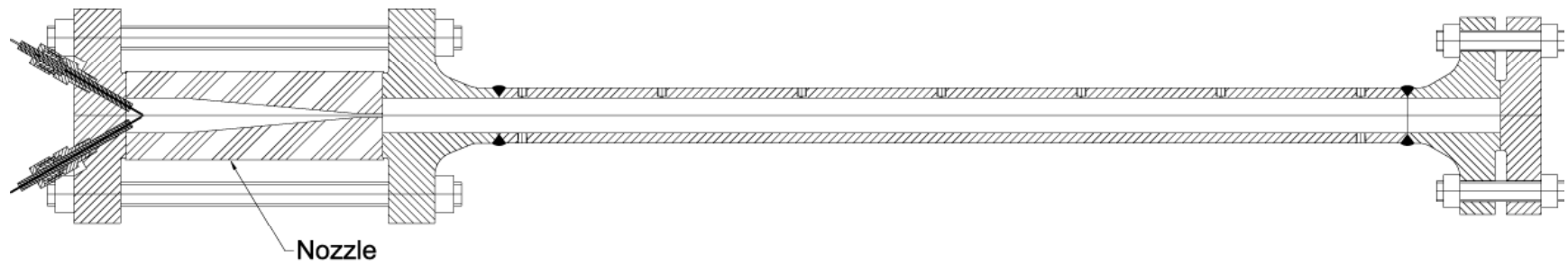
Figure 4. Detonation tube in initial and actuator configurations.
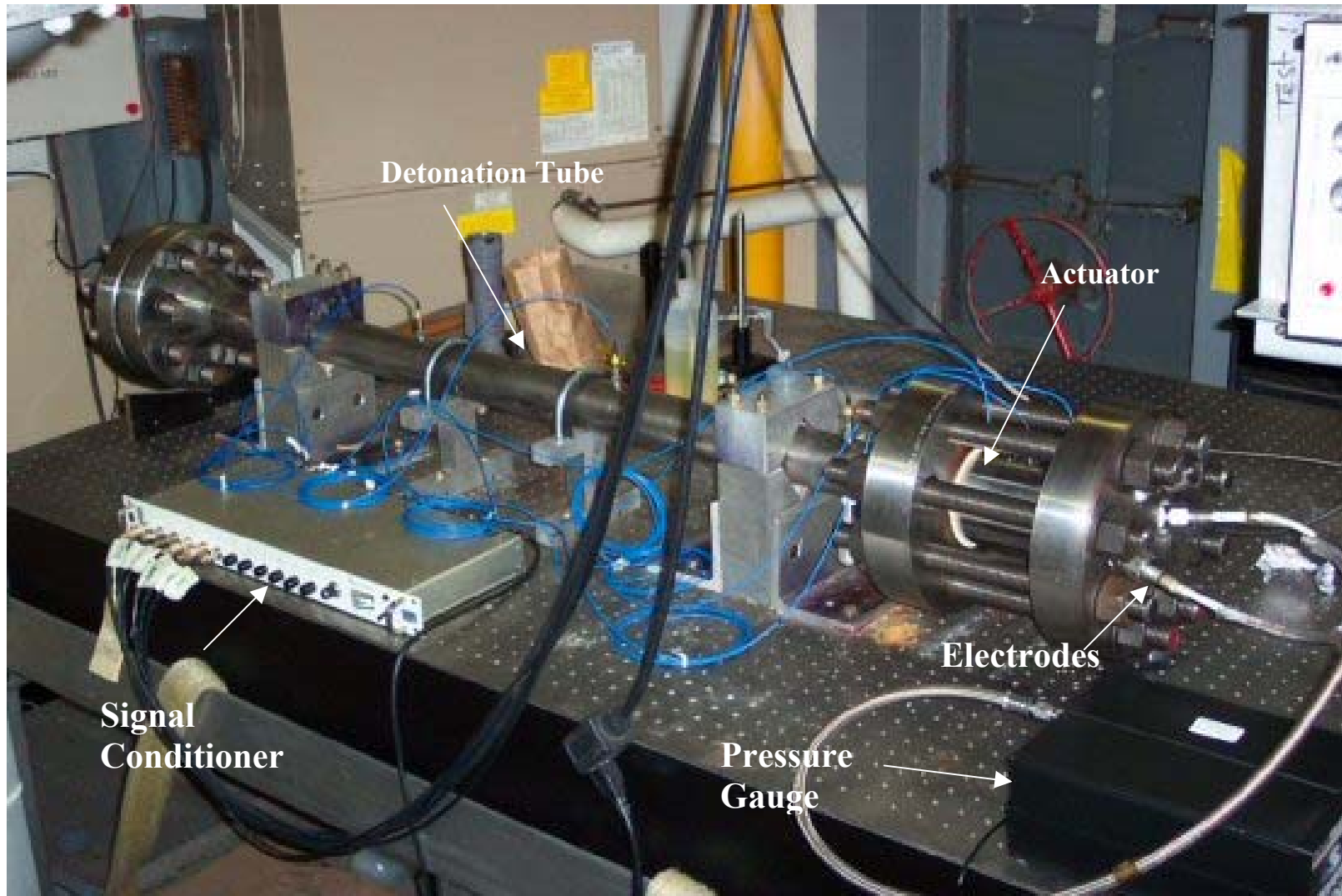
Figure 5. Detonation tube with an actuator installed.
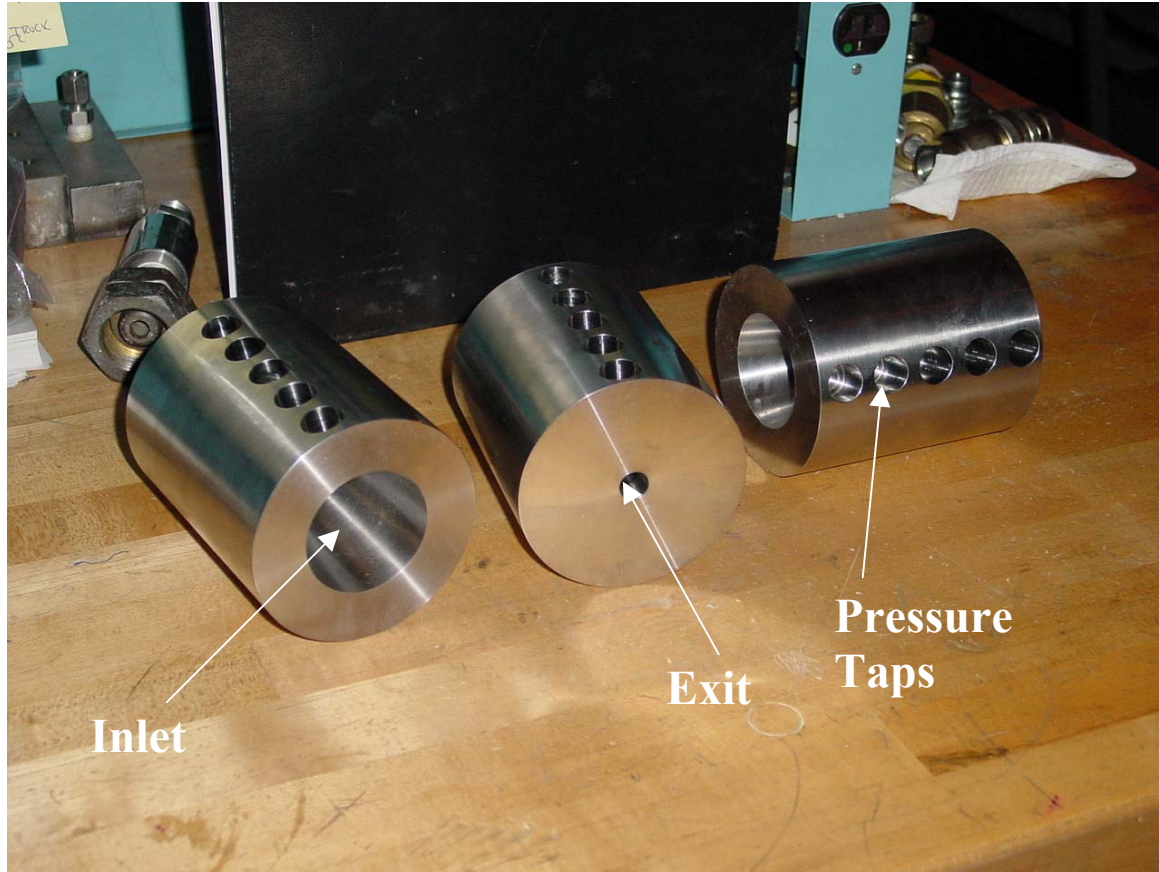
Figure 6. Detonation actuators.
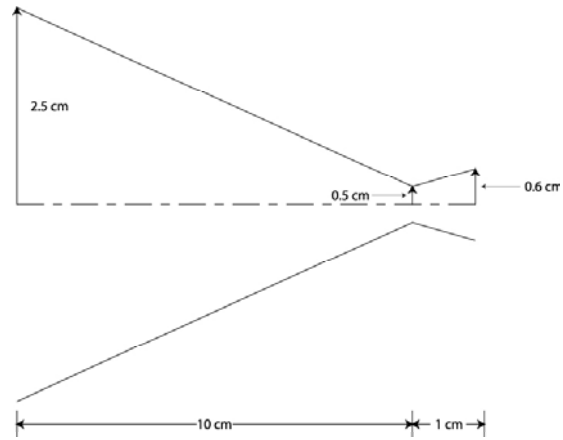
(a) Detonation Actuator A
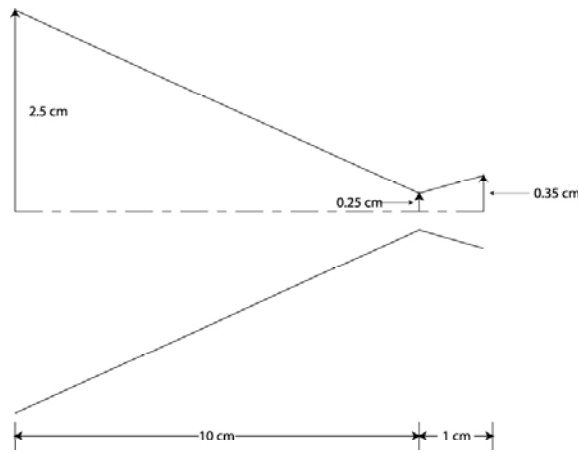
(b) Detonation Actuator B

Figure 7. Simplified schematics of detonation actuators.

2.5 cm

0.25 cm

0.35 cm

10 cm

1 cm

1 cm
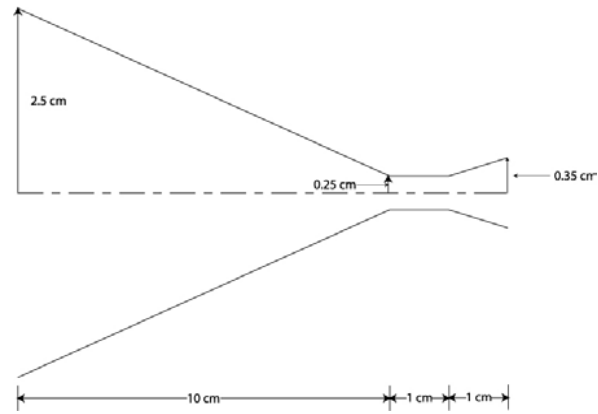
(c) Detonation Actuator C

Figure 7. Simplified schematics of detonation actuators, cont.
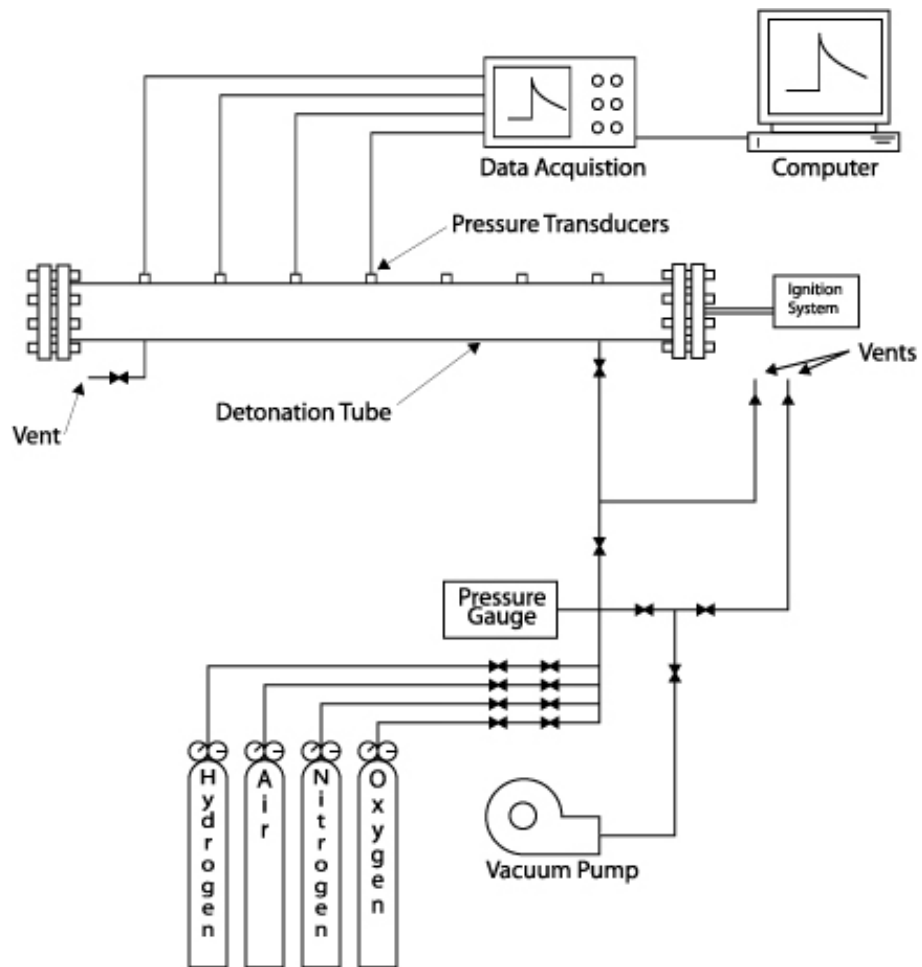
Figure 8. Simplified schematic of the detonation tube facility setup.
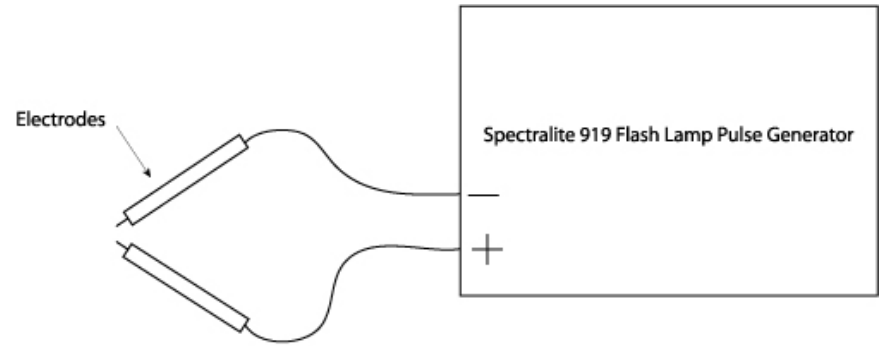
(a)
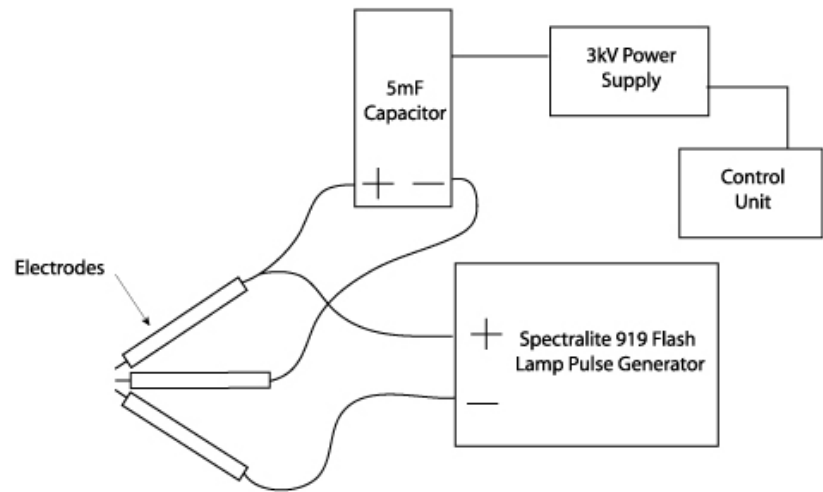
(b)

Figure 9. Simplified schematic of the initial and high-energy ignition systems.
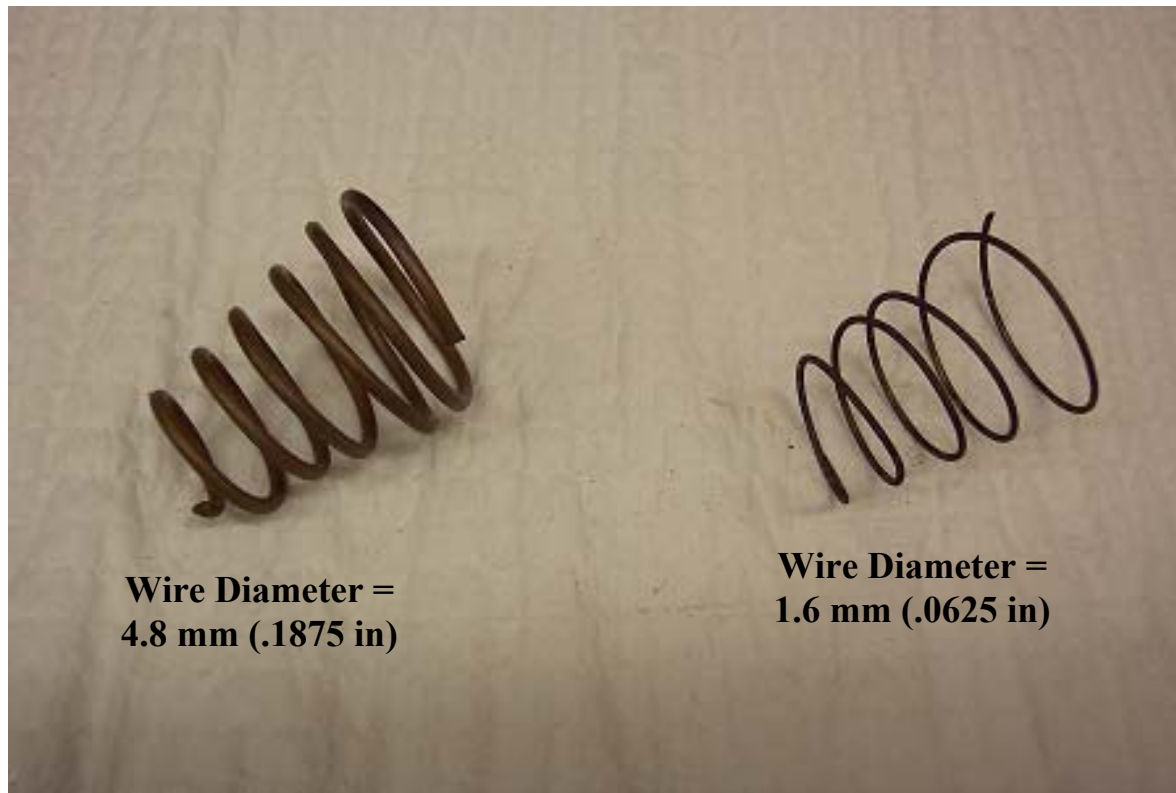
Figure 10(a). Shchelkin spirals used in the actuators.

Figure 10(b). Shchelkin spirals used in the constant area tube.

Figure 11. Shchelkin spiral installed in a detonation actuator.
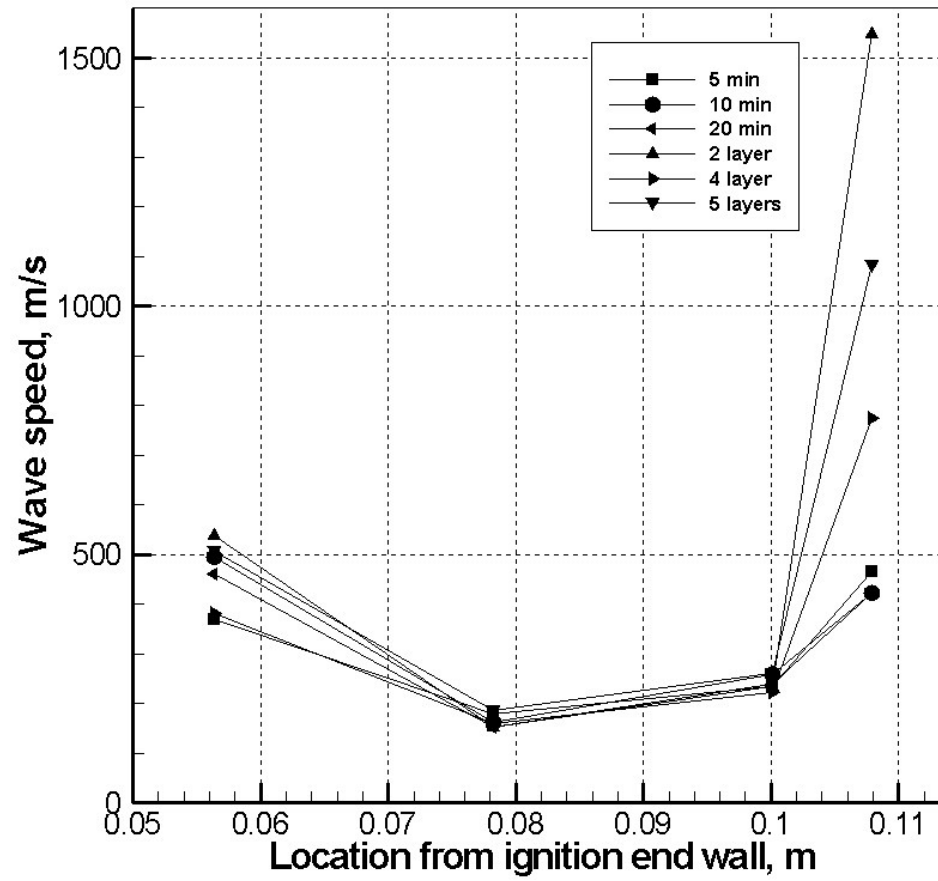
Figure 12. Wave speeds for various mixing techniques.
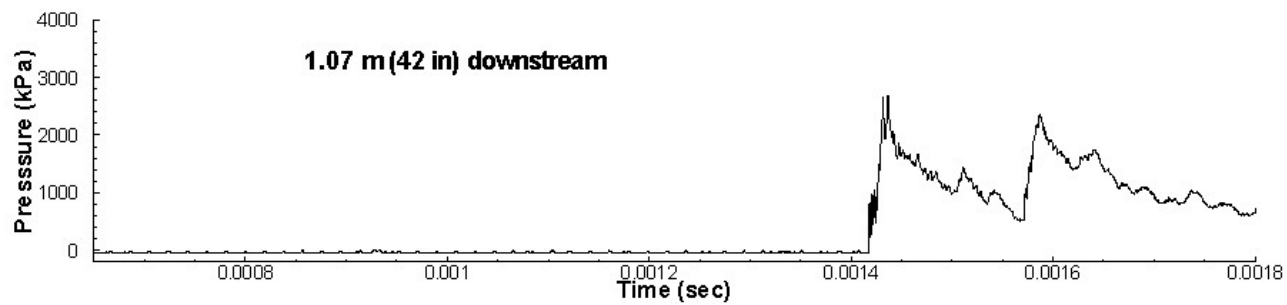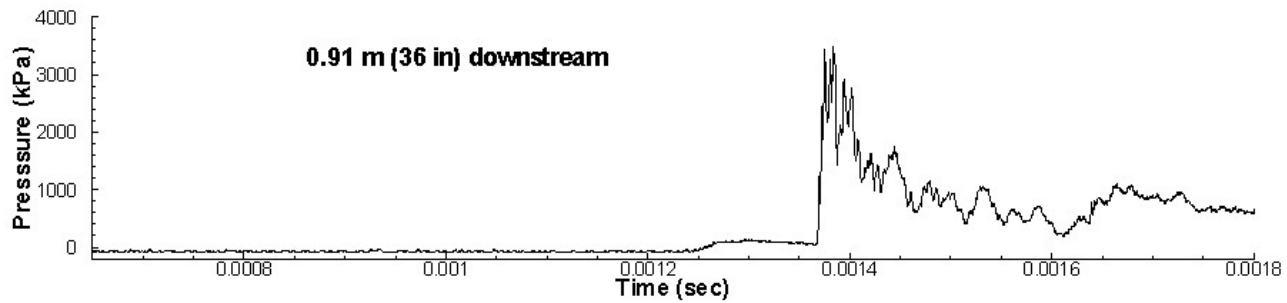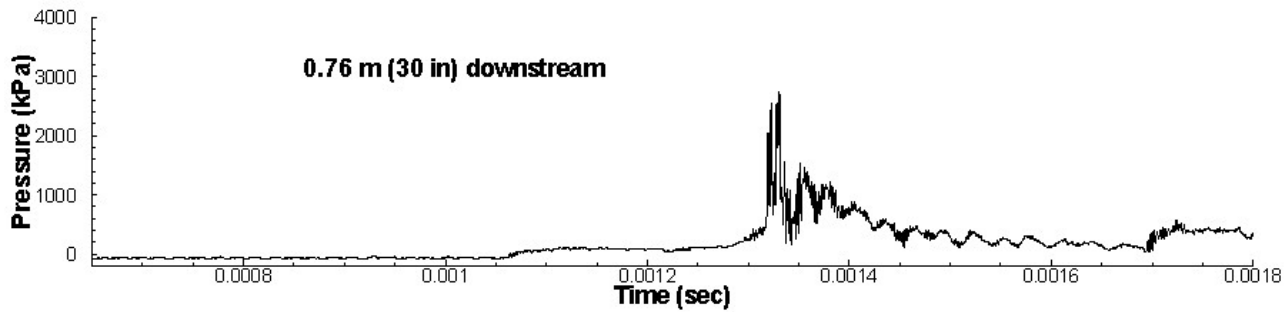
Figure 13. Pressure histories in the tube for a 103 kPa (15 psia) fill pressure
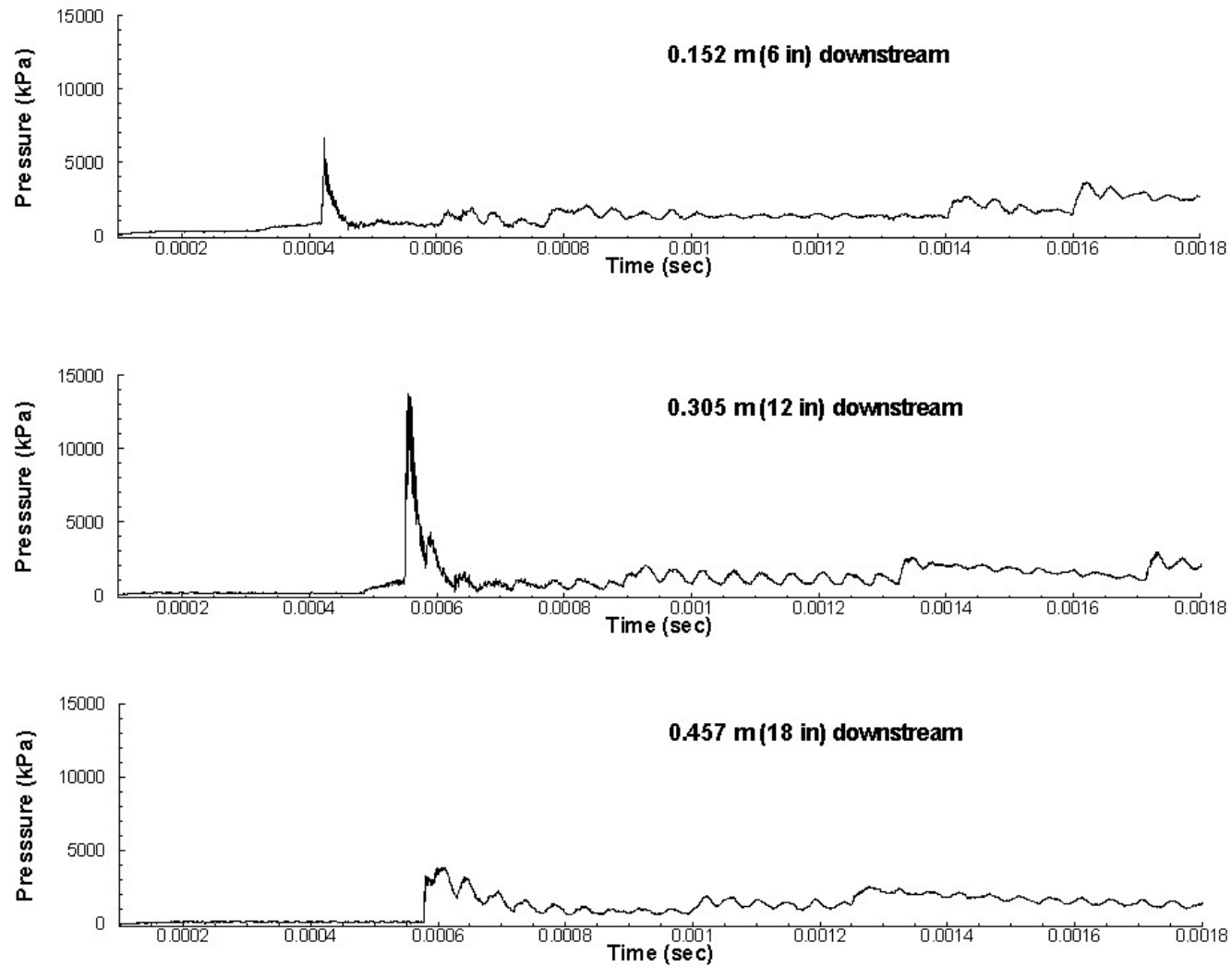
Figure 14. Pressure histories in the tube for a 207 kPa (30 psia) fill pressure.
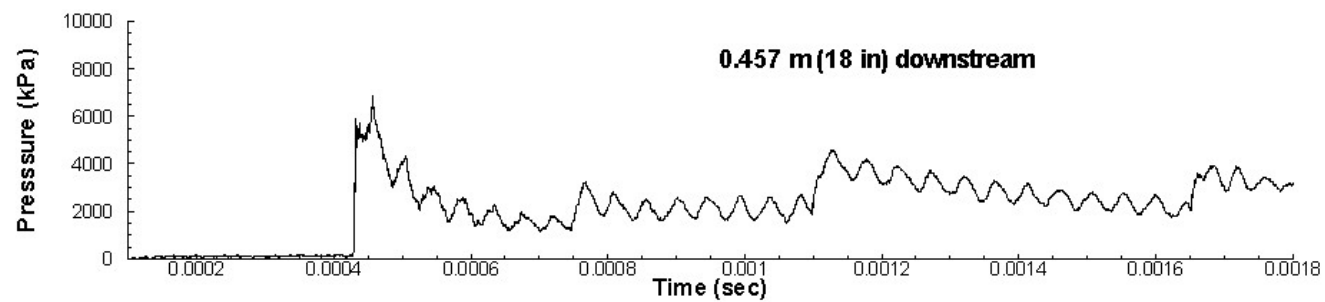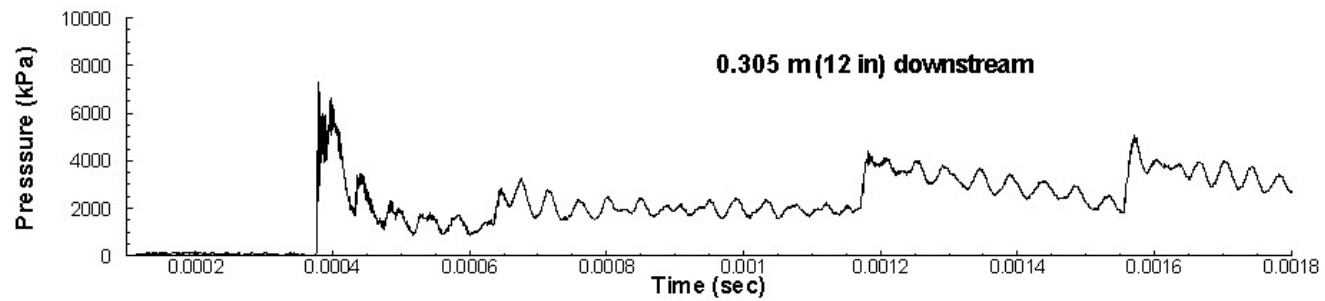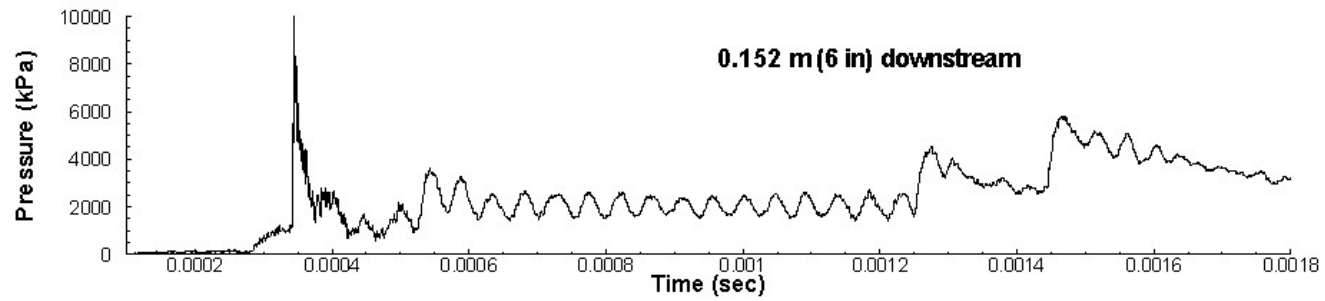
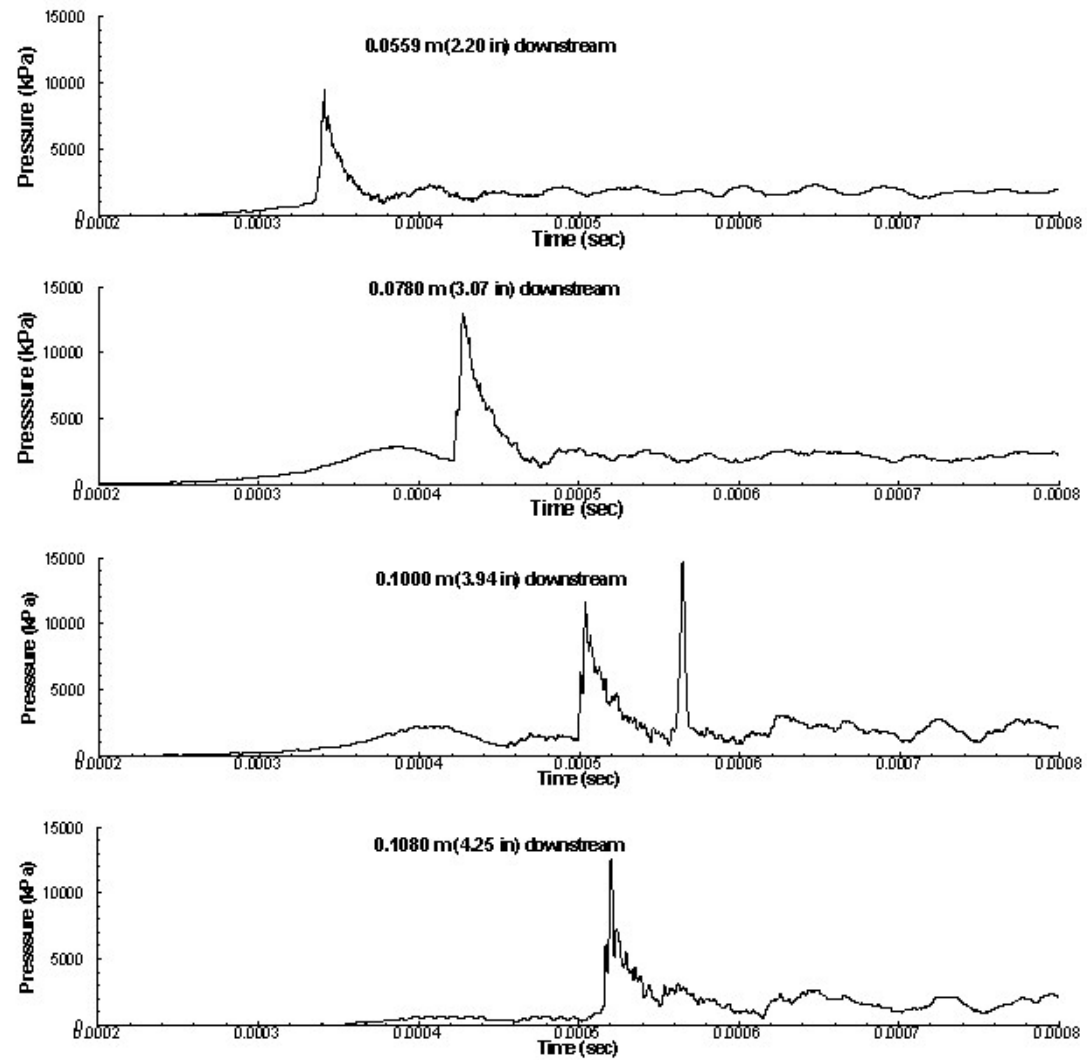Figure 15. Pressure histories in the tube for a 345 kPa (50 psia) fill pressure.
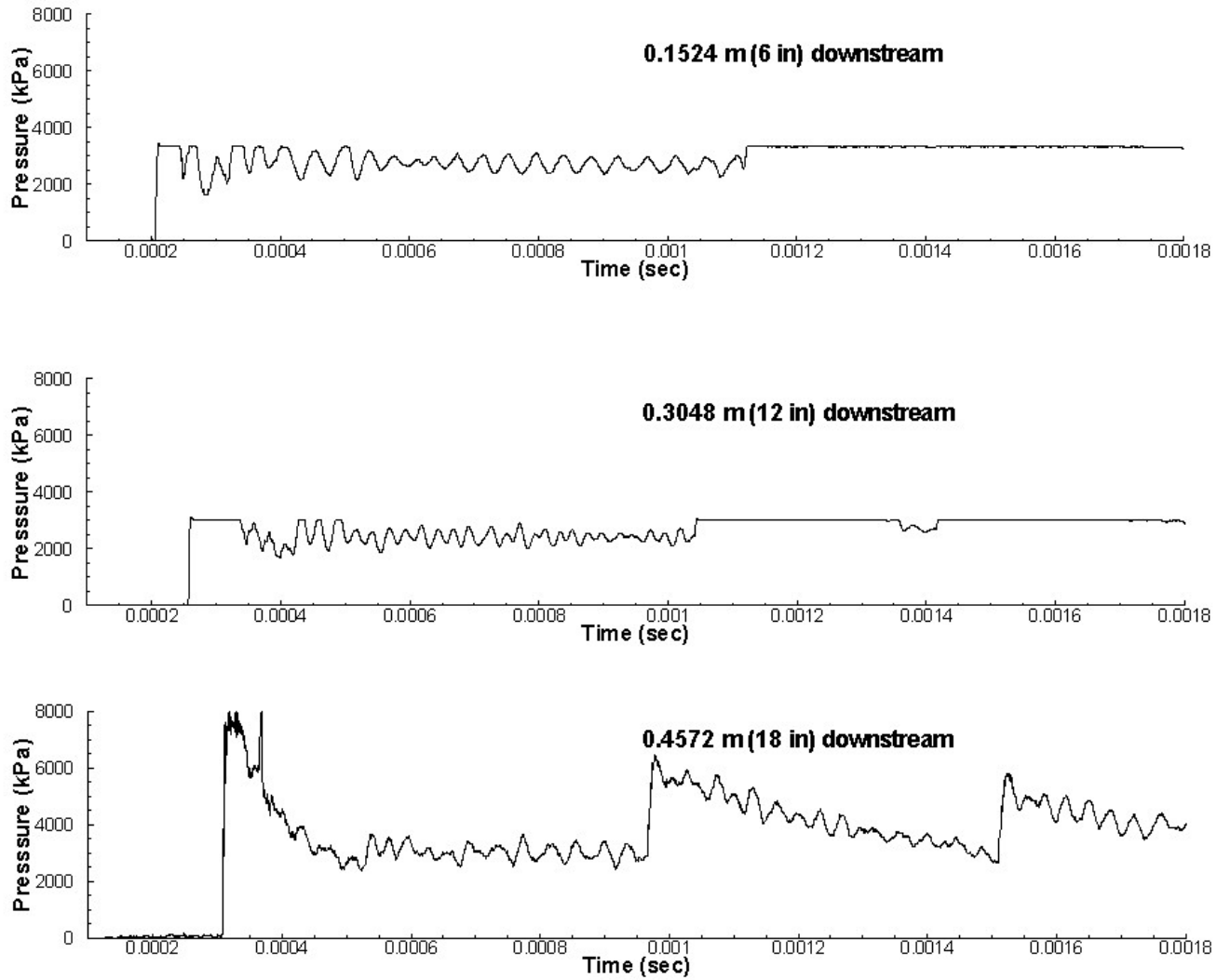
Figure 16. Pressure histories in the tube for a 483 kPa (70 psia) fill pressure.
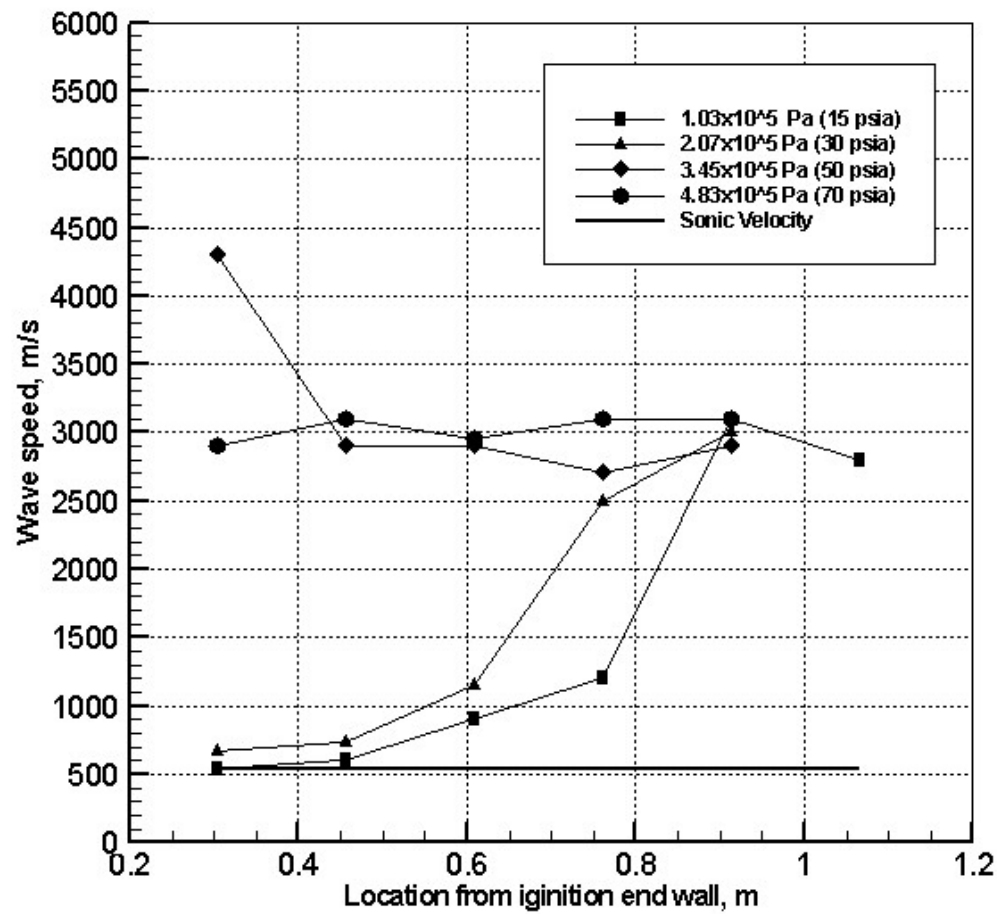
Figure 17. Wave speeds in the tube for various fill pressures.
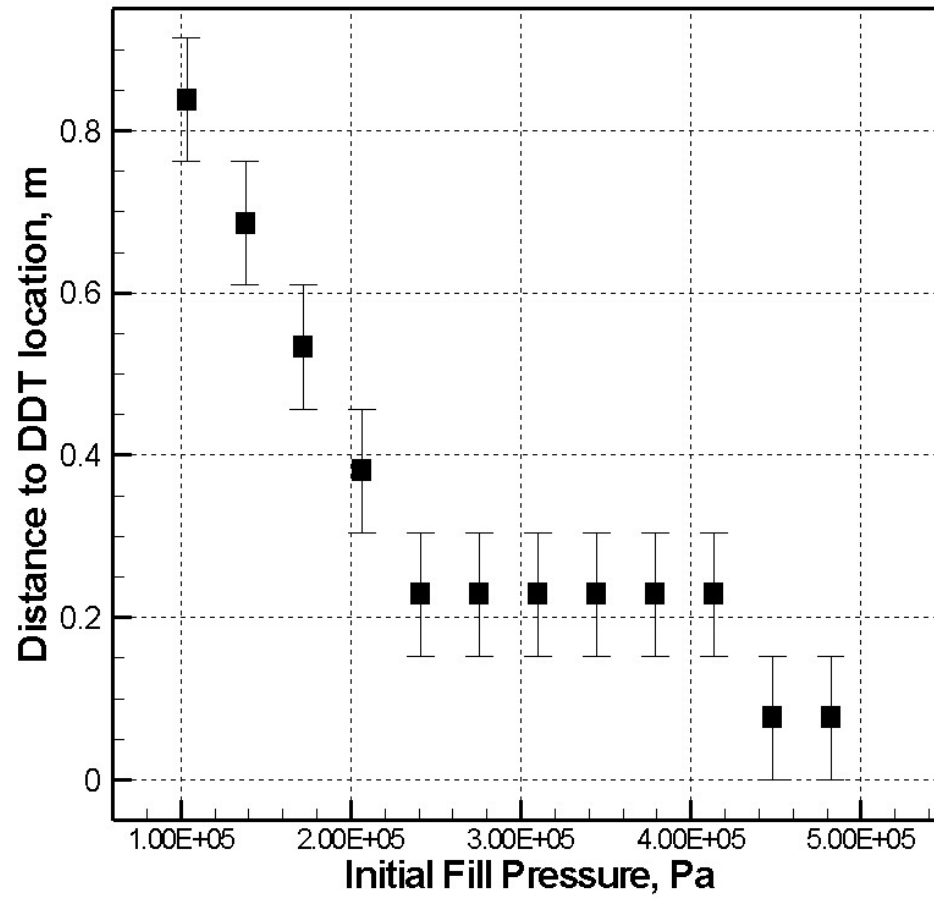
Figure 18. Distance required for DDT versus fill pressure.
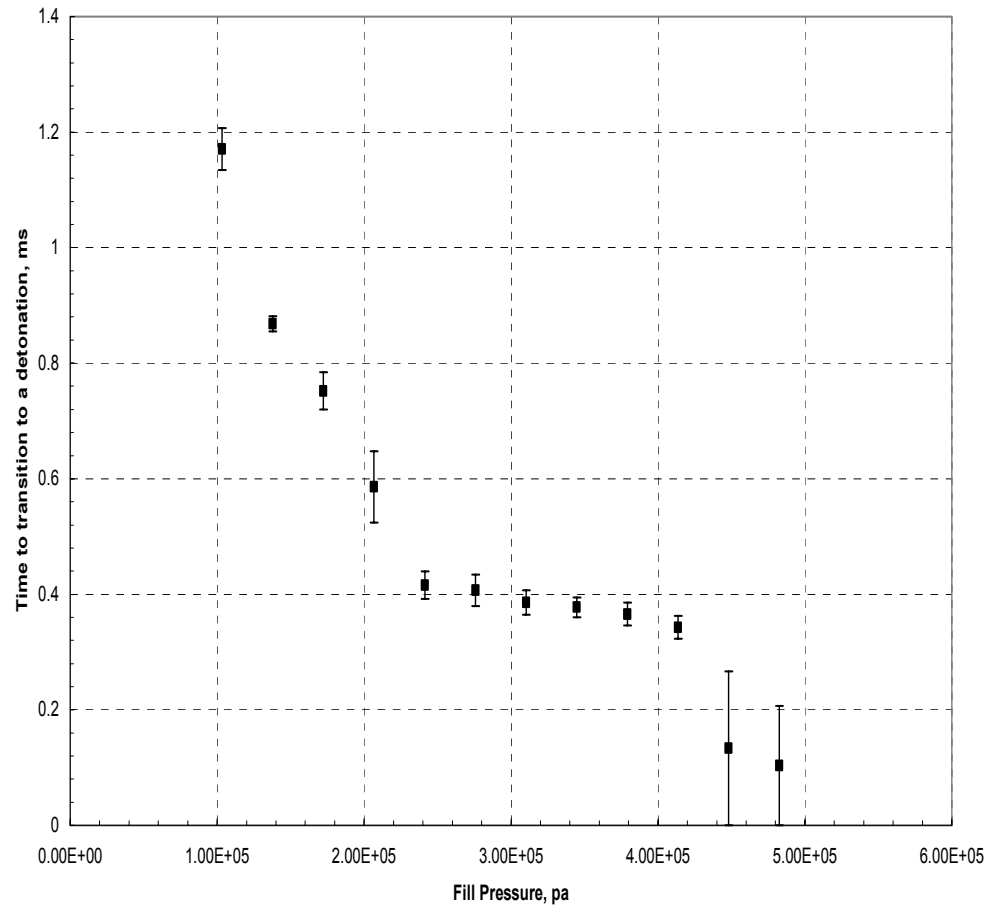
Figure 19. Time required for DDT versus fill pressure.
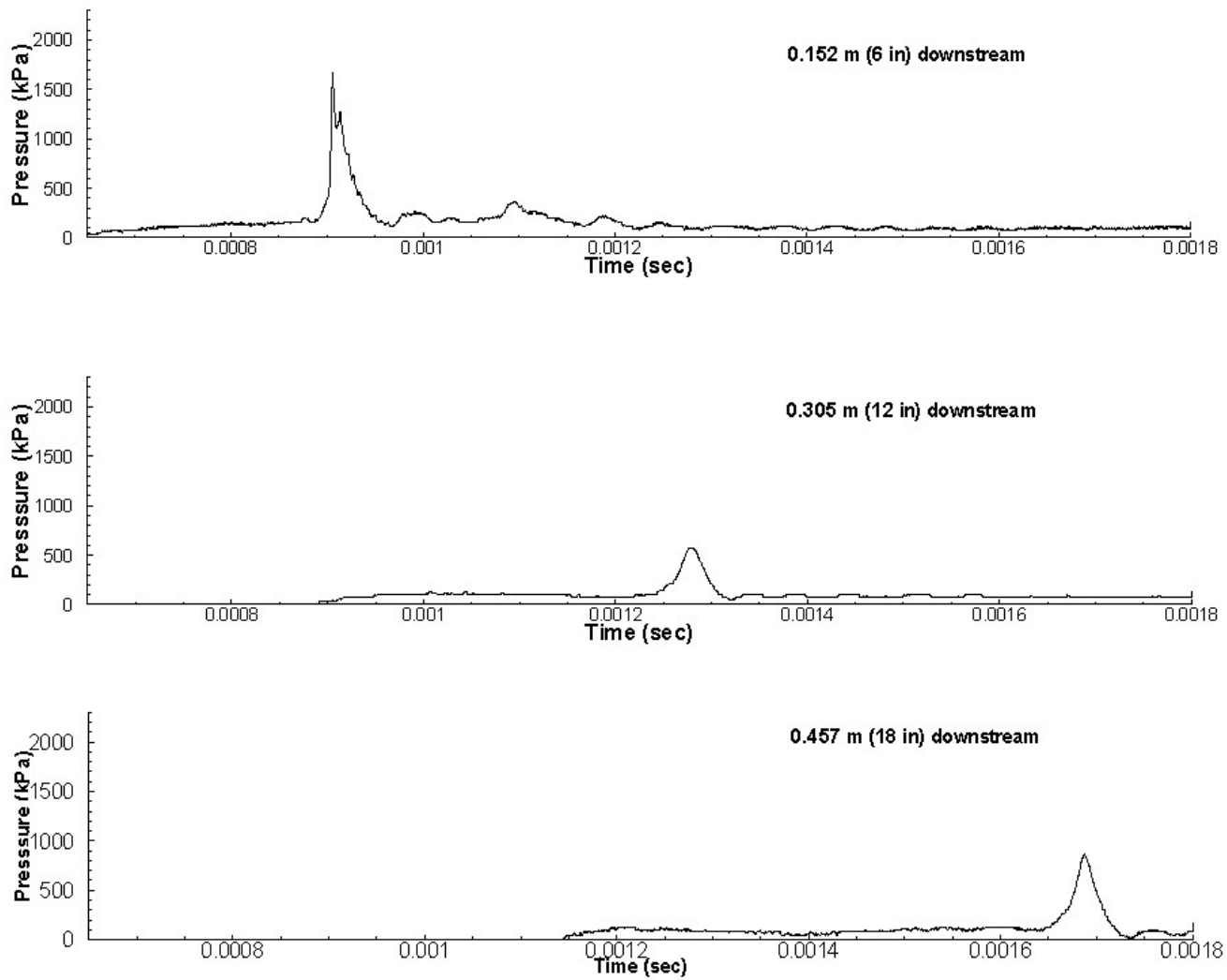
Figure 20. Pressure histories in the tube with an equivalence ratio of 0.3.
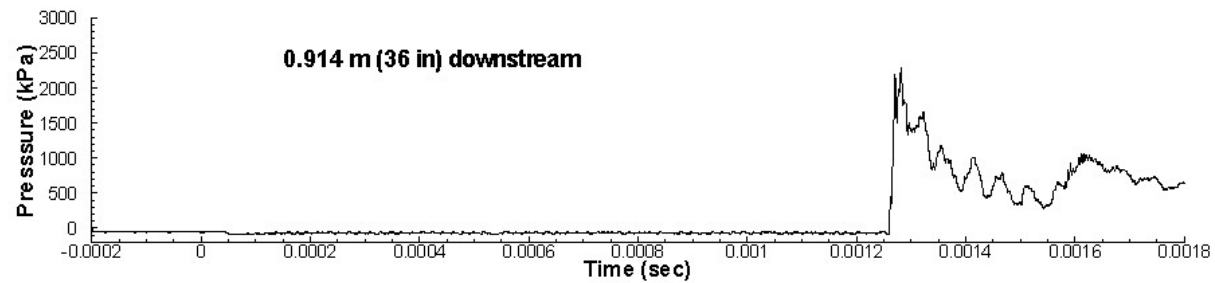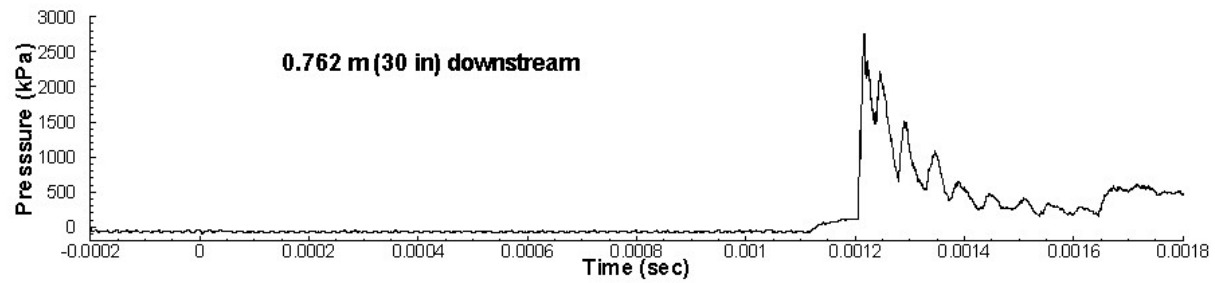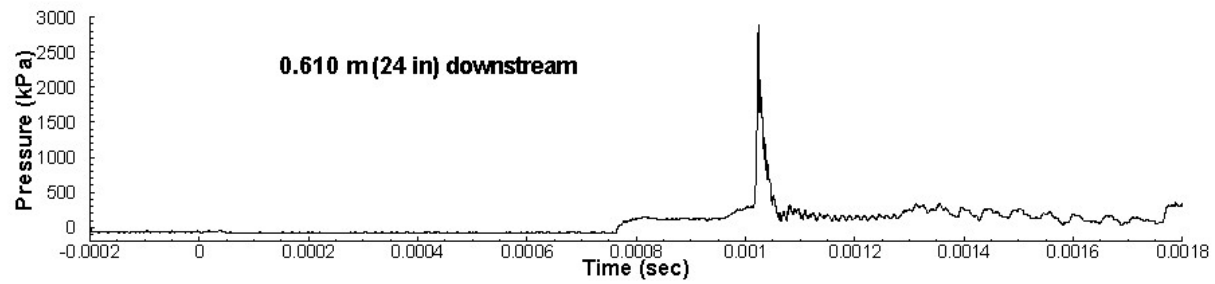
Figure 21. Pressure histories in the tube with an equivalence ratio of 0.5.
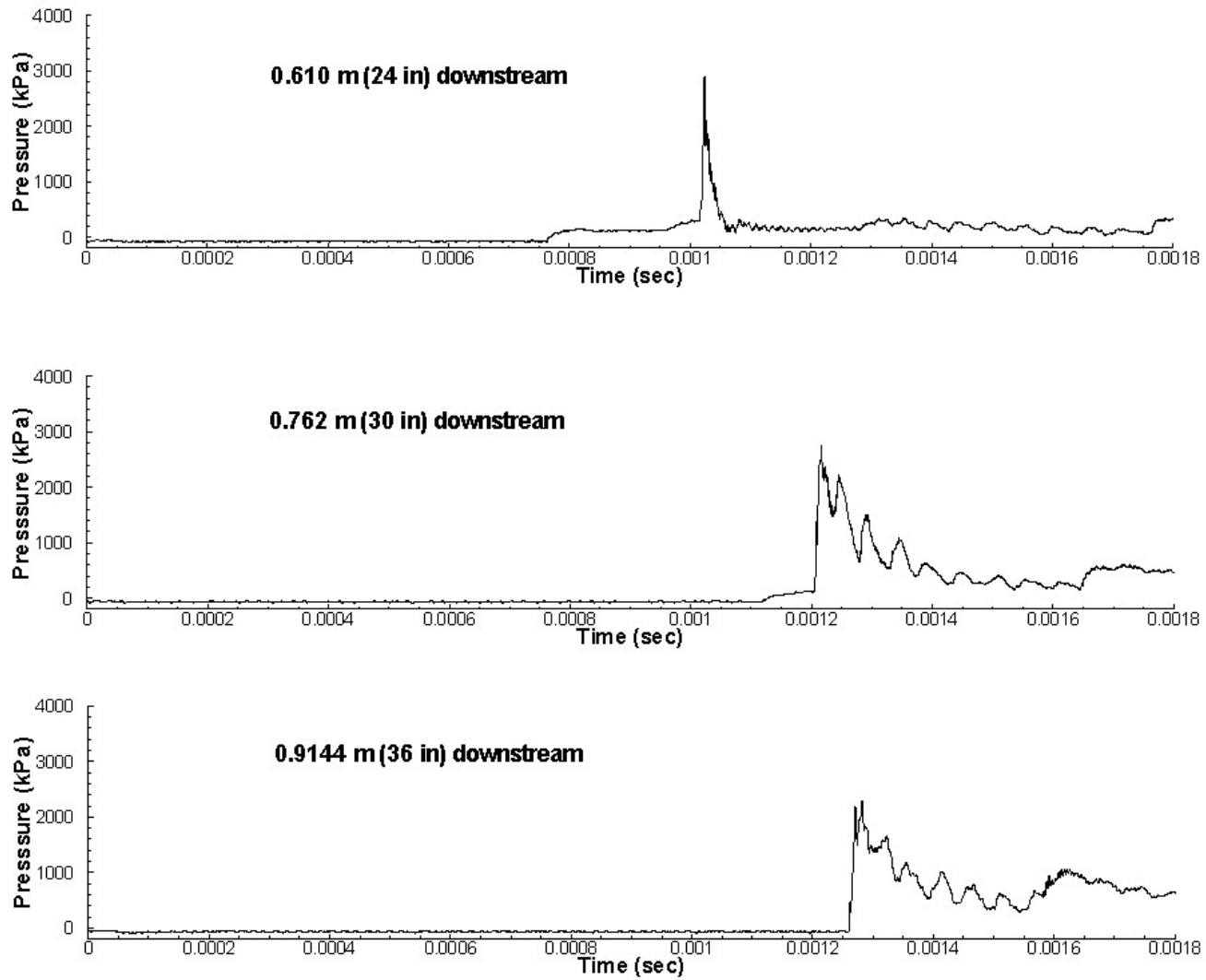
Figure 22. Pressure histories in the tube with an equivalence ratio of 0.7.
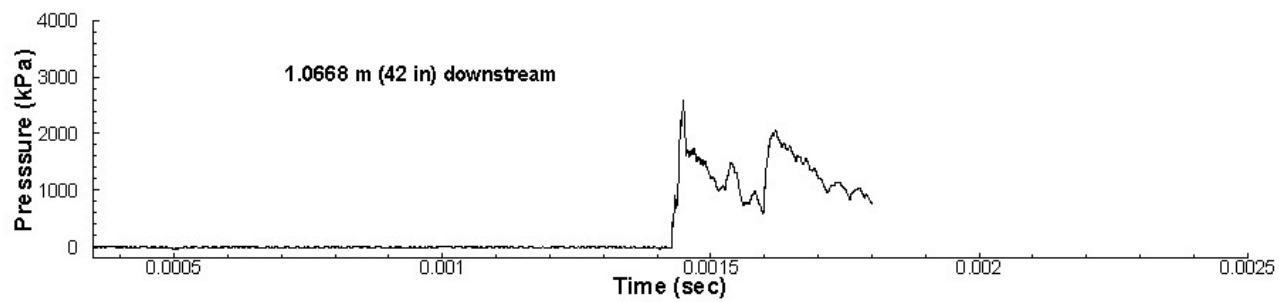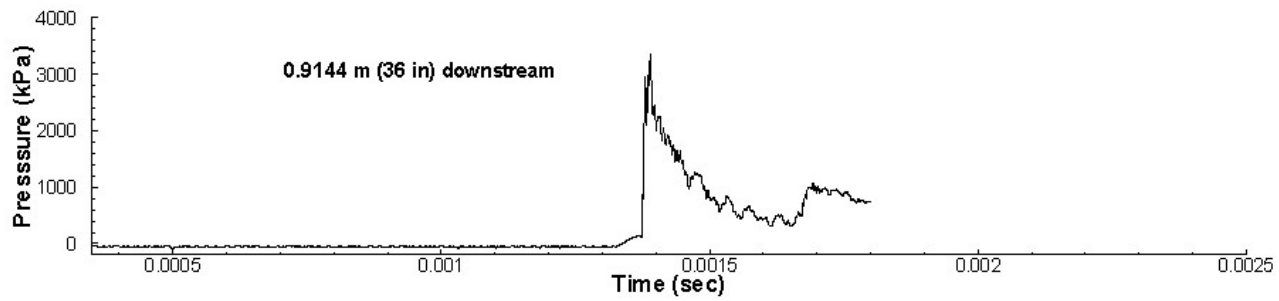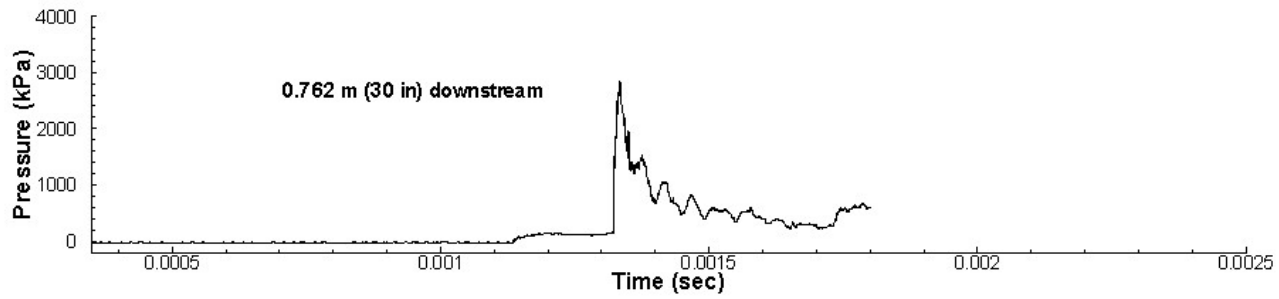
Figure 23. Pressure histories in the tube with an equivalence ratio of 0.9.
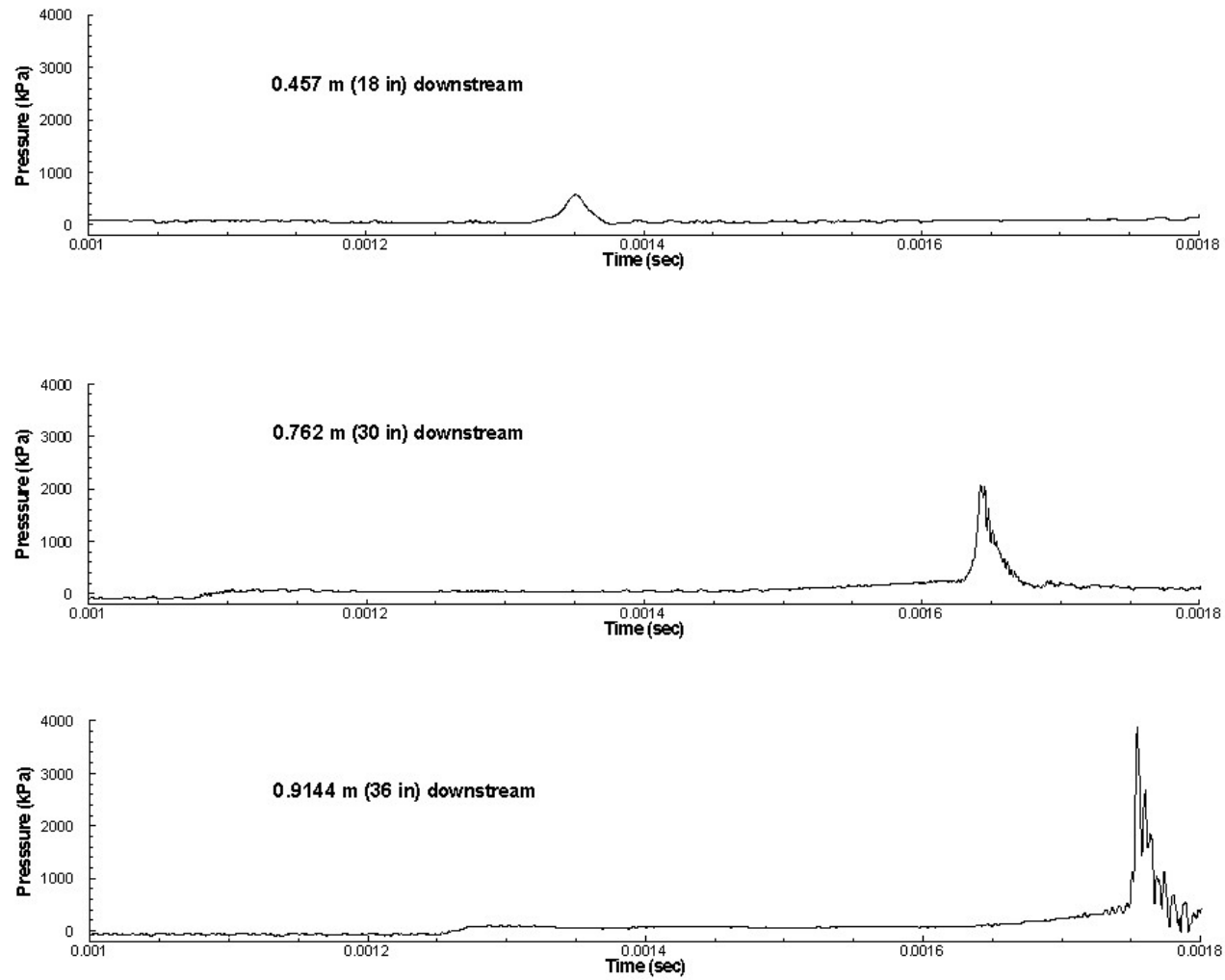
Figure 24. Pressure histories in the tube with an equivalence ratio of 1.1.
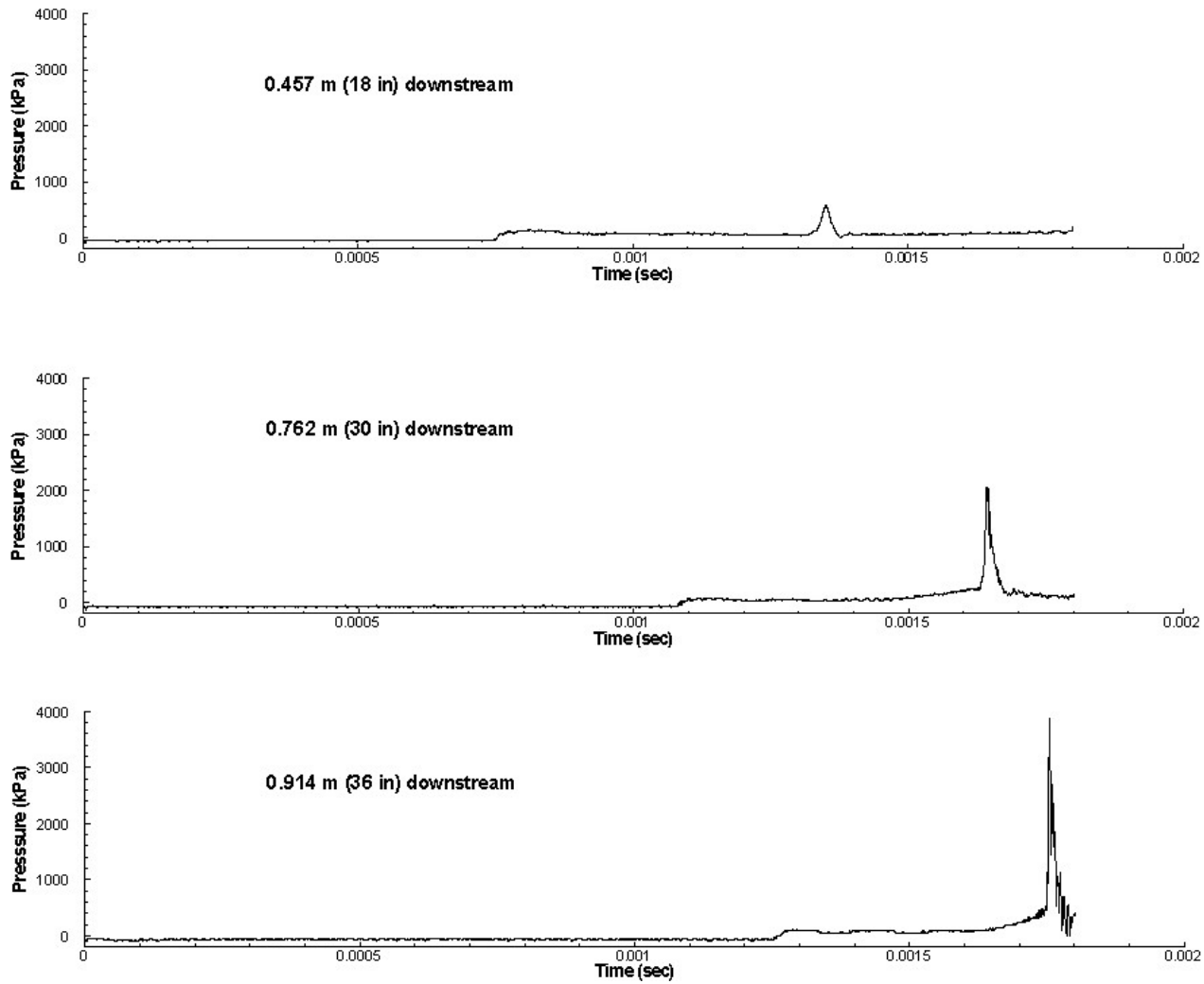
Figure 25. Pressure histories in the tube with an equivalence ratio of 1.3.
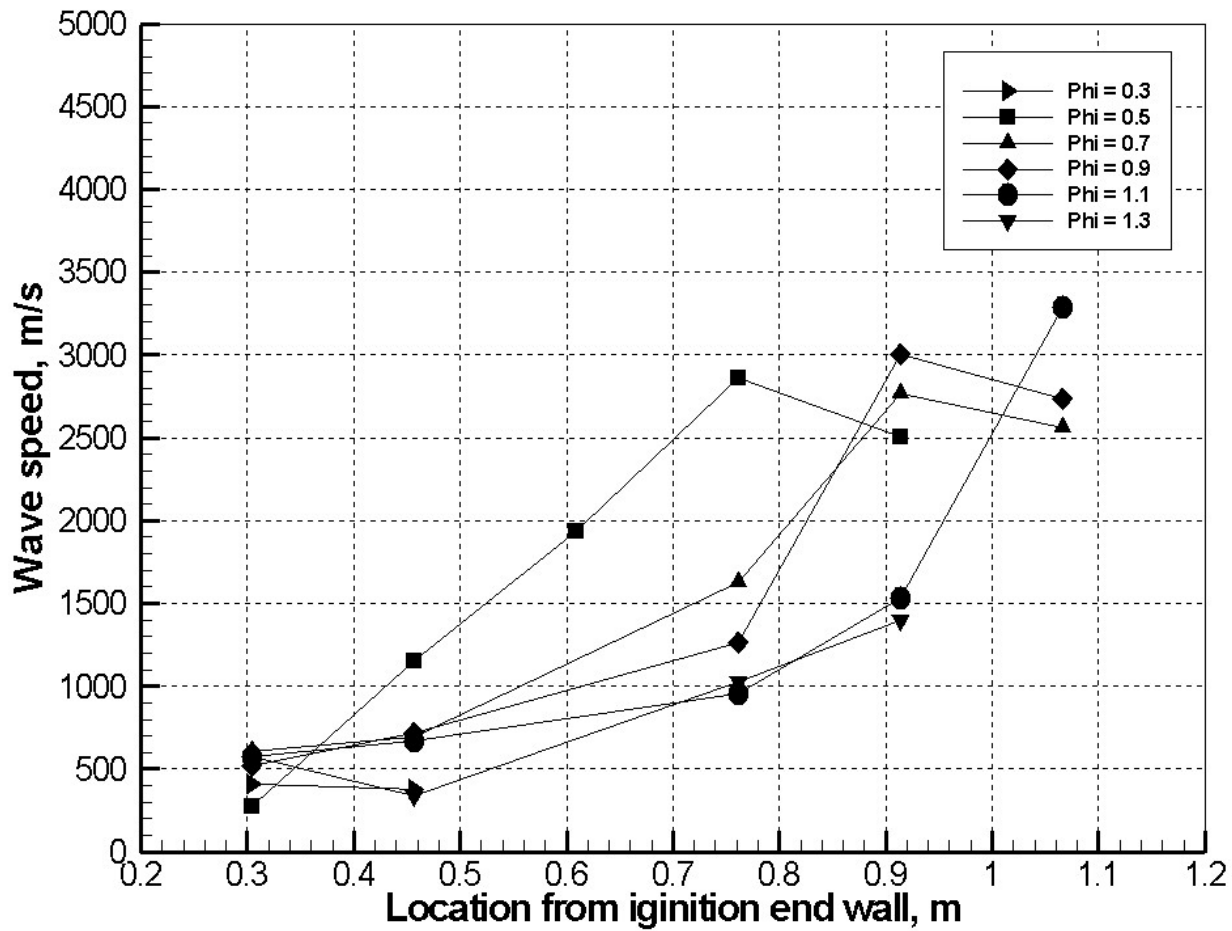
Figure 26. Wave speeds in the tube for various equivalence ratios.
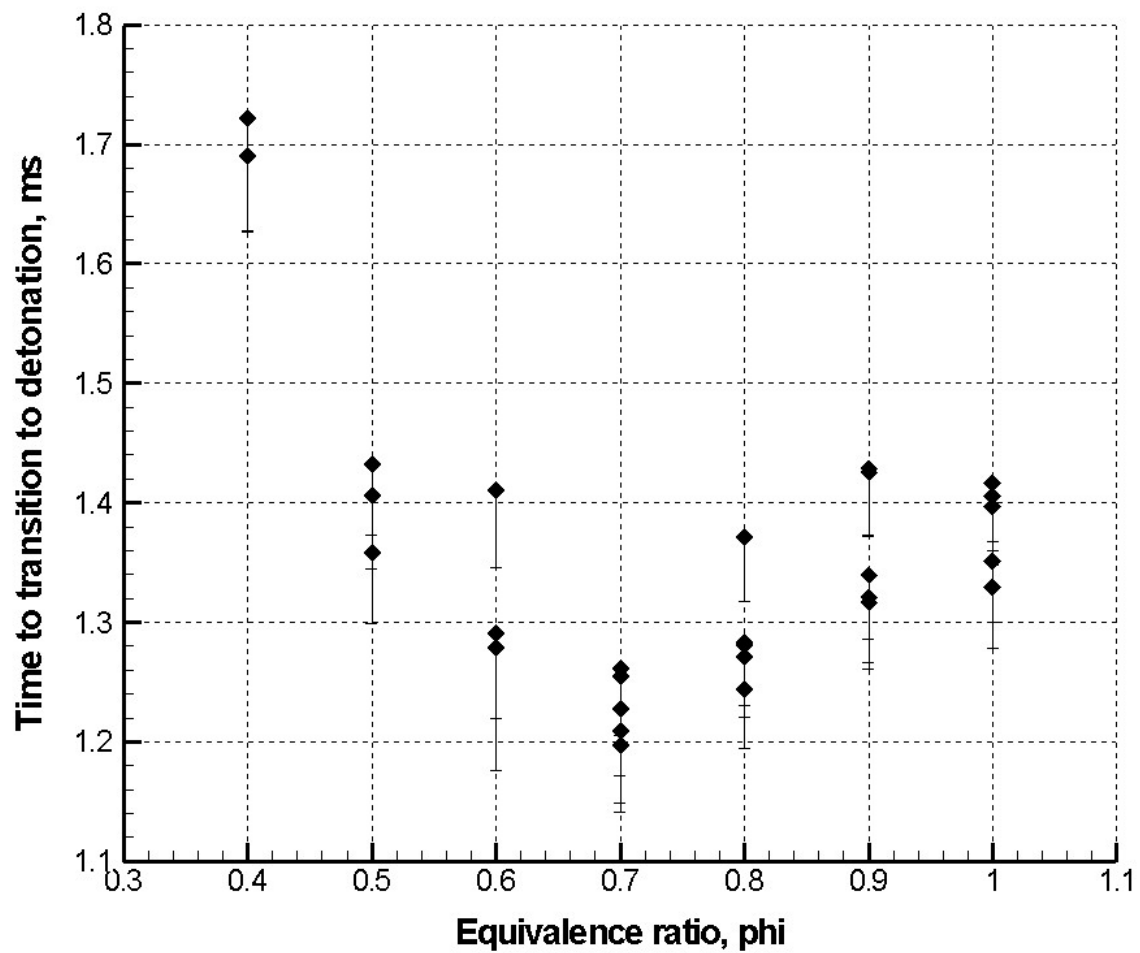
Figure 27. Time required for DDT versus equivalence ratio.
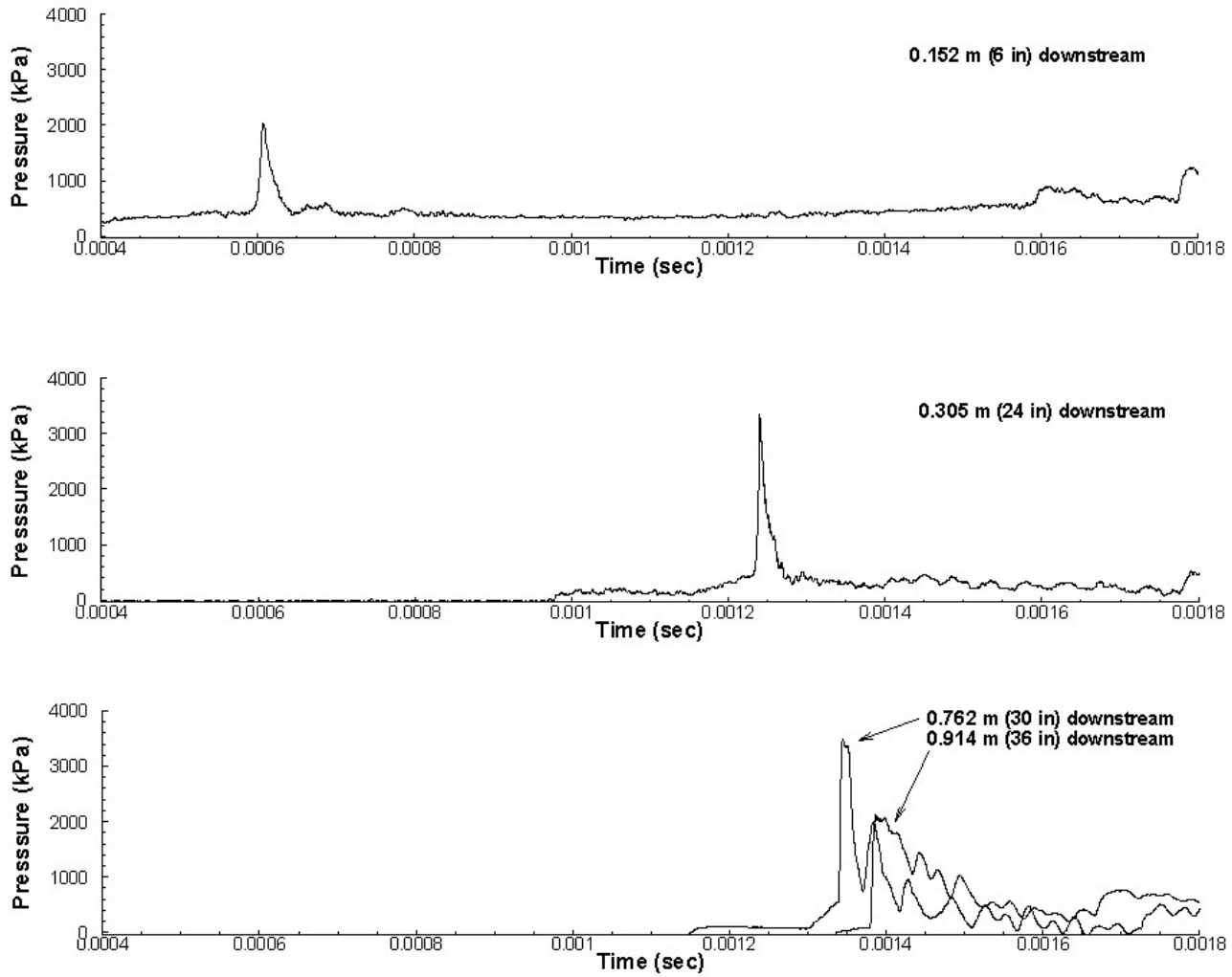
Figure 28. Pressure histories in the tube with an ignition energy of 0.025J.
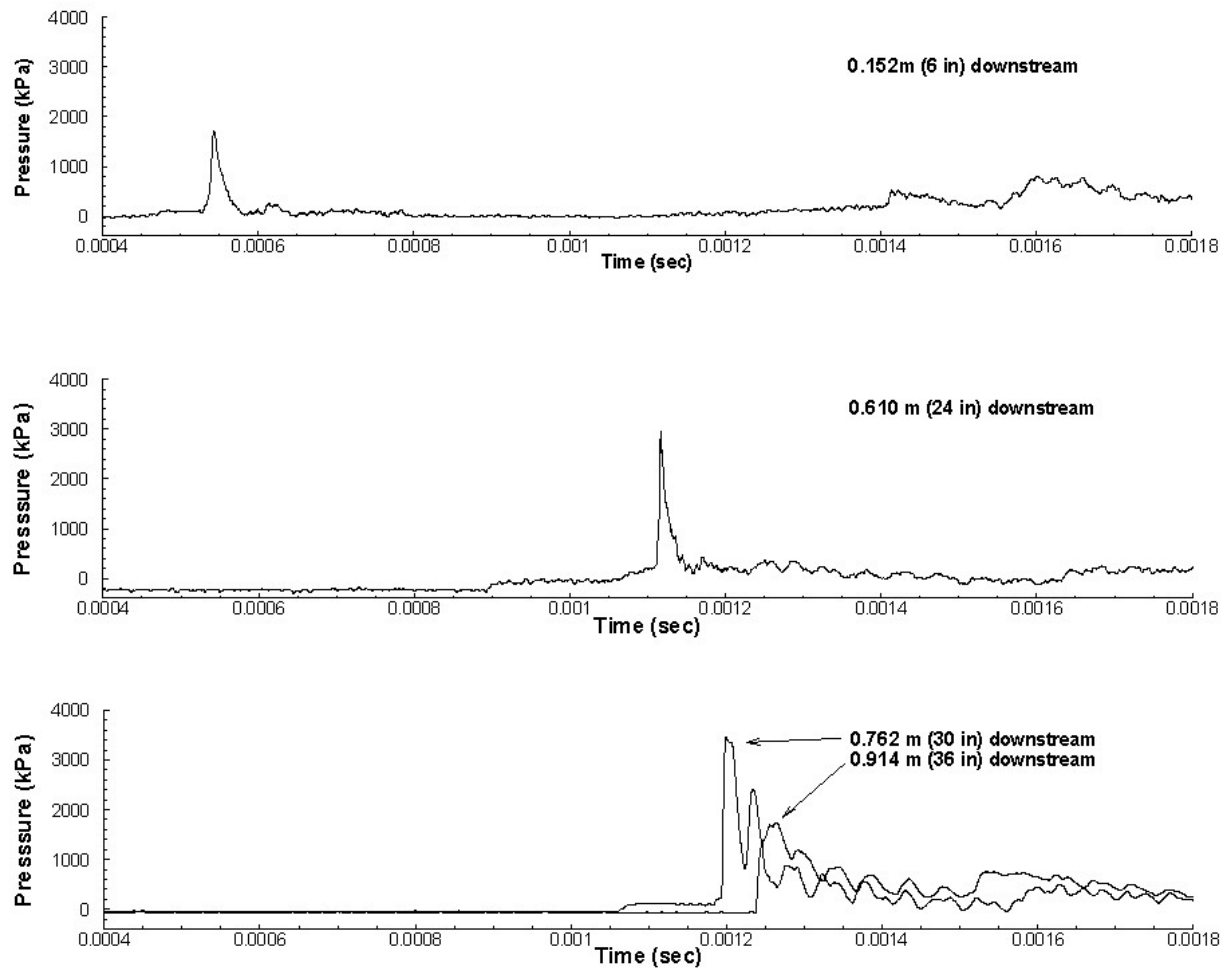
Figure 29. Pressure histories in the tube with an ignition energy of 0.25J.
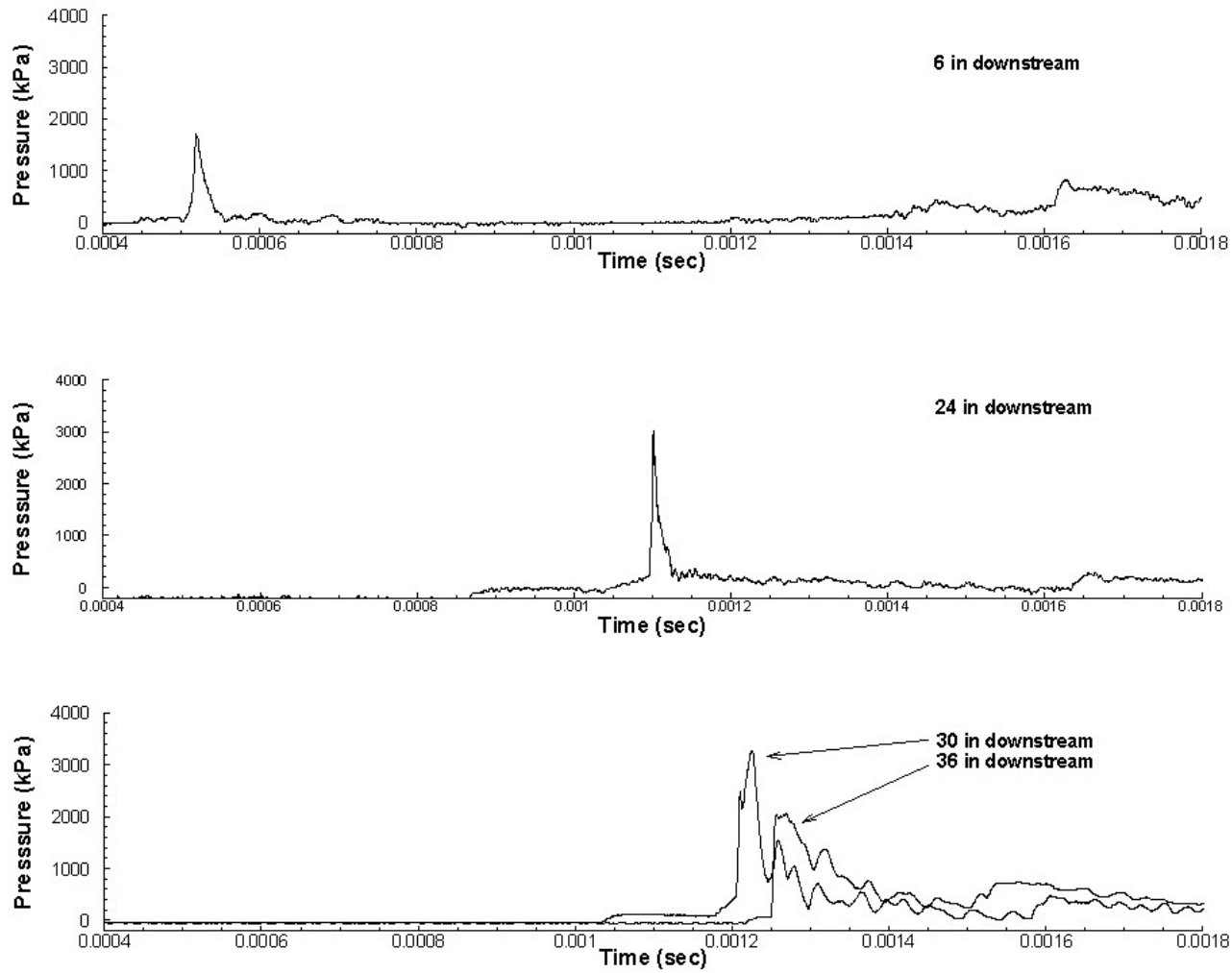
Figure 30. Pressure histories in the tube with an ignition energy of 2.5J.
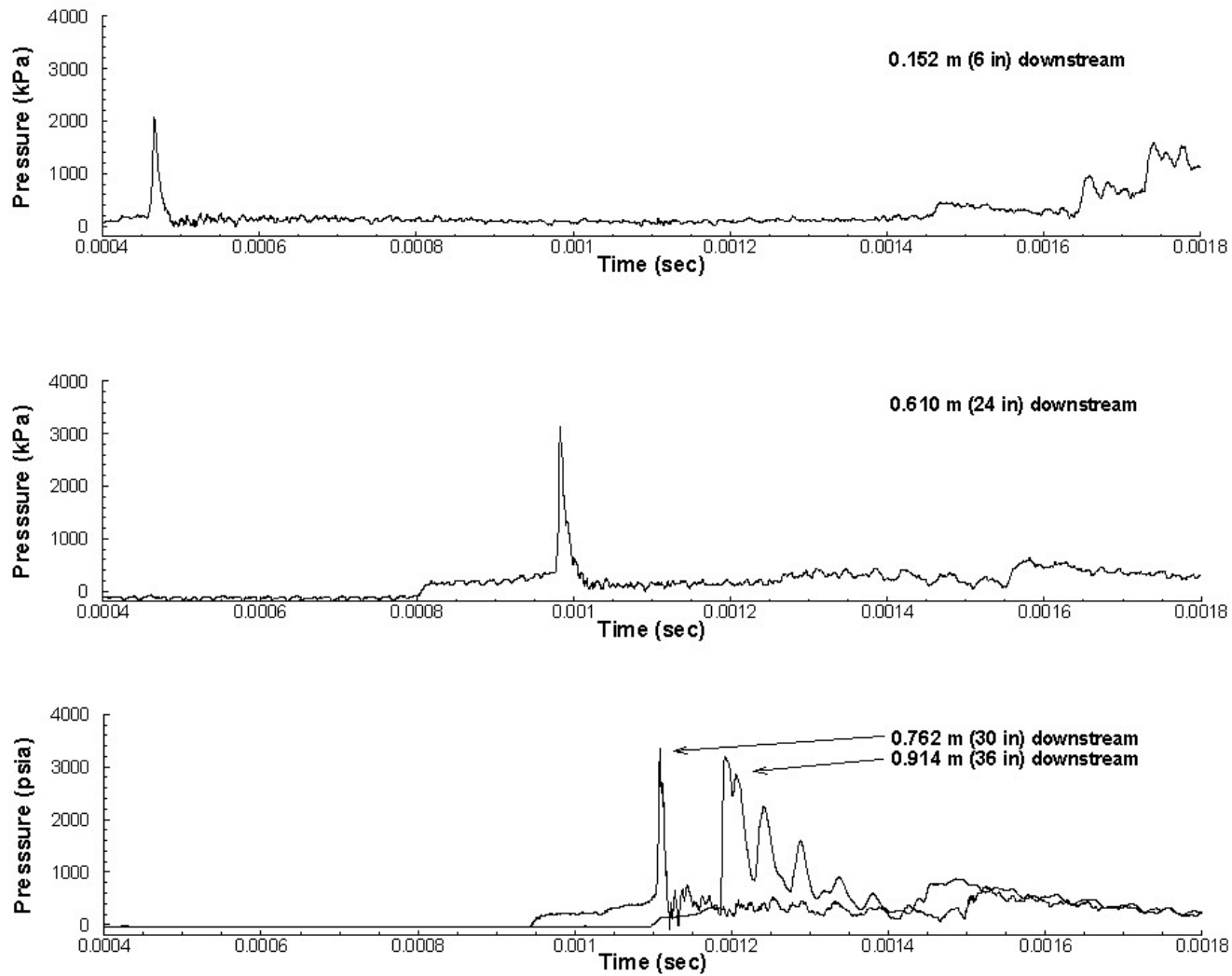
Figure 31. Pressure histories in the tube with an ignition energy of 5.0J.
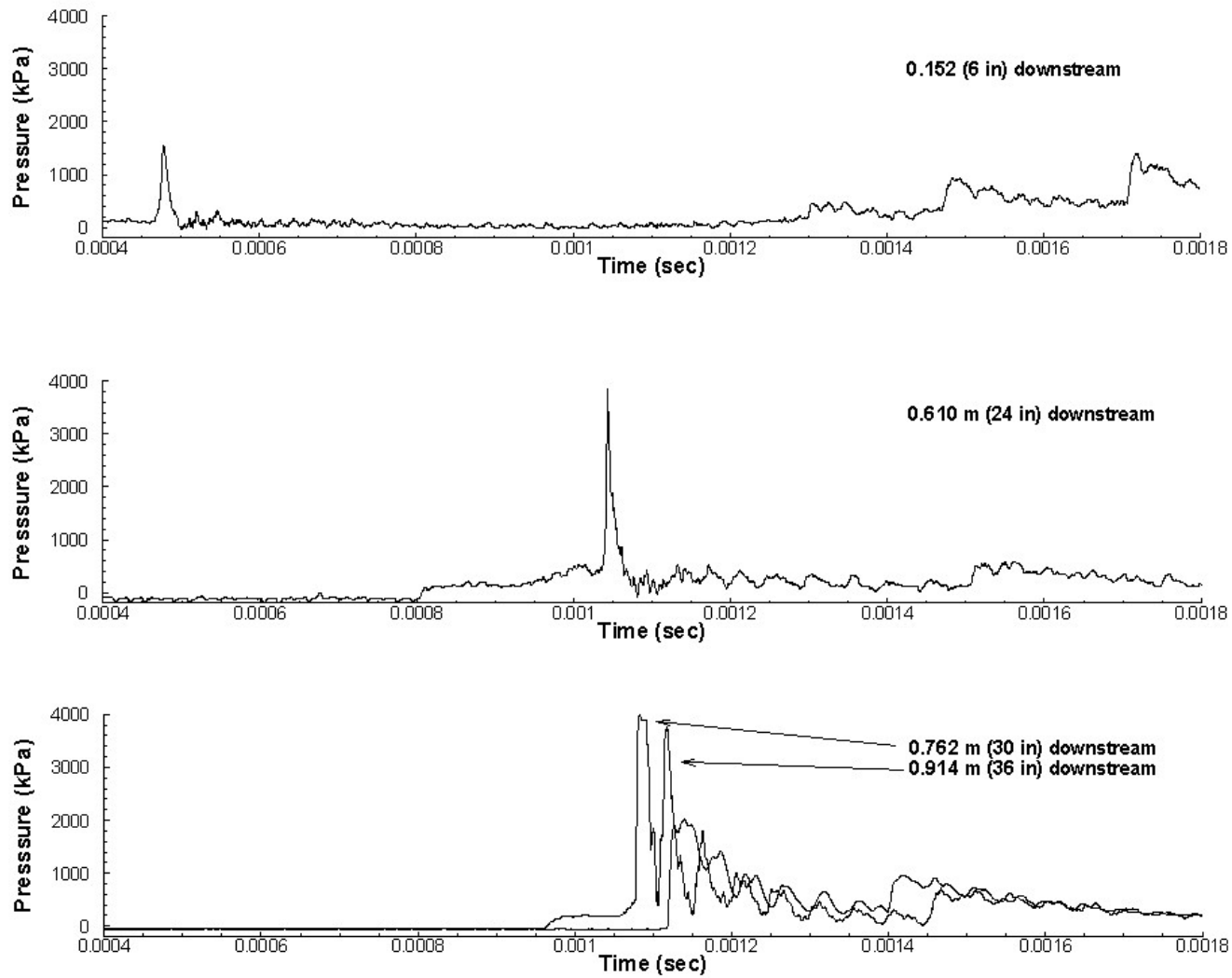
Figure 32. Pressure histories in the tube with an ignition energy of 10.0J.
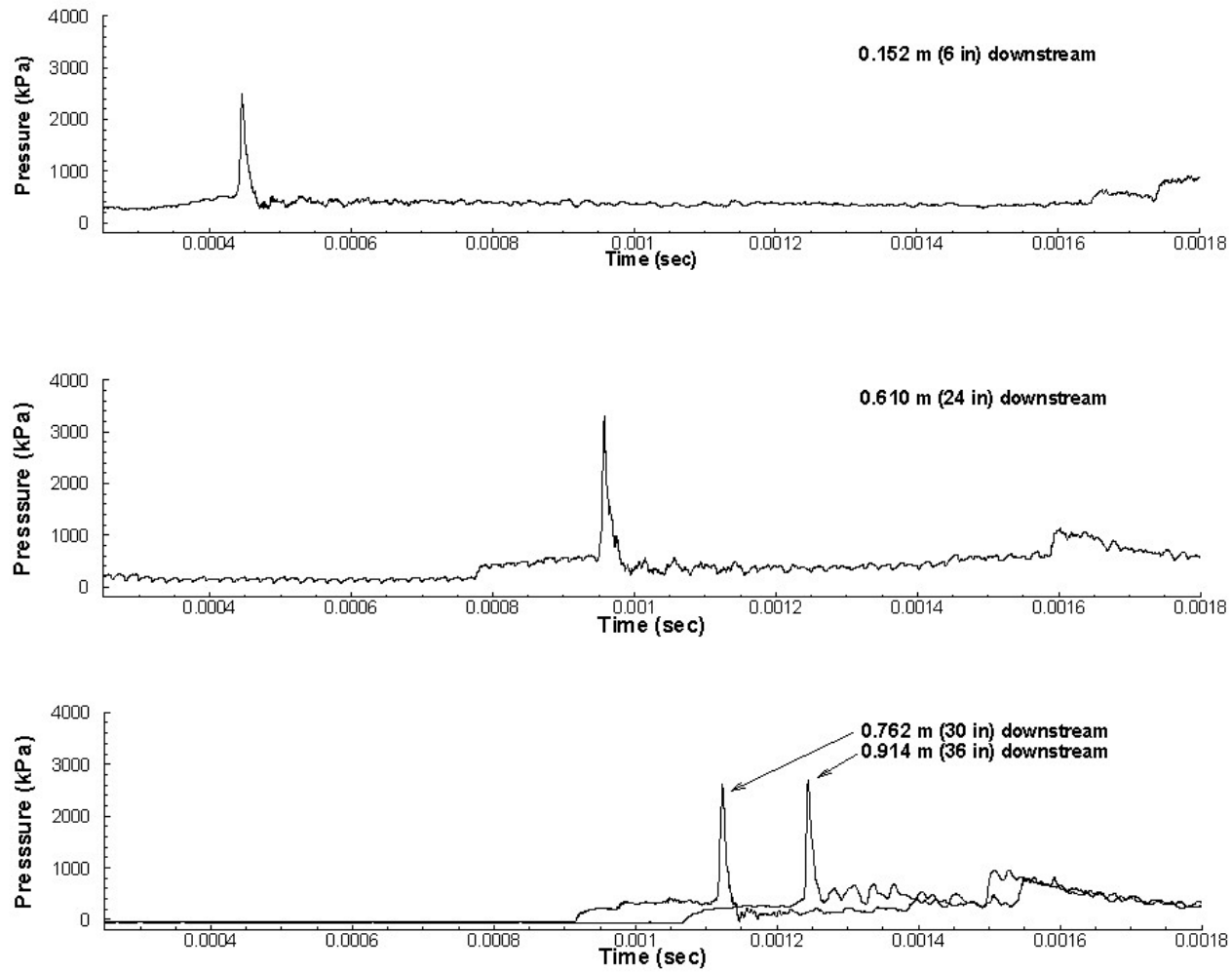
Figure 33. Pressure histories in the tube with an ignition energy of 15.0J.
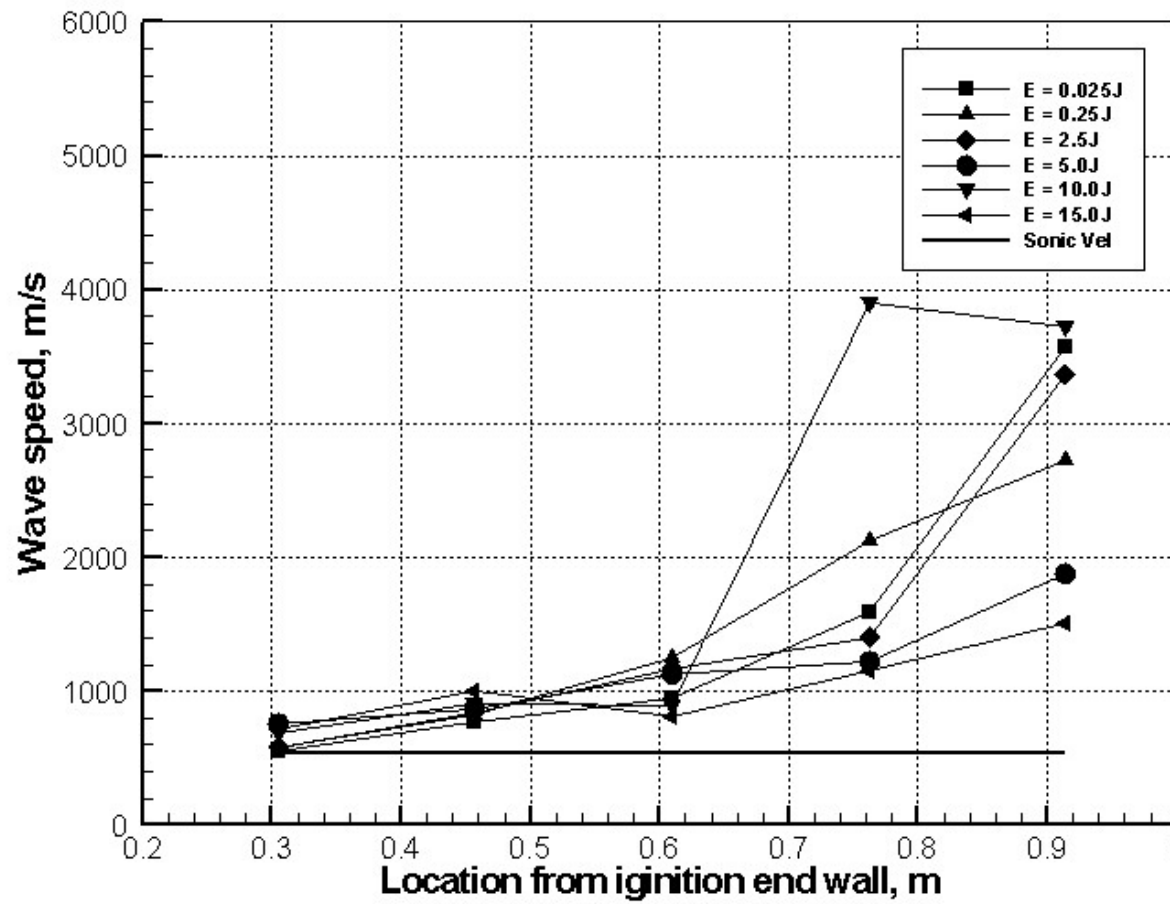
Figure 34. Wave speeds in the tube for various ignition energies.
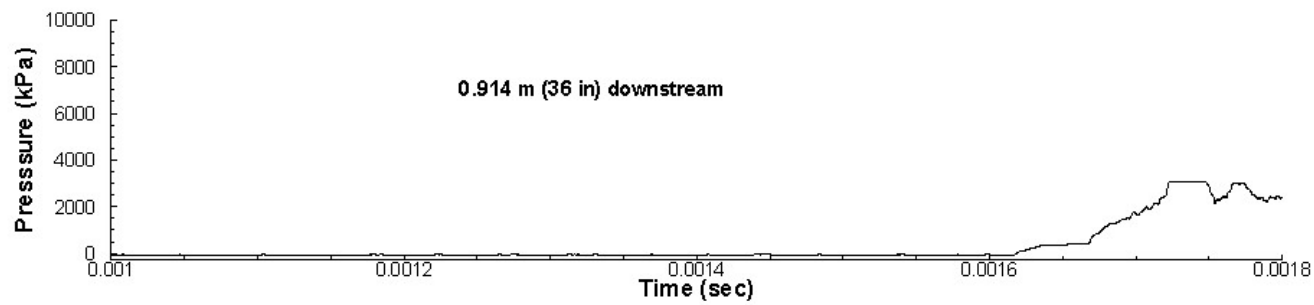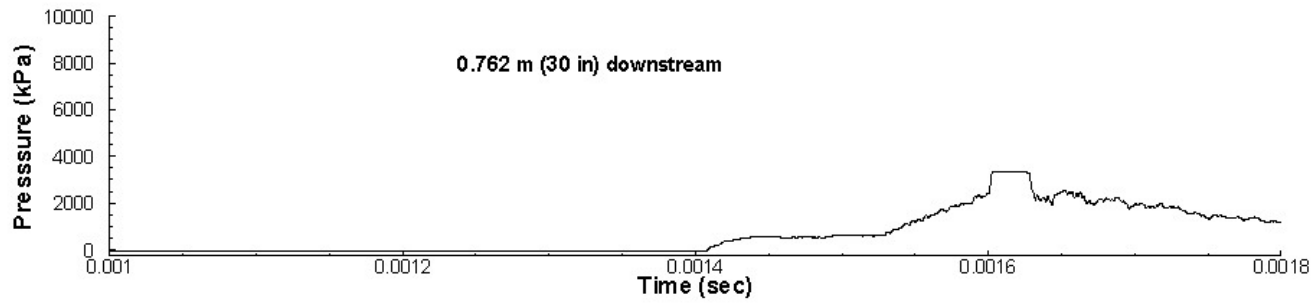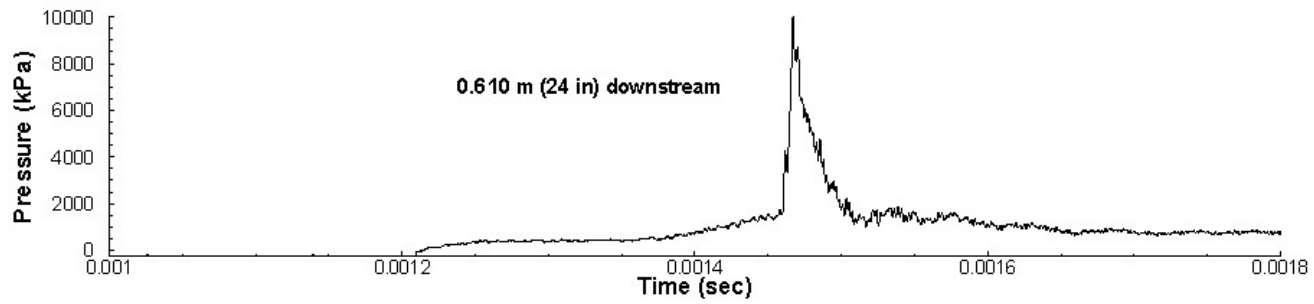
Figure 35. Pressure histories in the tube with a composition fraction of 0.25.
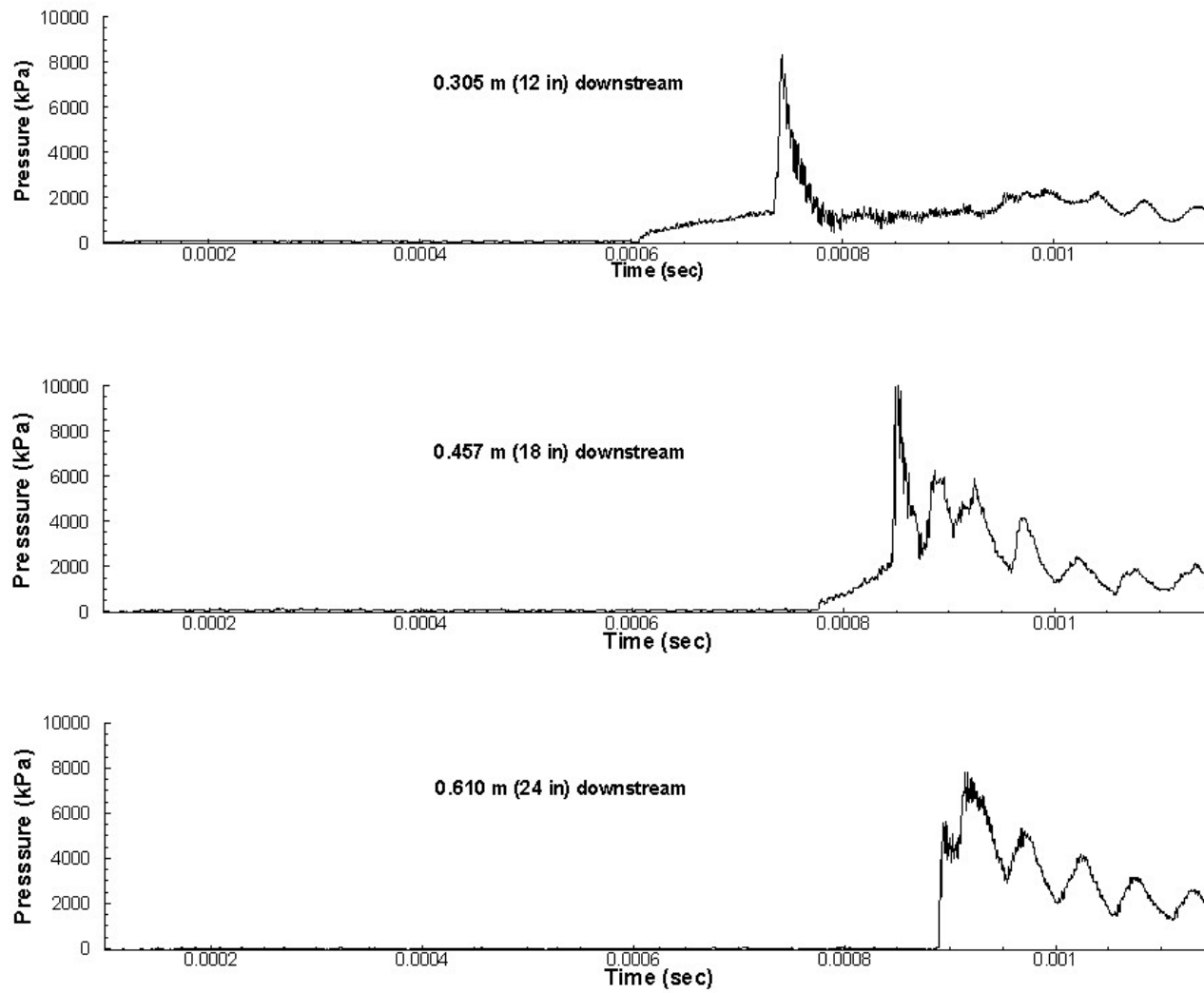
Figure 36. Pressure histories in the tube with a composition fraction of 0.50.
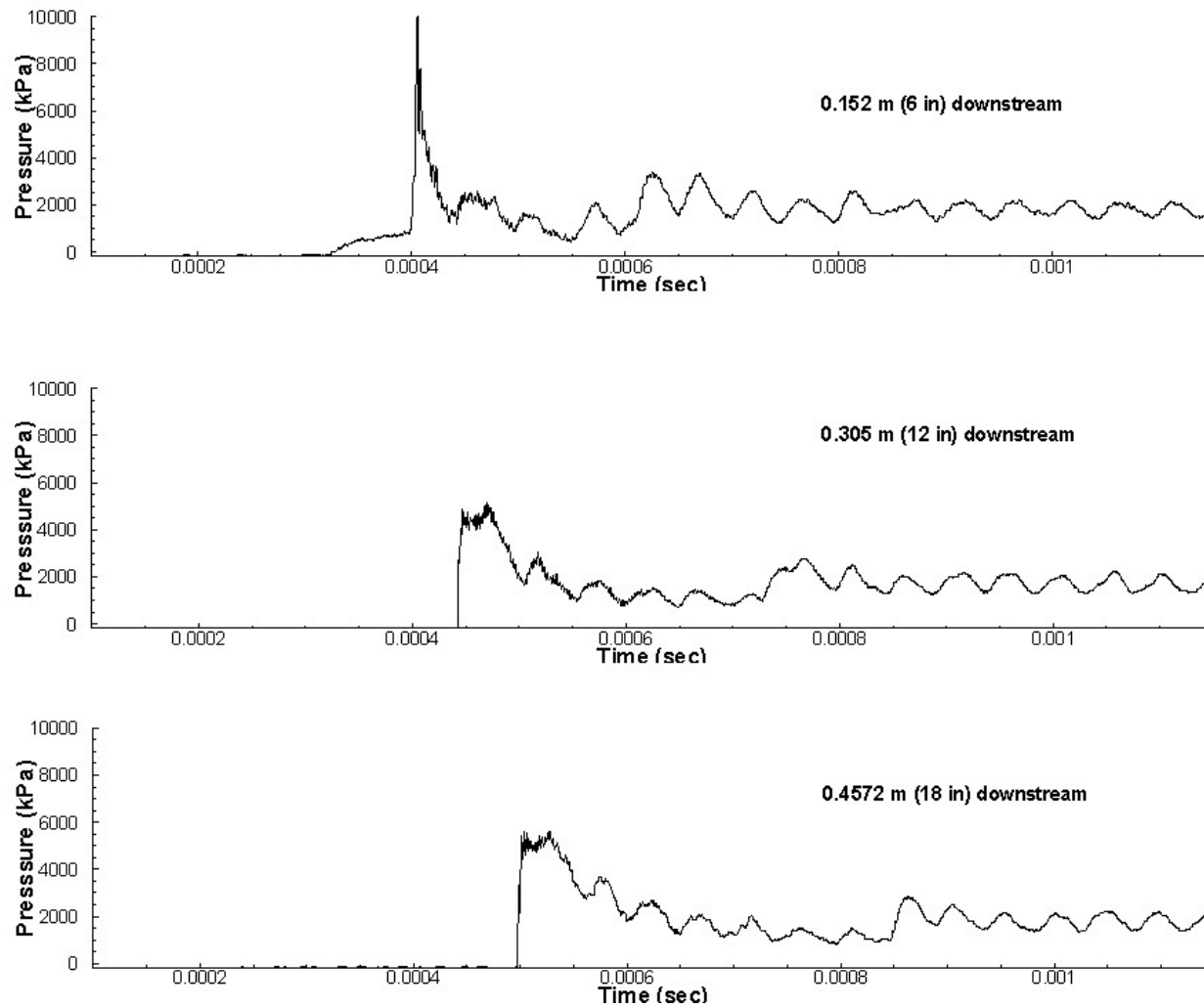
Figure 37. Pressure histories in the tube with a composition fraction of 0.75.
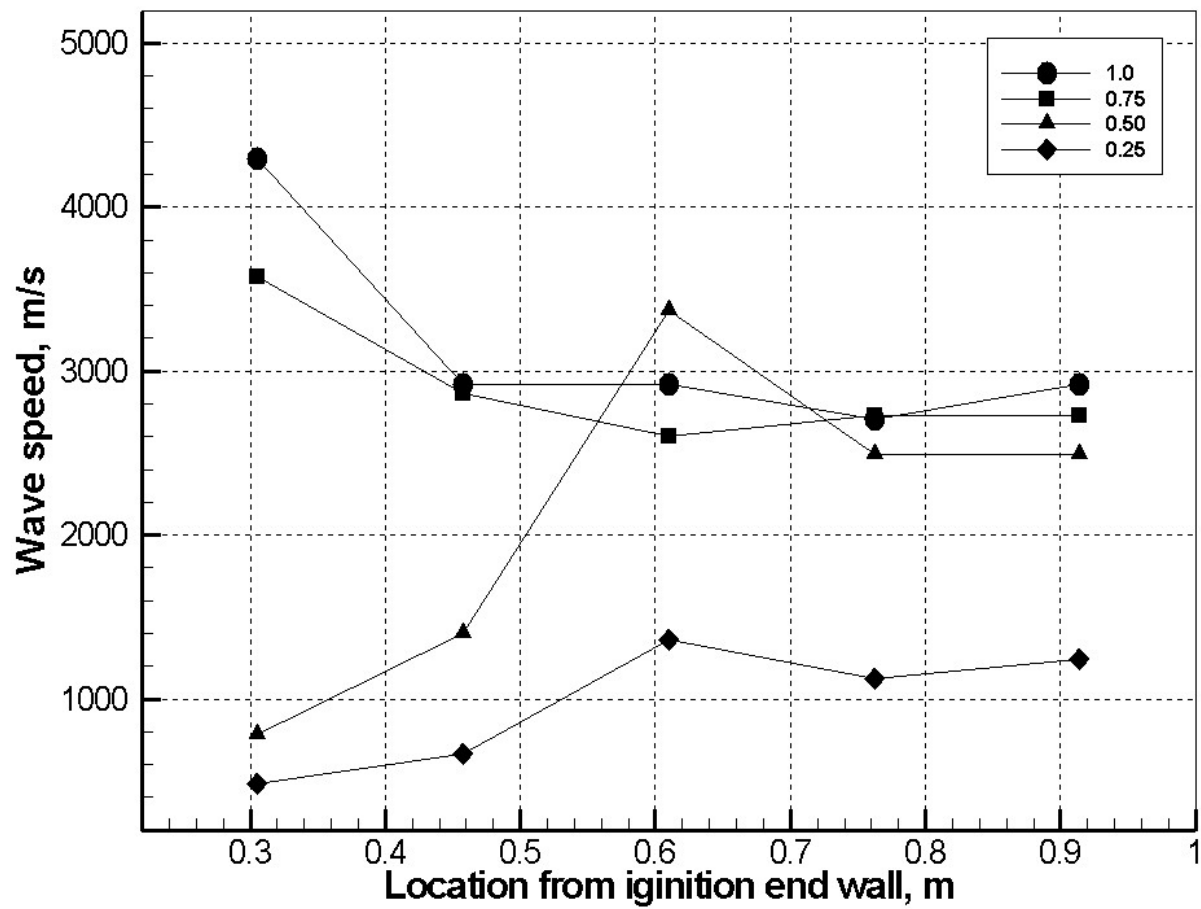
Figure 38. Wave speeds in the tube for various composition fractions.
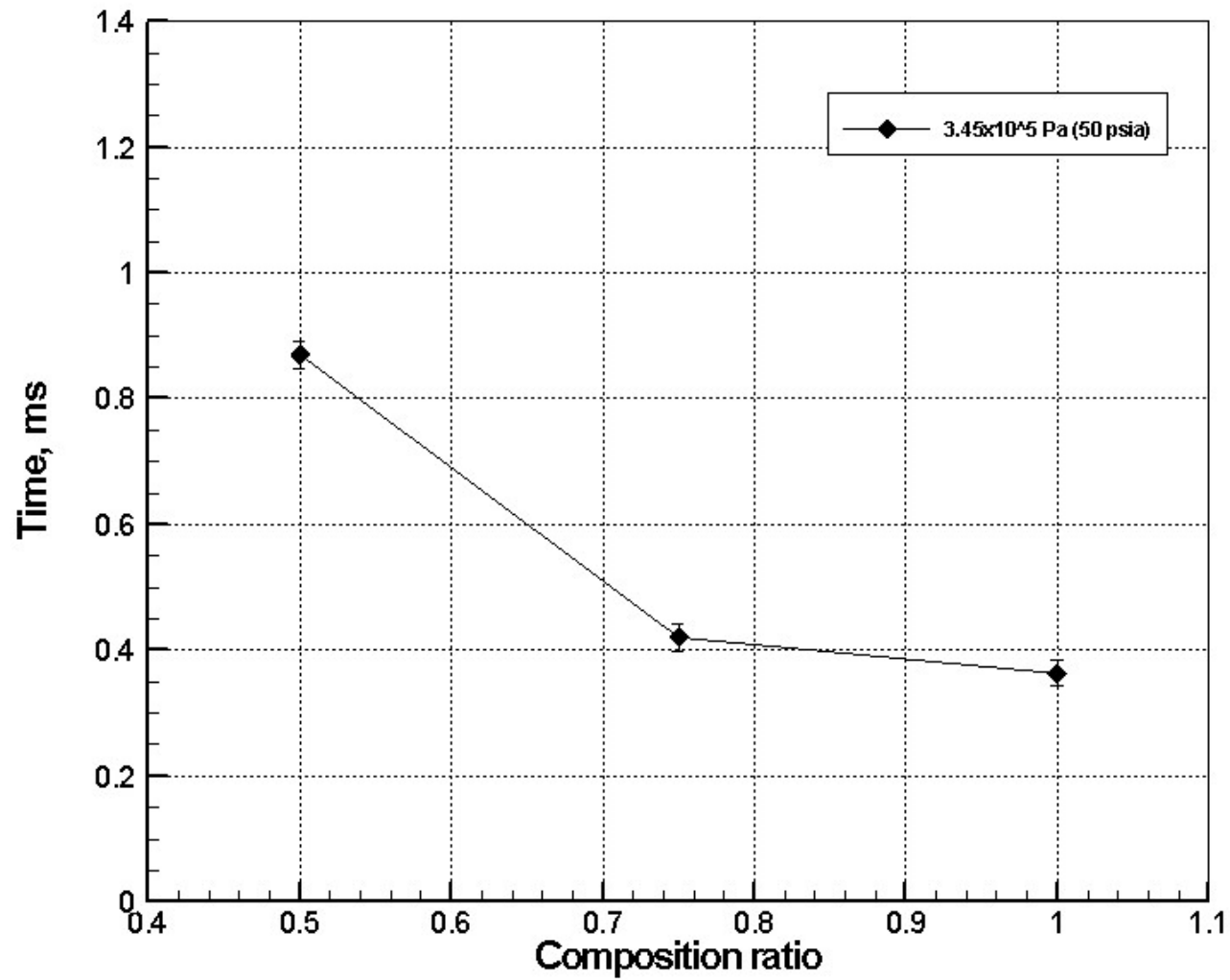
Figure 39. Time required for DDT versus the composition fraction.
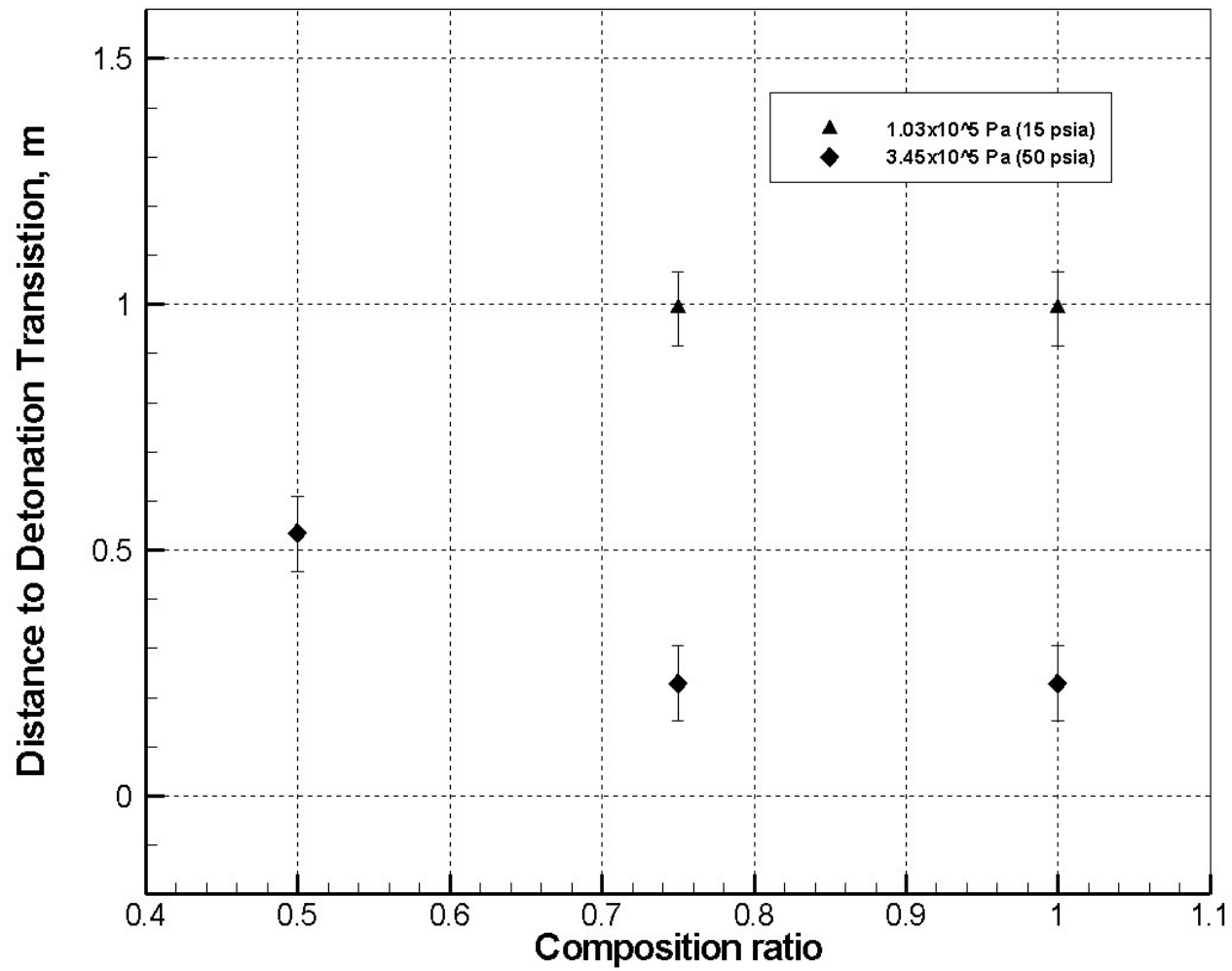
Figure 40. Distance required for DDT versus composition fraction.
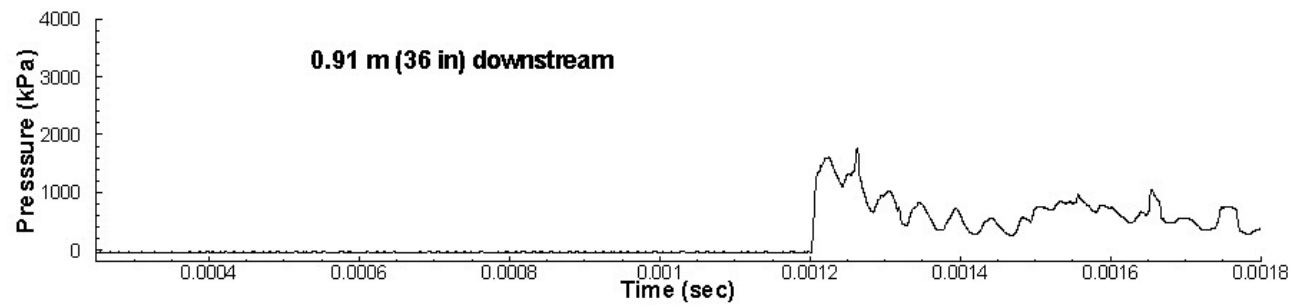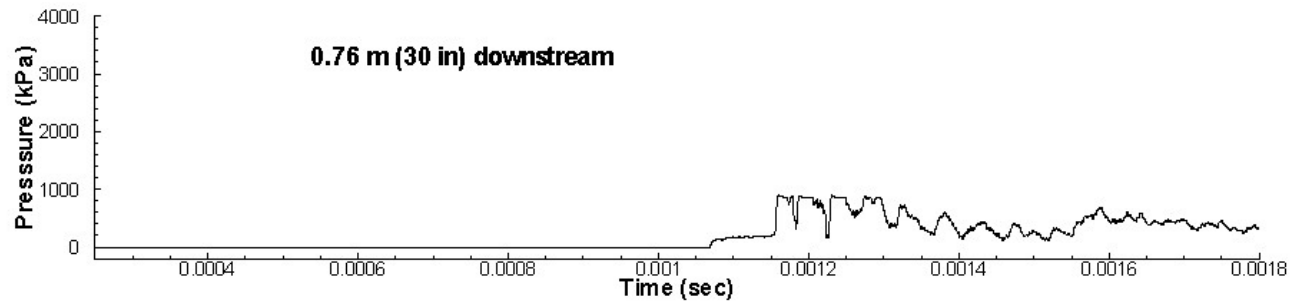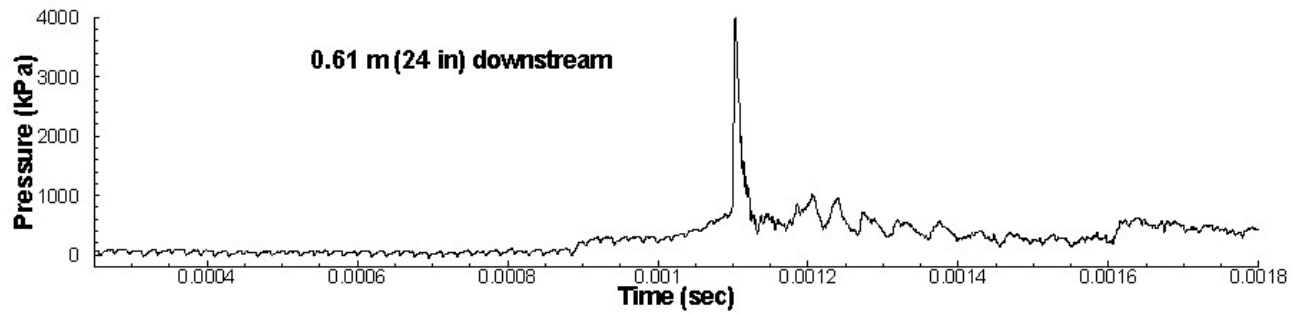
Figure 41. Pressure histories in the tube at a 103 kPa (15 psia) fill pressure using a spiral.
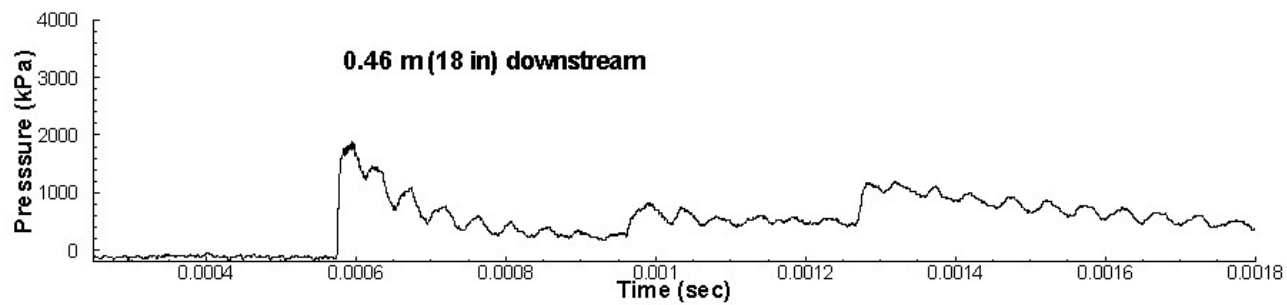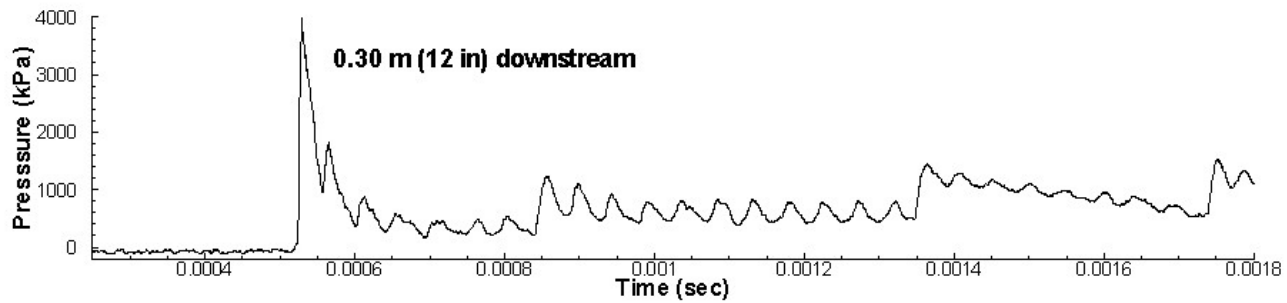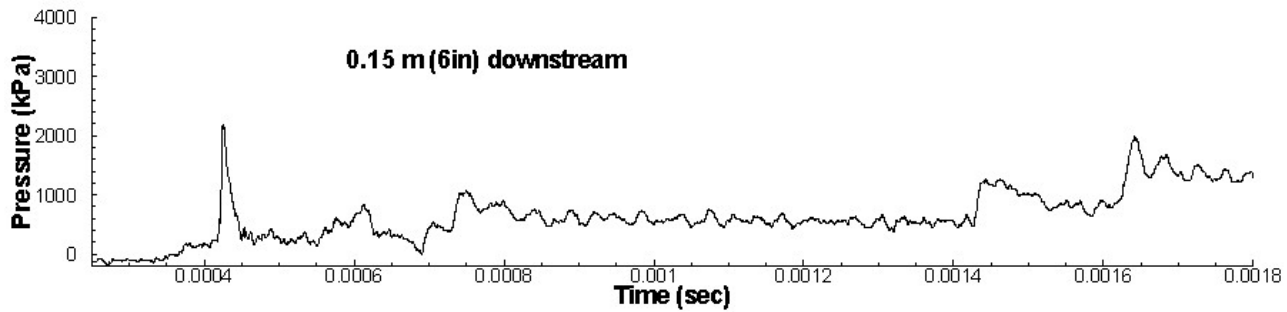
Figure 42. Pressure histories in the tube at a 207 kPa (30 psia) fill pressure using a spiral.
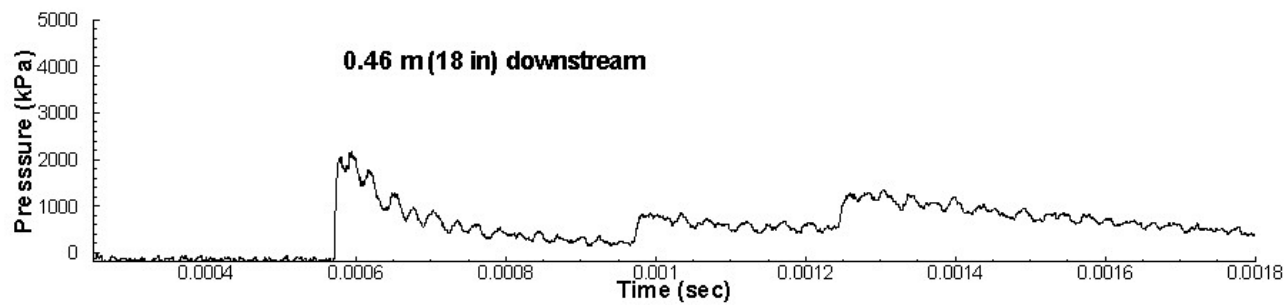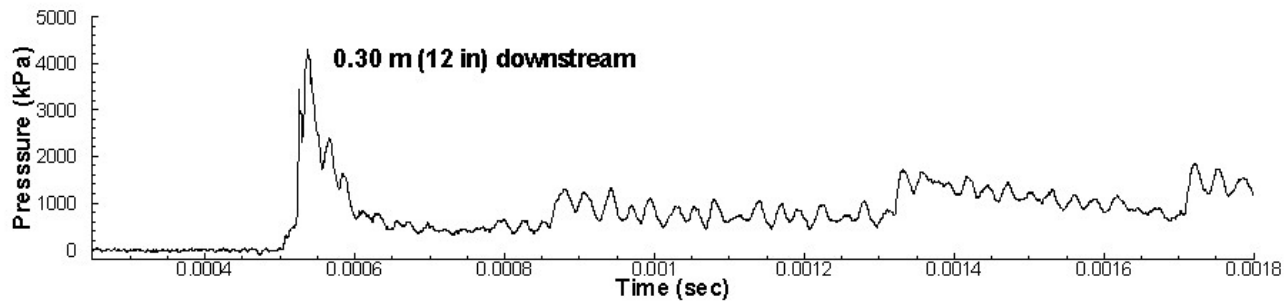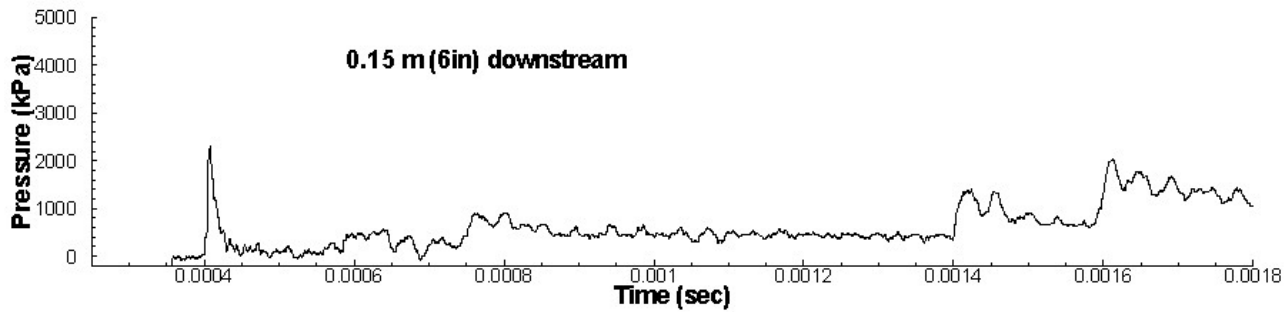
Figure 43. Pressure histories in the tube at a 345 kPa (50 psia) fill pressure using a spiral.
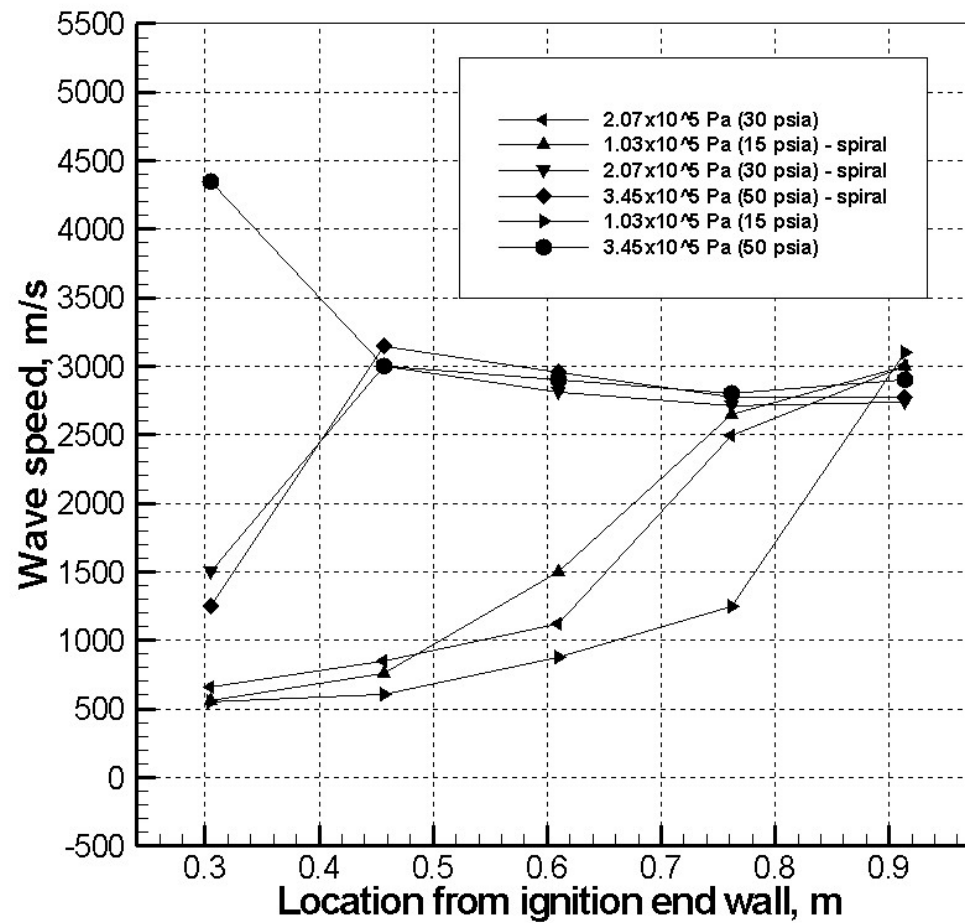
Figure 44. Comparison of wave speeds in the tube with and without a spiral.
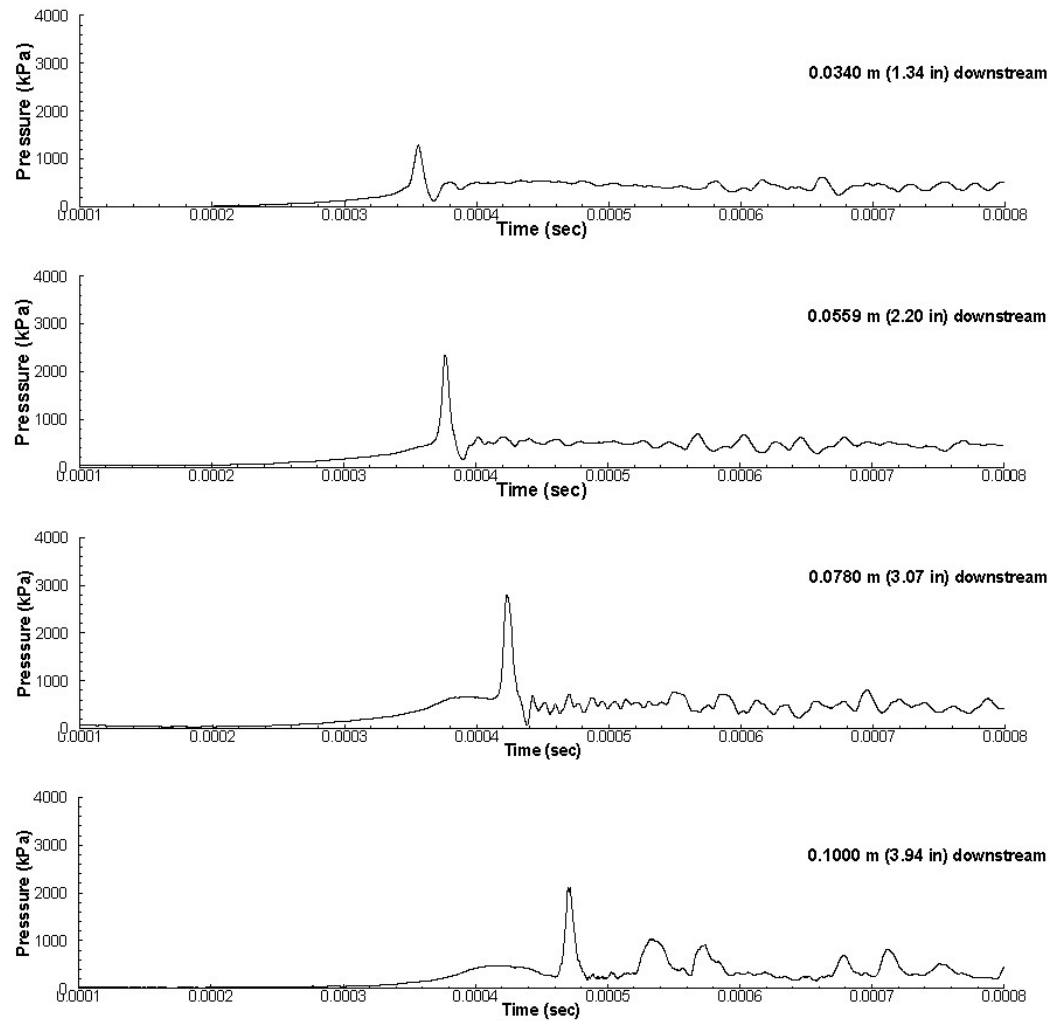
Figure 45. Pressure histories in actuator A with a 103 kPa (15 psia) fill pressure.
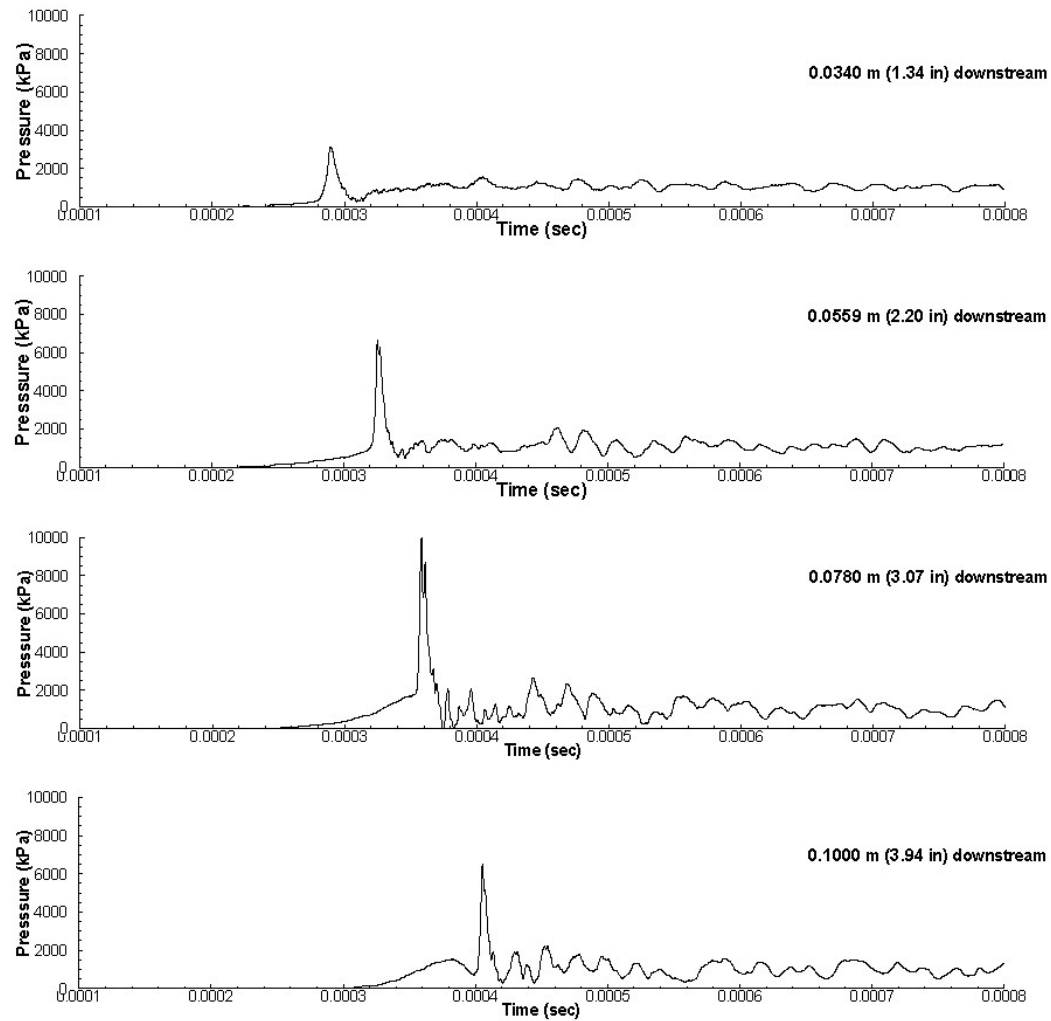
Figure 46. Pressure histories in actuator A with a 207 kPa (30 psia) fill pressure.
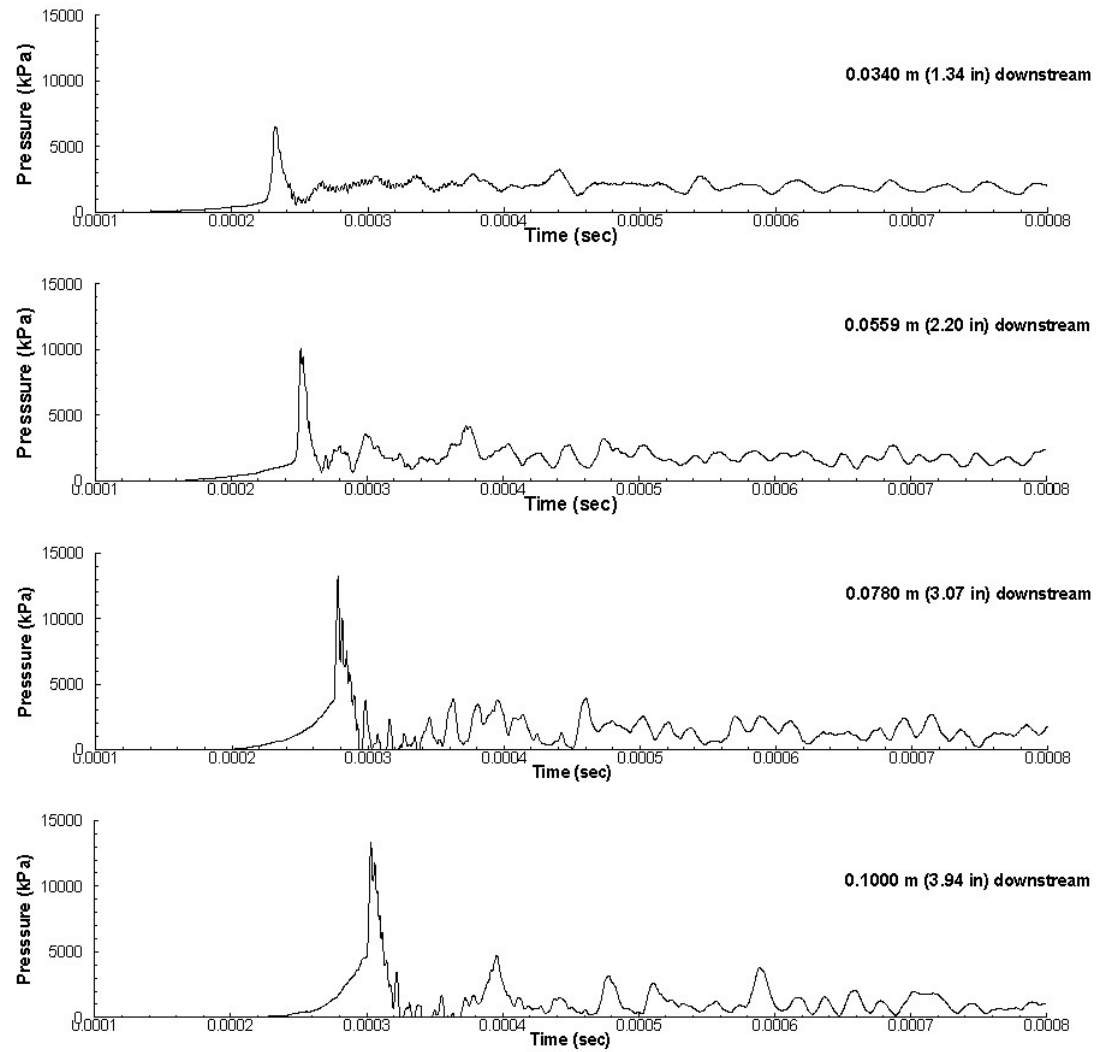
Figure 47. Pressure histories in actuator A with a 345 kPa (50 psia) fill pressure.
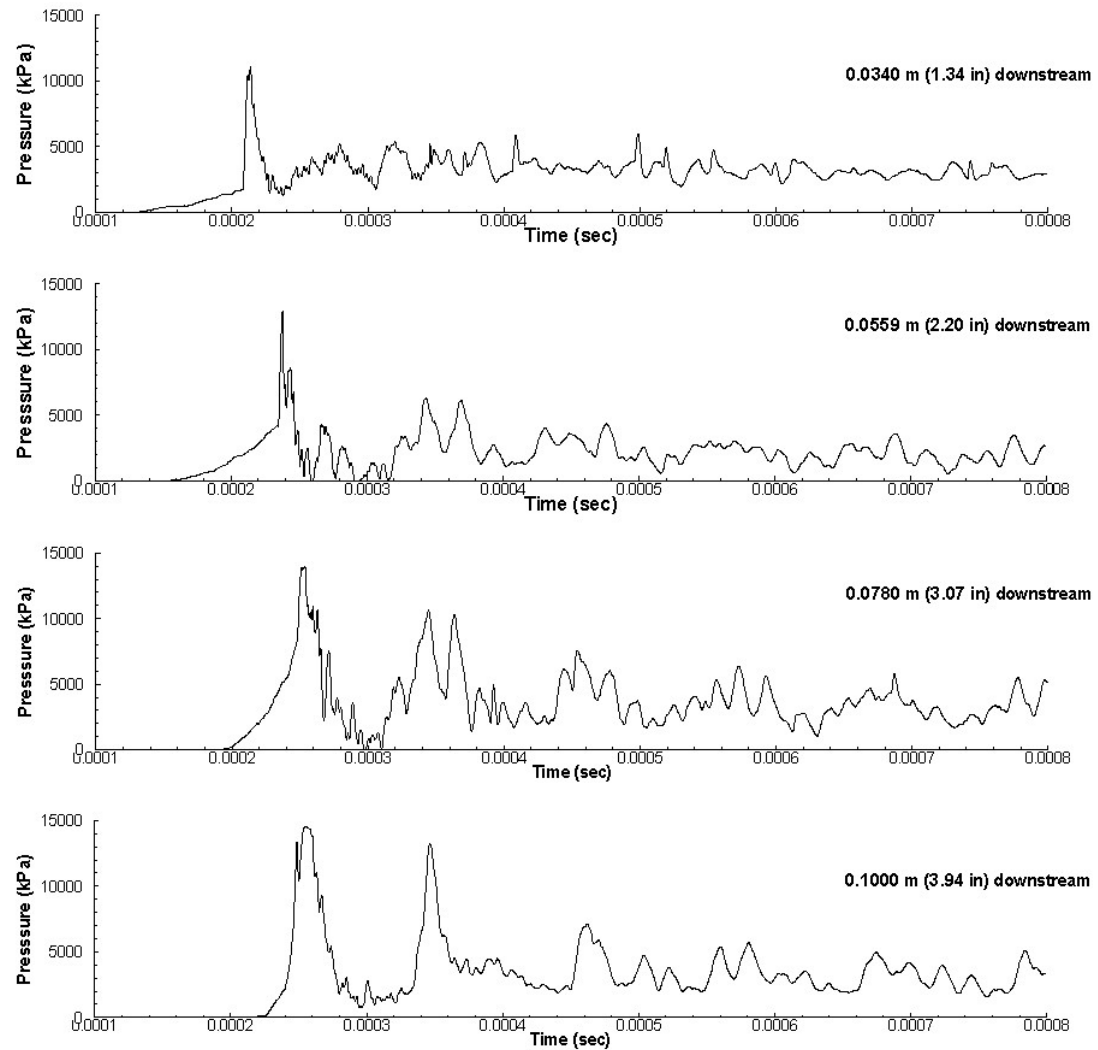
Figure 48. Pressure histories in actuator A with a 483 kPa (70 psia) fill pressure.
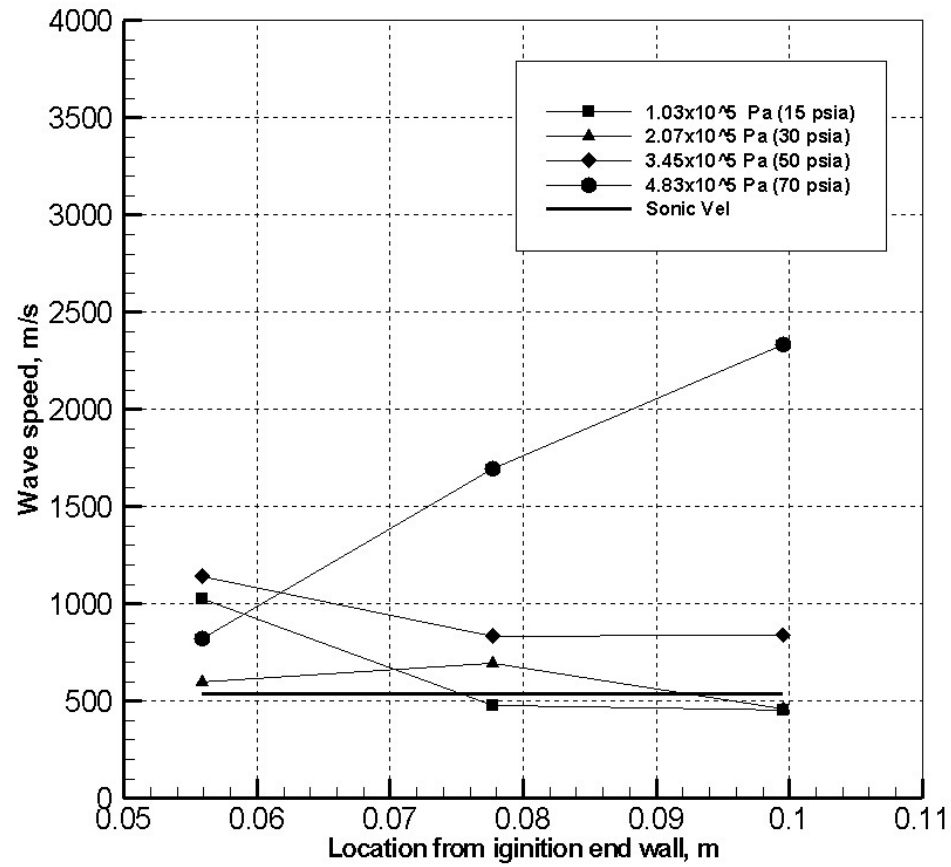
Figure 49. Wave speeds for each fill pressure case using actuator A.
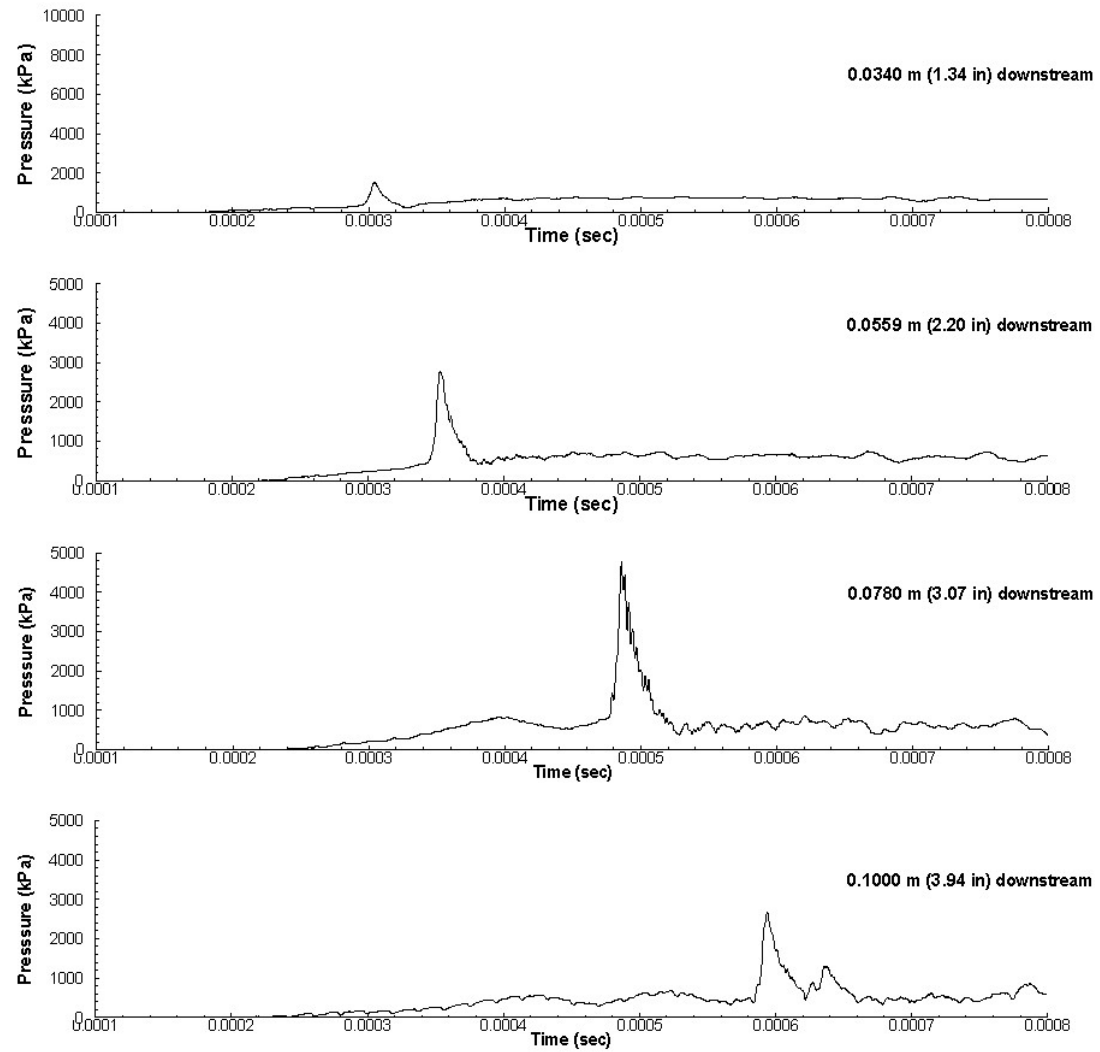
Figure 50. Pressure histories in actuator B with a 103 kPa (15 psia) fill pressure.
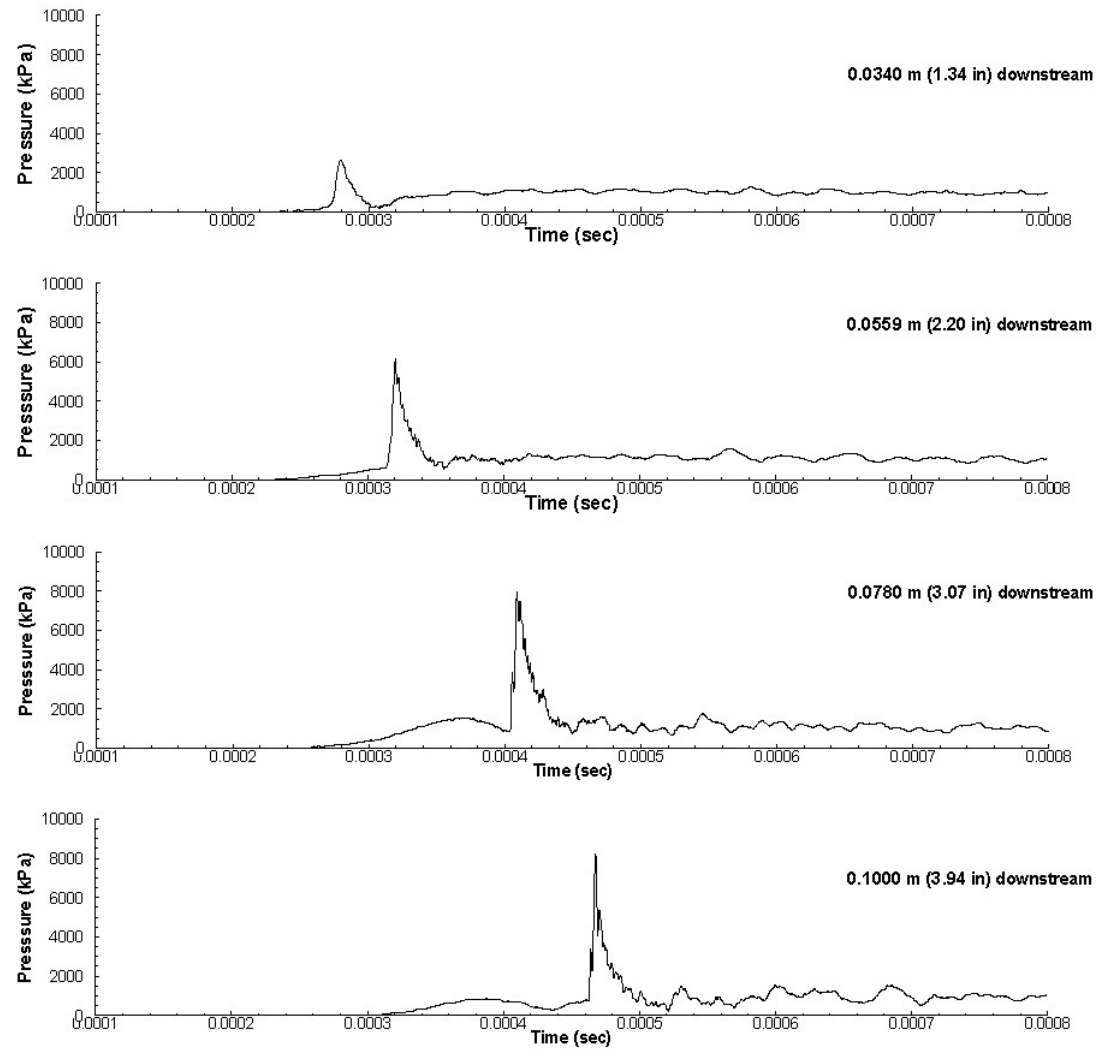
Figure 51. Pressure histories in actuator B with a 207 kPa (30 psia) fill pressure.
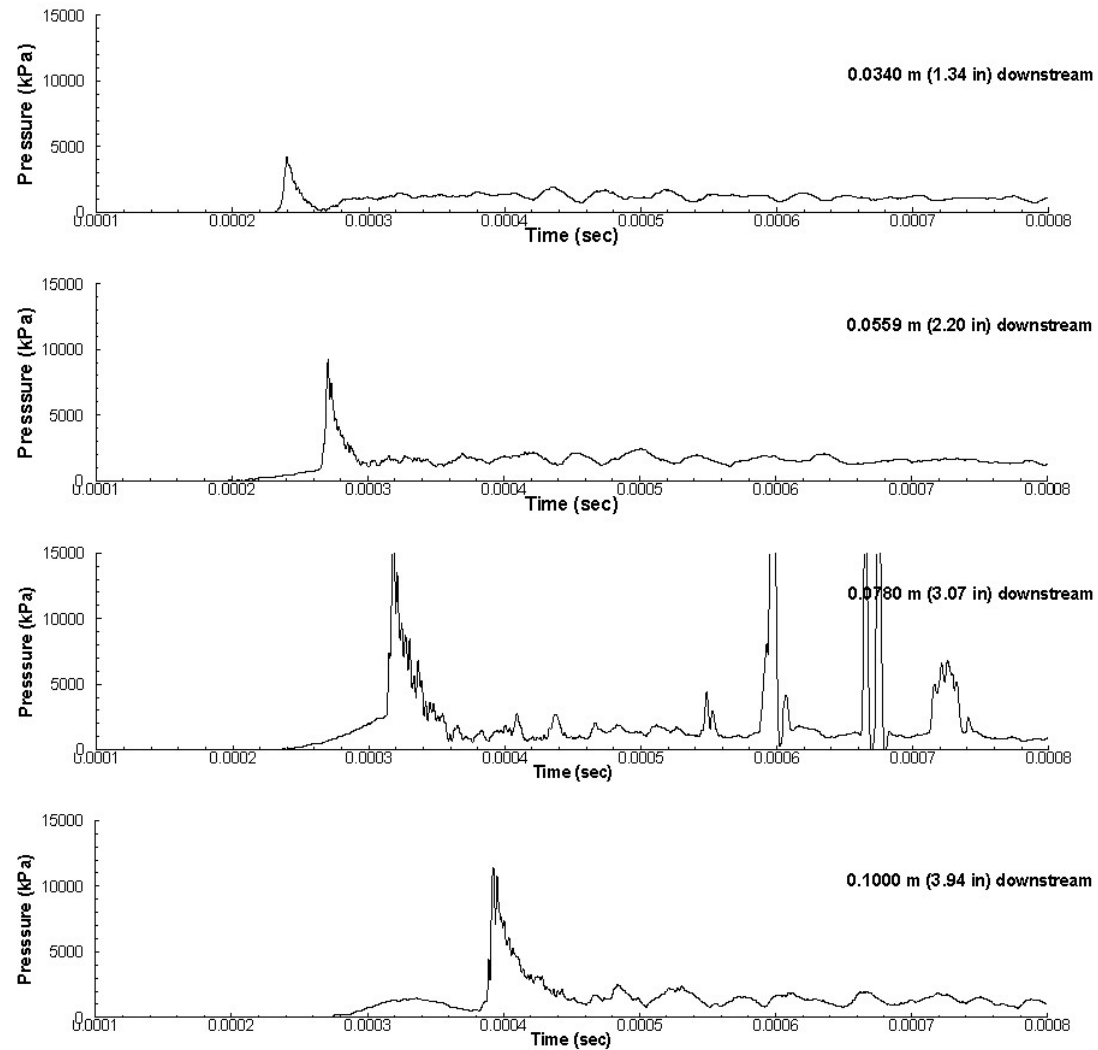
Figure 52. Pressure histories in actuator B with a 345 kPa (50 psia) fill pressure.
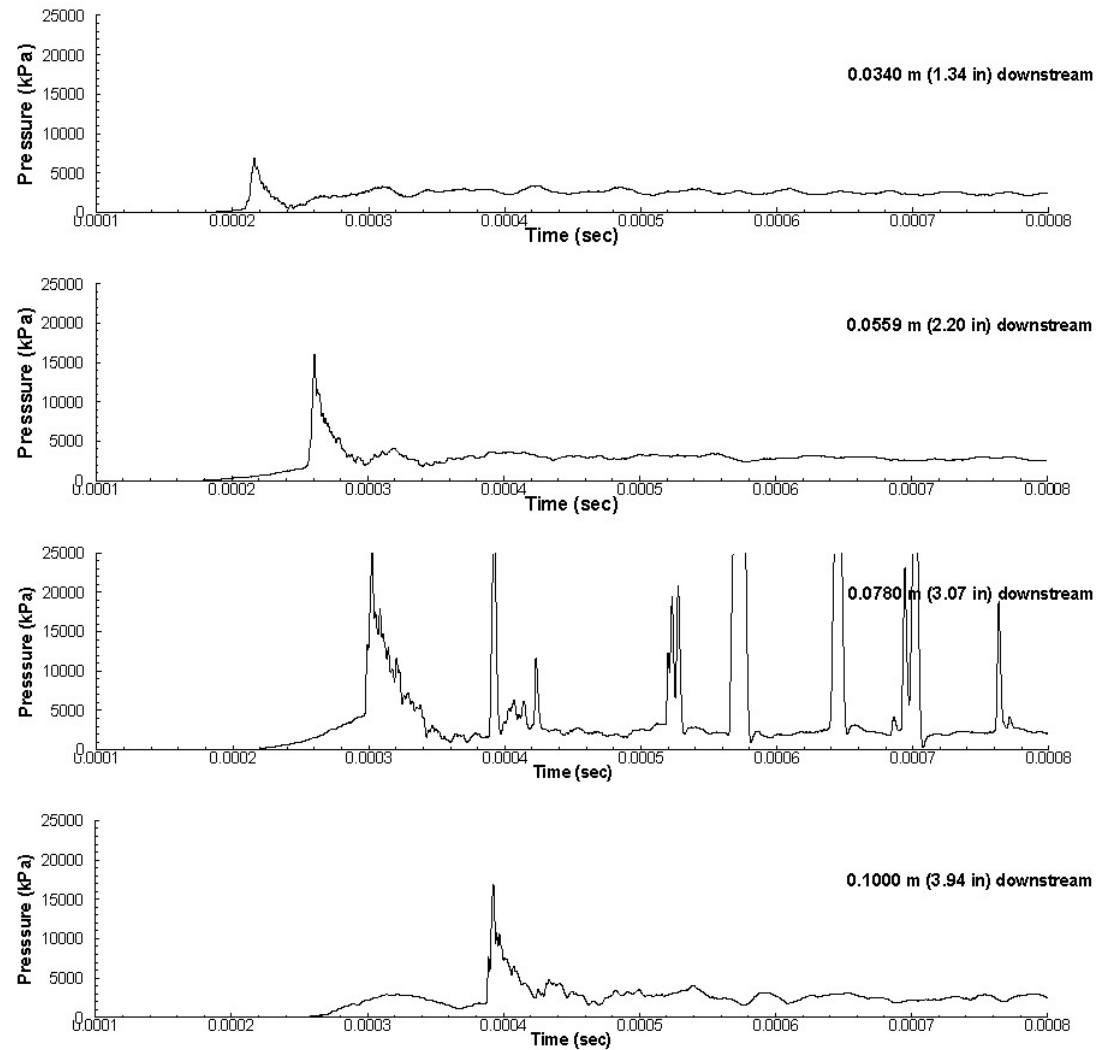
Figure 53. Pressure histories in actuator B with a 483 kPa (70 psia) fill pressure.
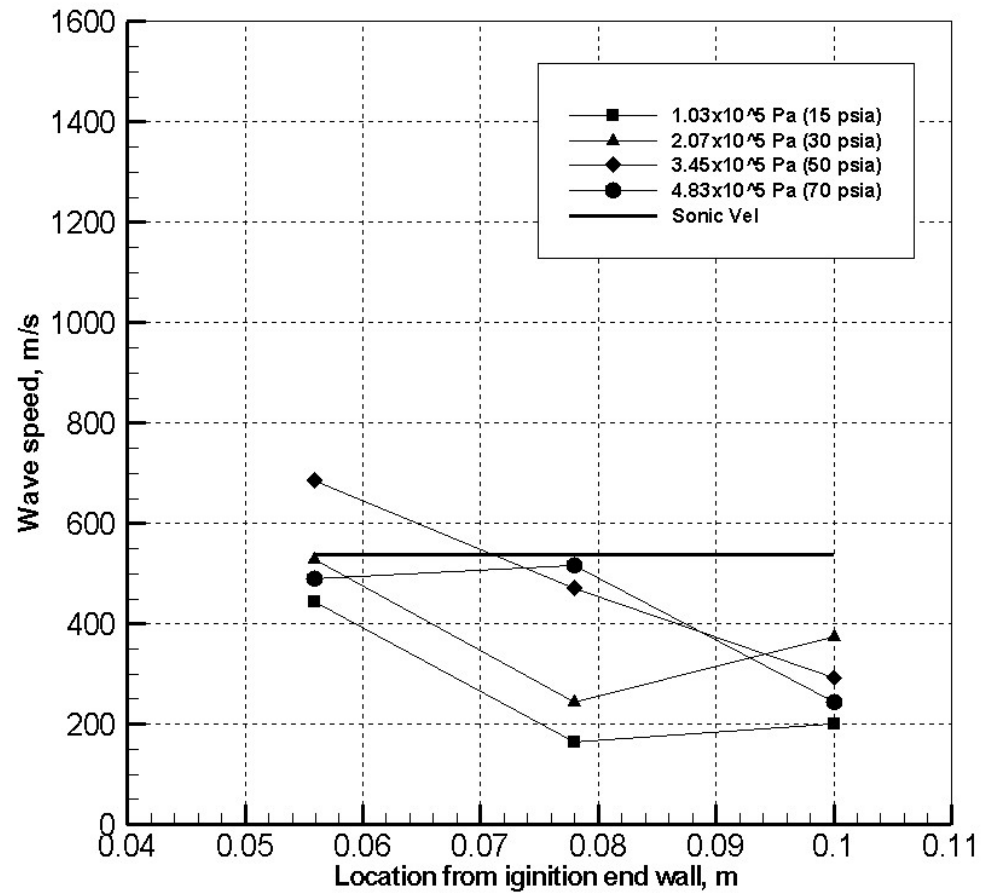
Figure 54. Wave speeds for each fill pressure case using actuator B.
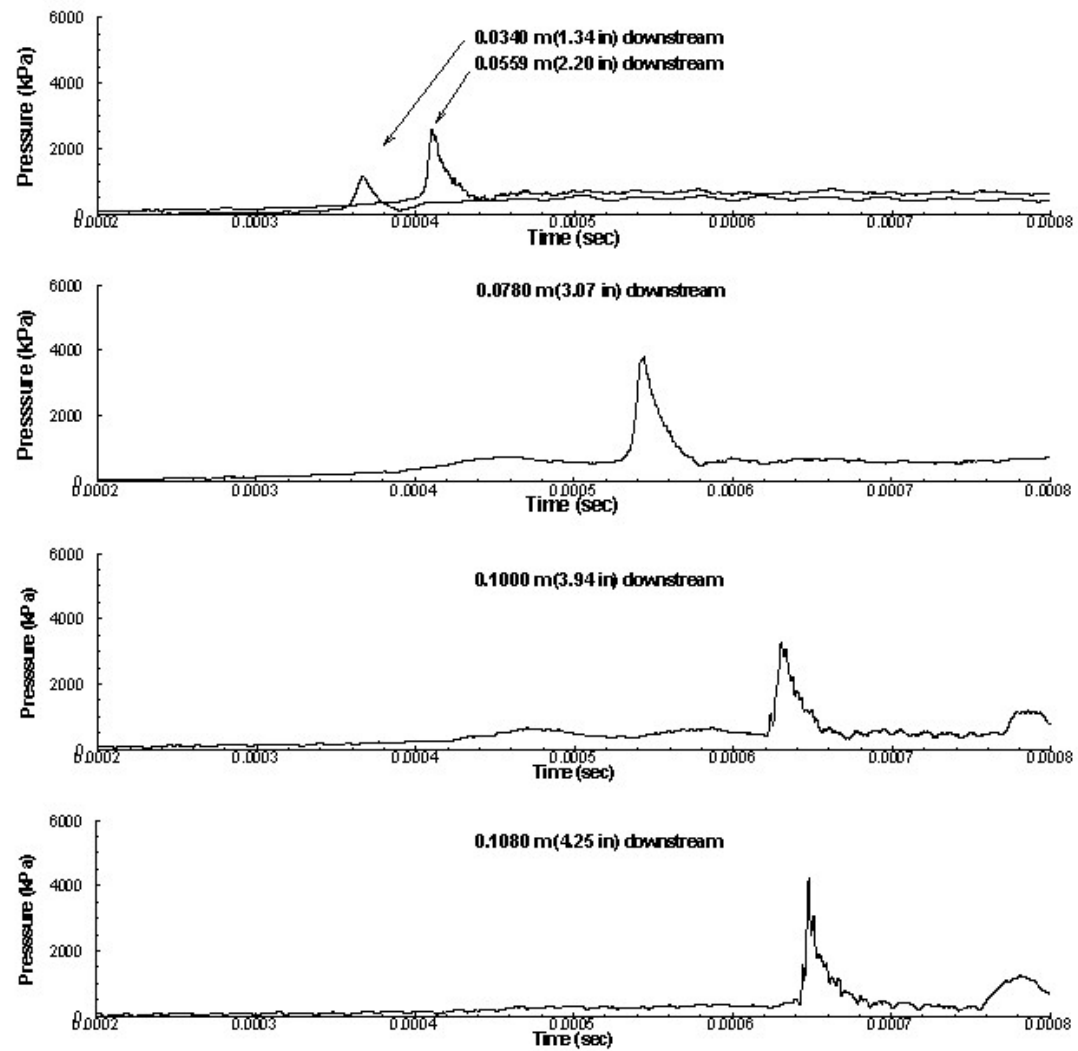
Figure 55. Pressure histories in actuator C with a 103 kPa (15 psia) fill pressure.
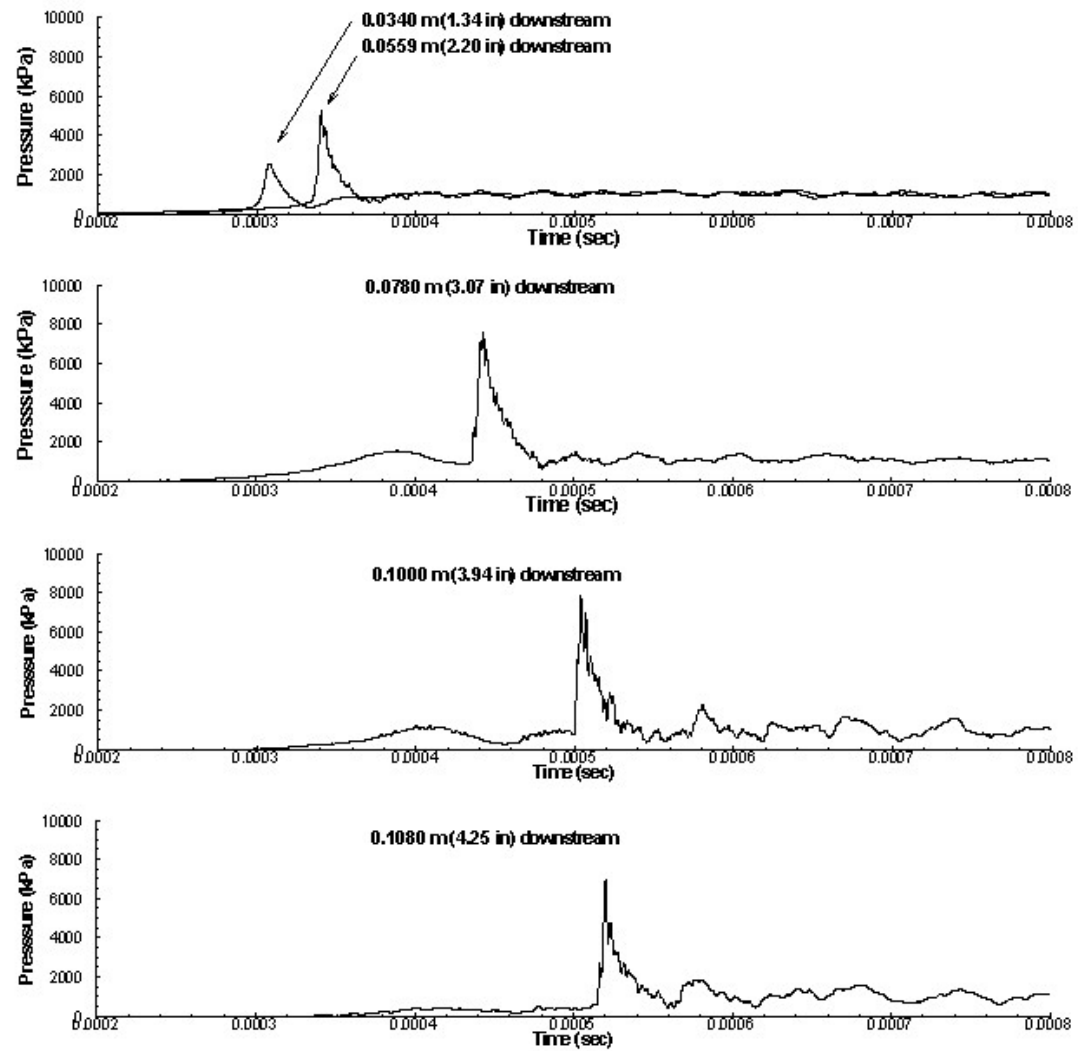
Figure 56. Pressure histories in actuator C with a 207 kPa (30 psia) fill pressure.

Figure 57. Pressure histories in actuator C with a 345 kPa (50 psia) fill pressure.
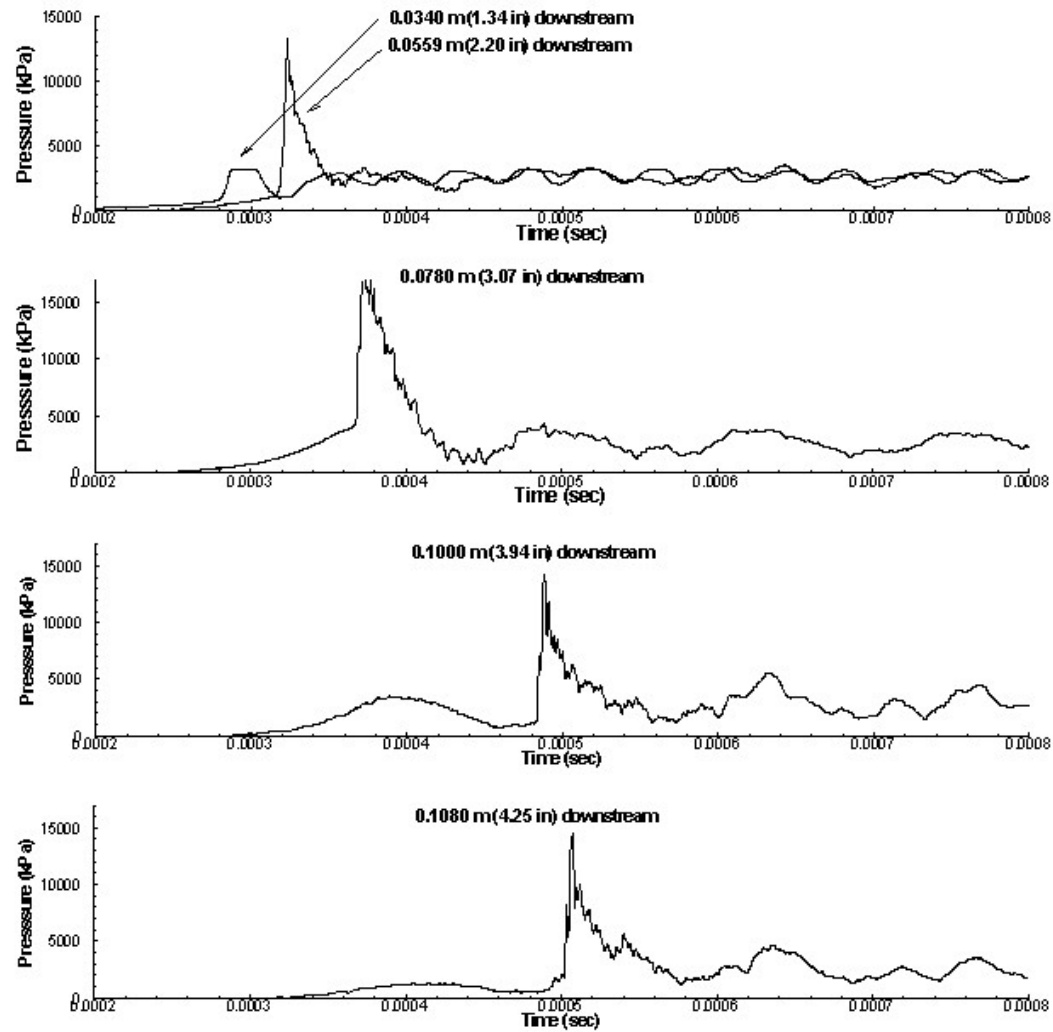
Figure 58. Pressure histories in actuator C with a 483 kPa (70 psia) fill pressure.
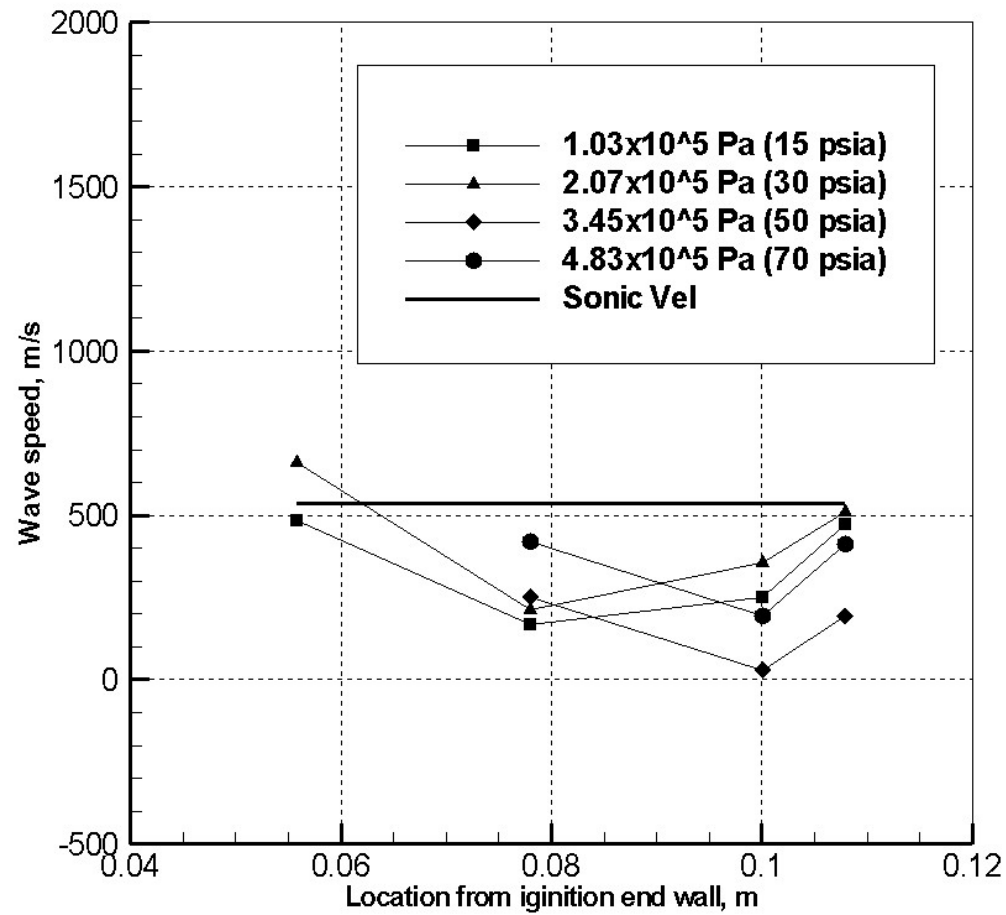
Figure 59. Wave speeds for each fill pressure case using actuator C.
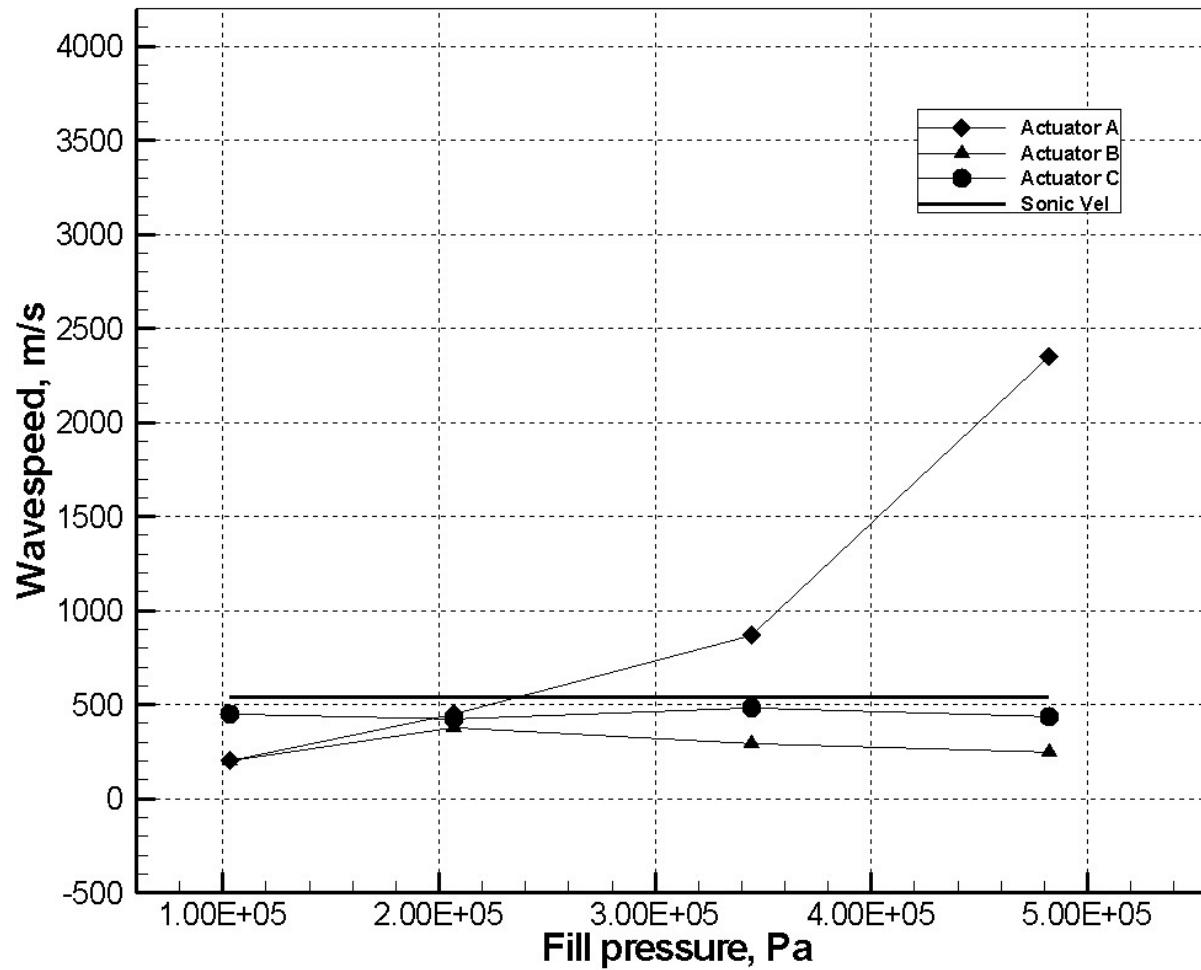
Figure 60. Exit wave speeds for each actuator at various fill pressures.
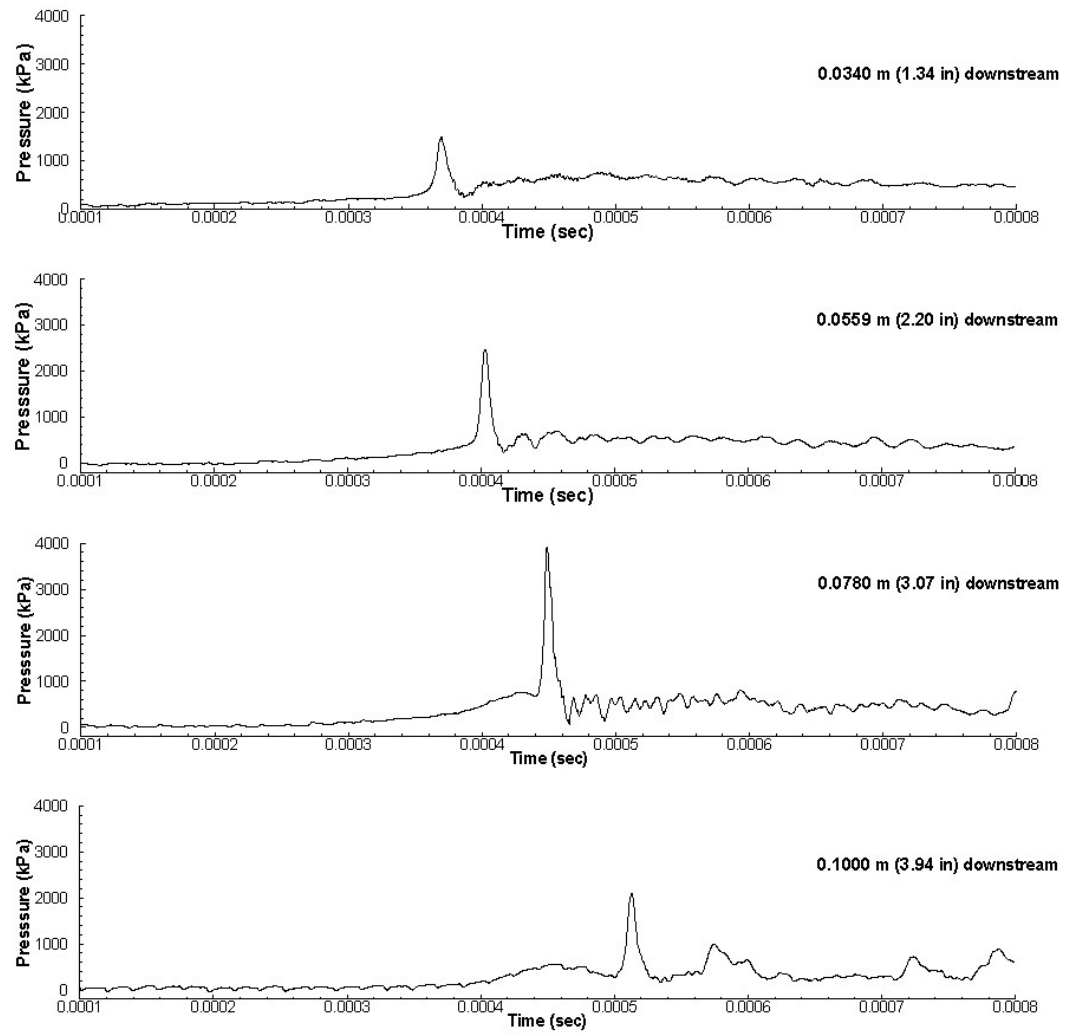
Figure 61. Pressure histories in actuator A with an equivalence ratio=0.7.
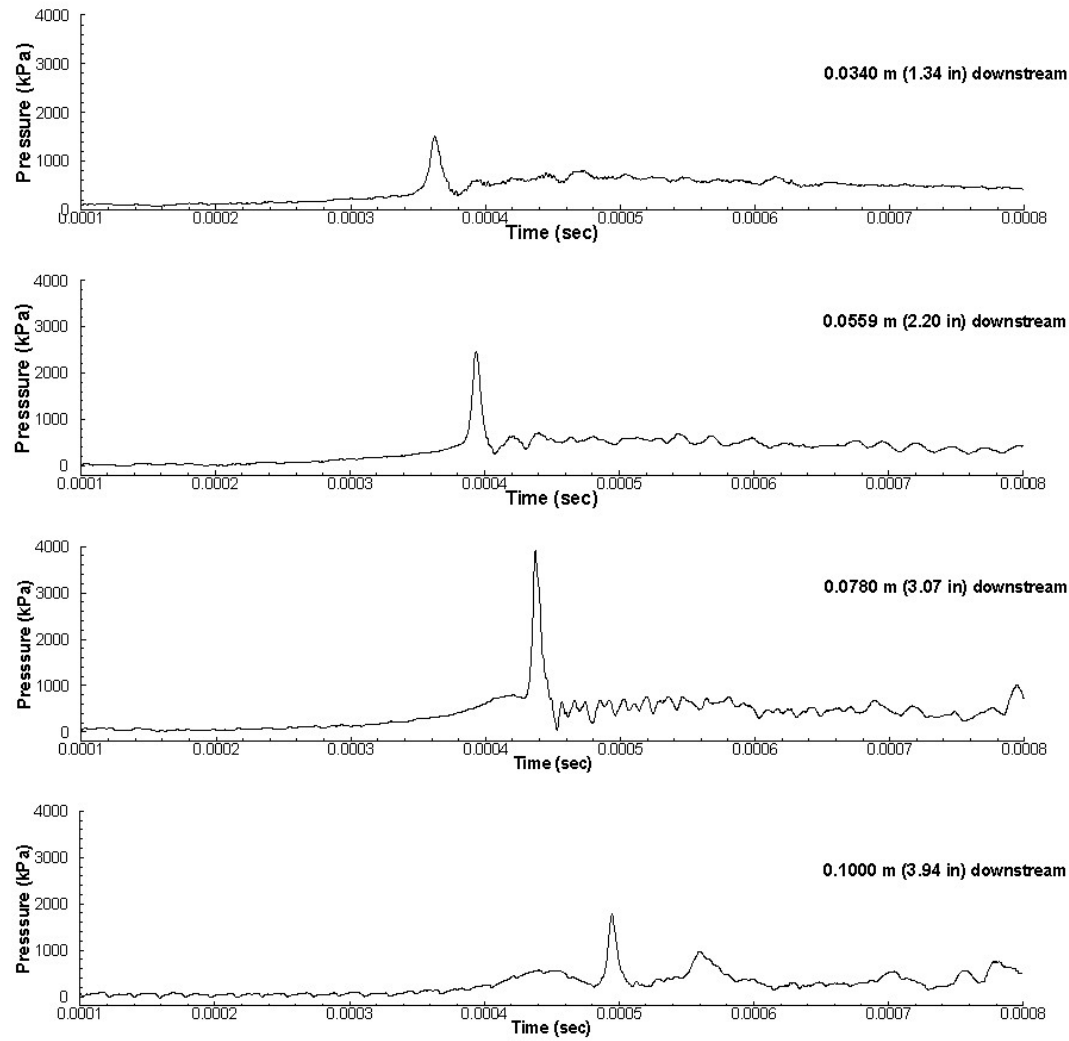
Figure 62. Pressure histories in actuator A with an equivalence ratio=0.9.
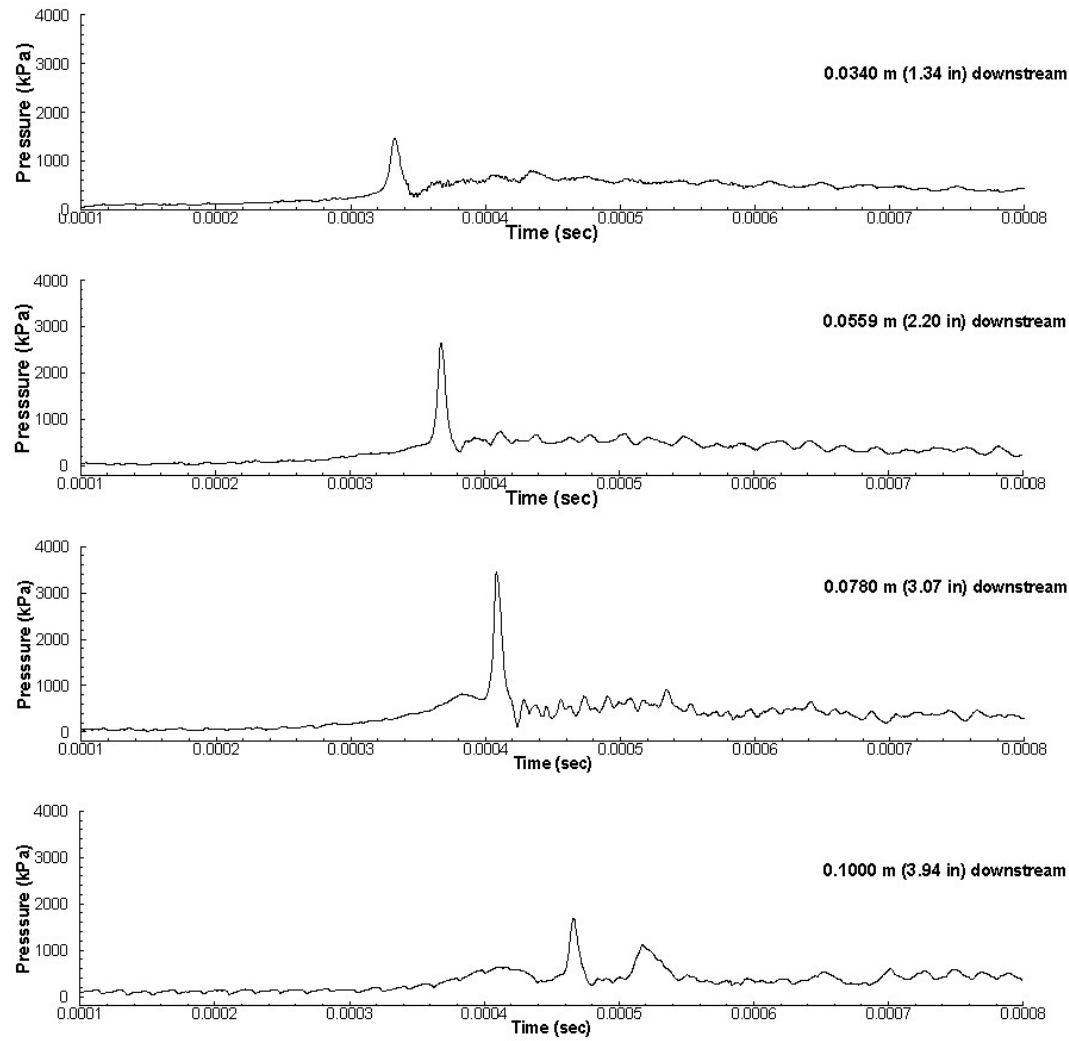
Figure 63. Pressure histories in actuator A with an equivalence ratio=1.1.
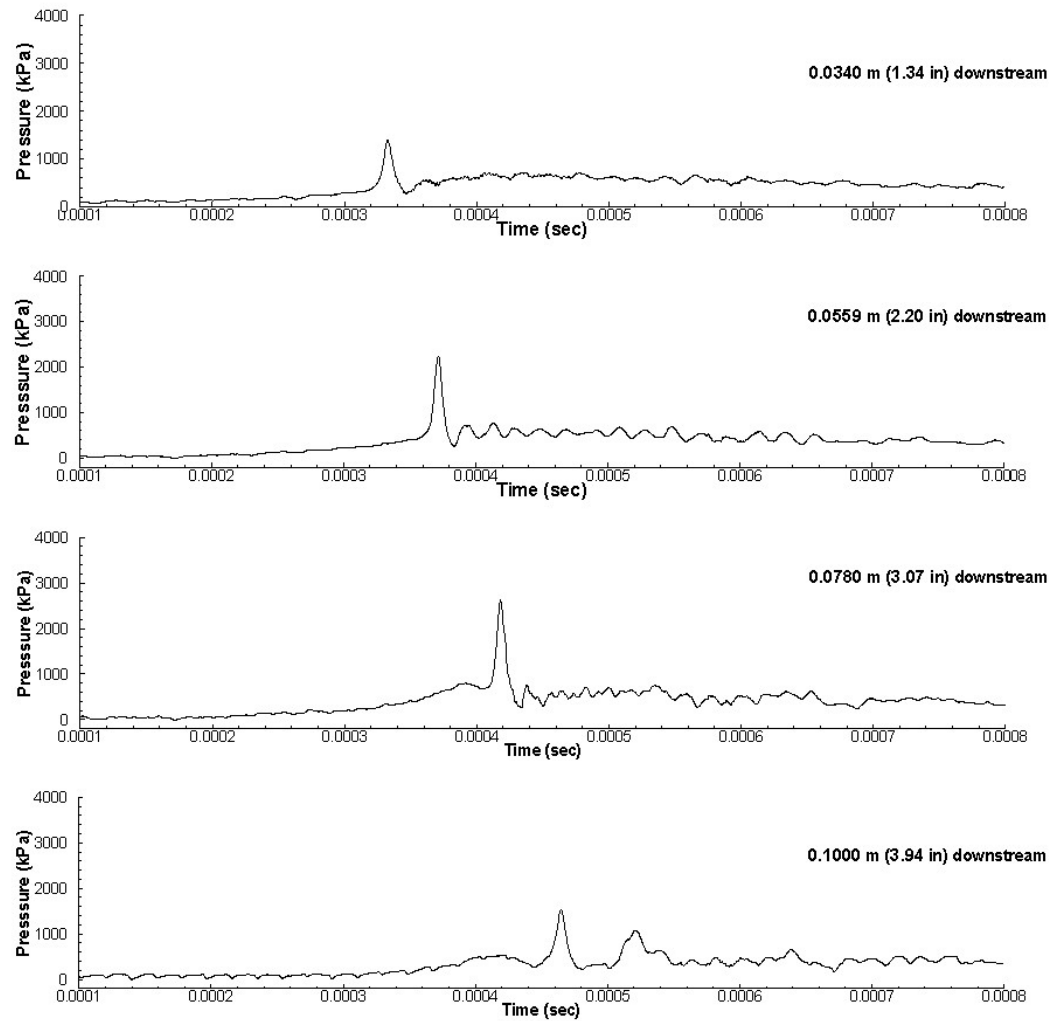
Figure 64. Pressure histories in actuator A with an equivalence ratio=1.3.
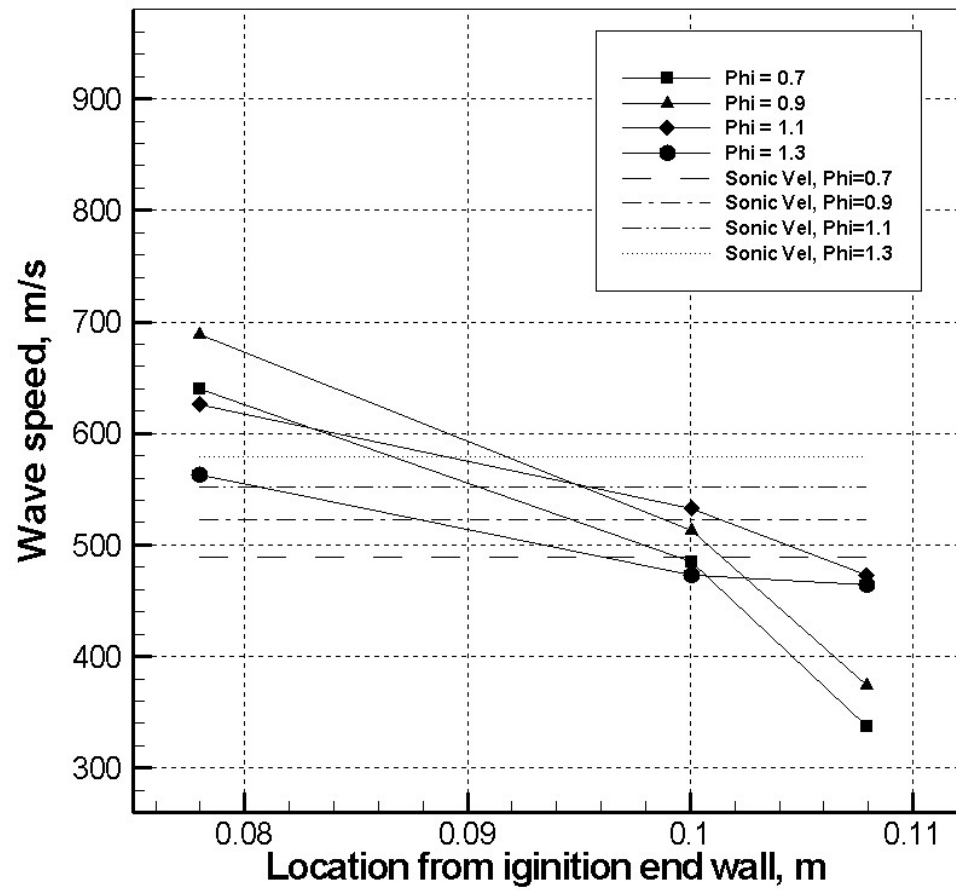
Figure 65. Wave speeds for each equivalence ratio case using actuator A.
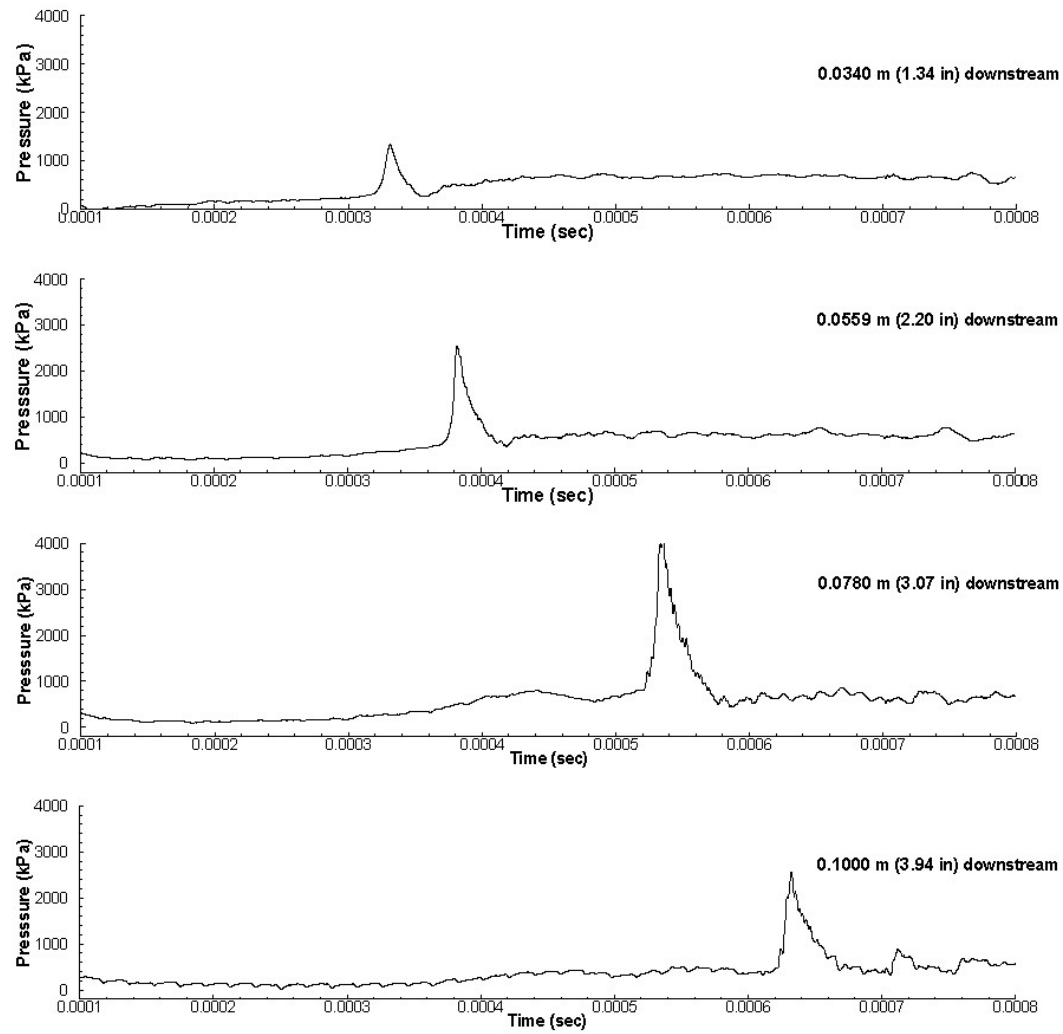
Figure 66.   Pressure histories in actuator B with an equivalence ratio=0.7.
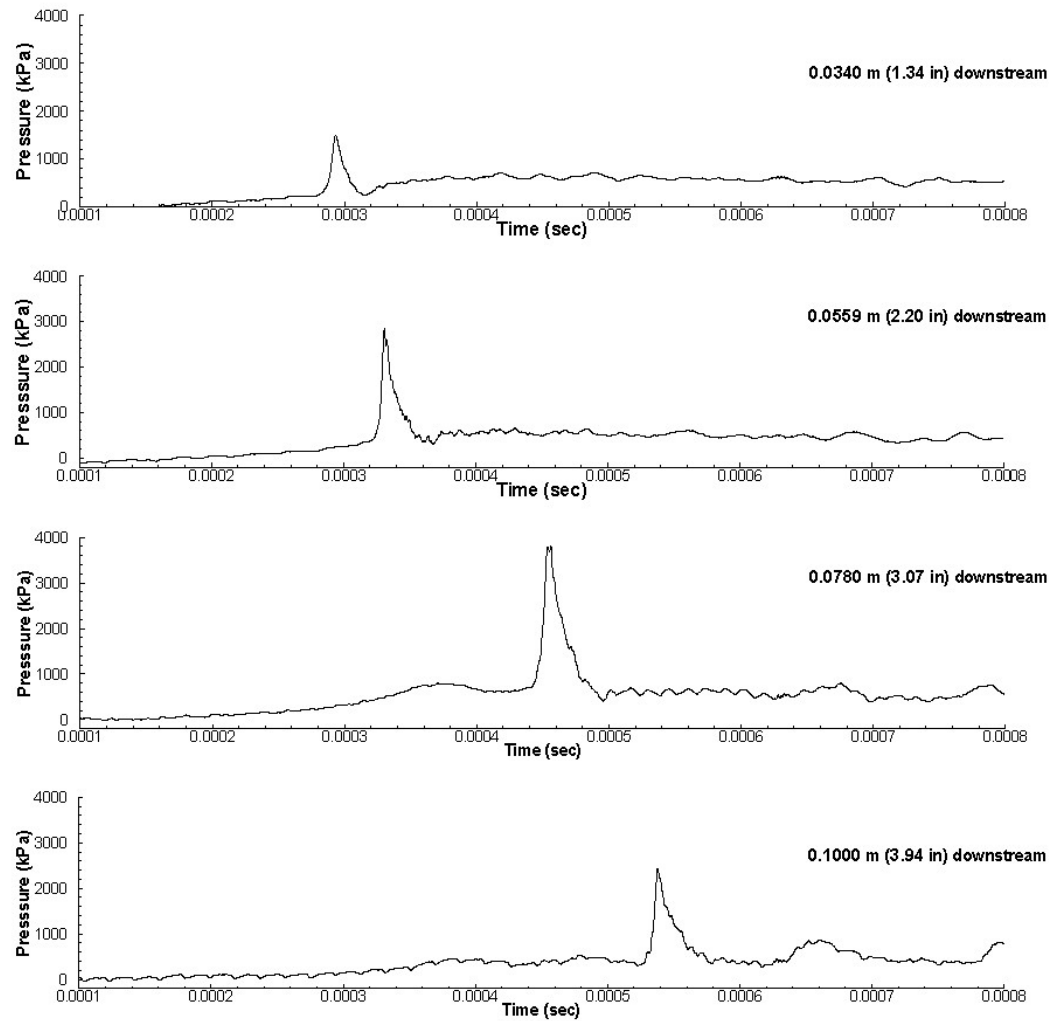
Figure 67. Pressure histories in actuator B with an equivalence ratio=1.3.
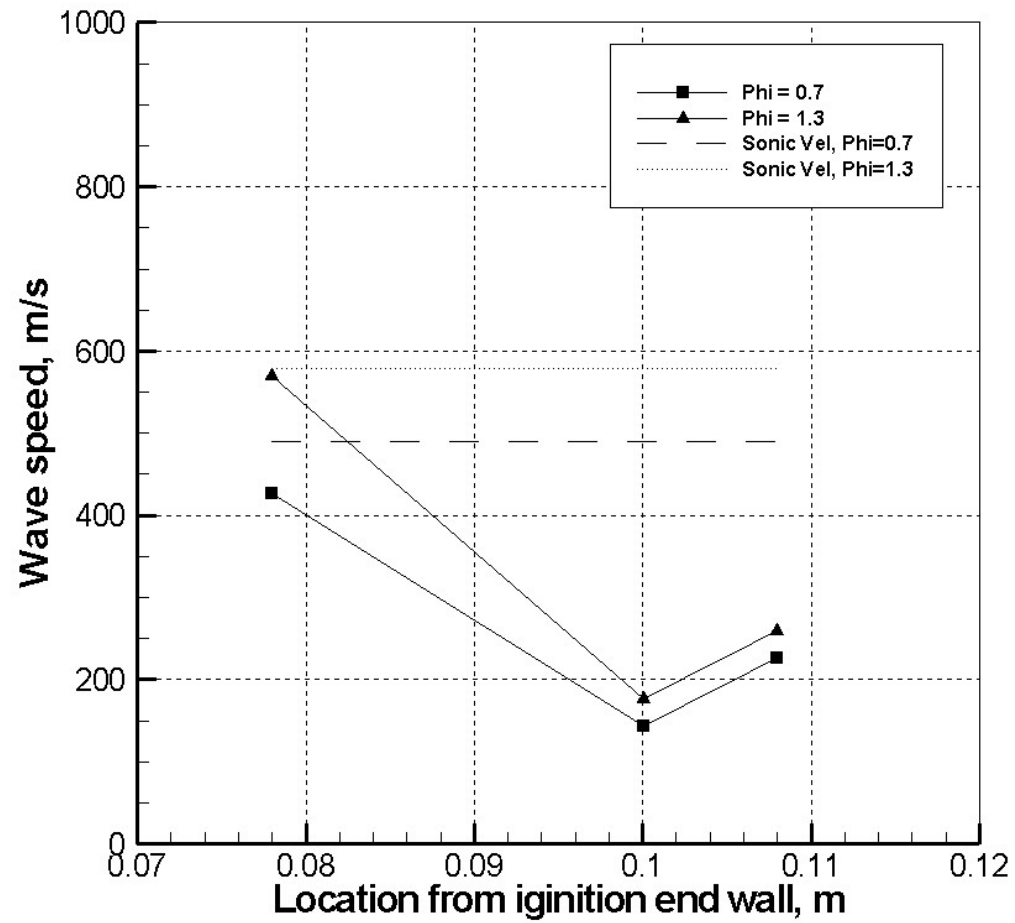
Figure 68. Wave speeds for each equivalence ratio case using actuator B.
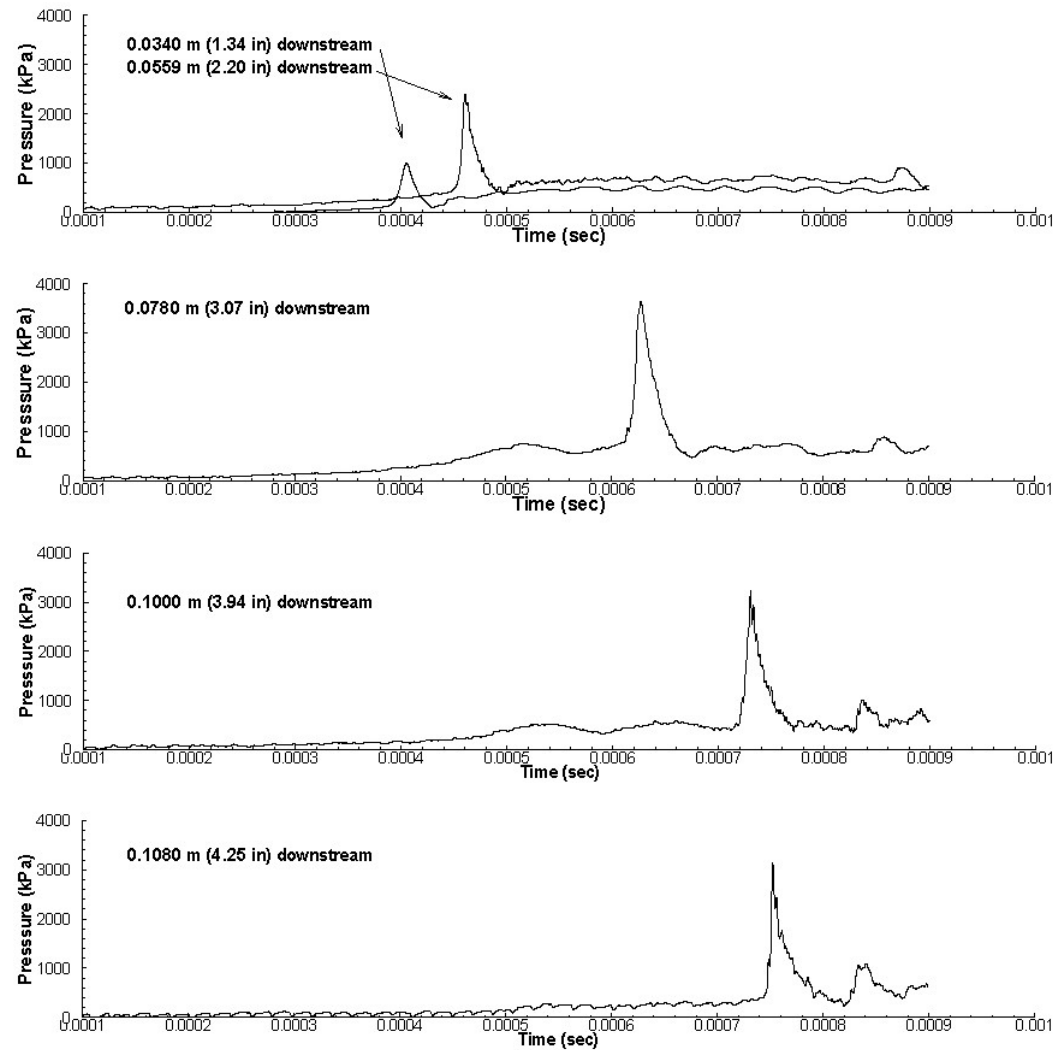
Figure 69. Pressure histories in actuator C with an equivalence ratio=0.7.
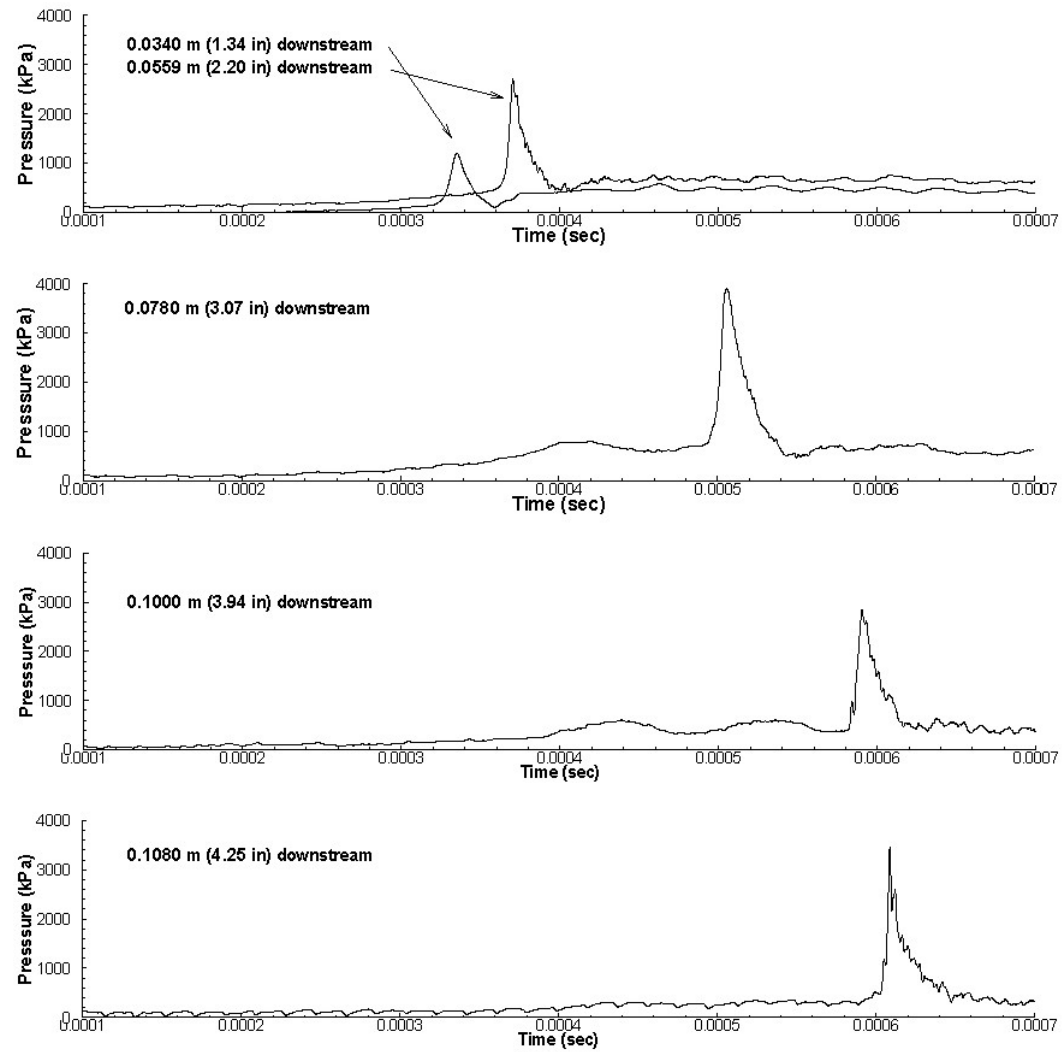
Figure 70. Pressure histories in actuator C with an equivalence ratio=1.3.
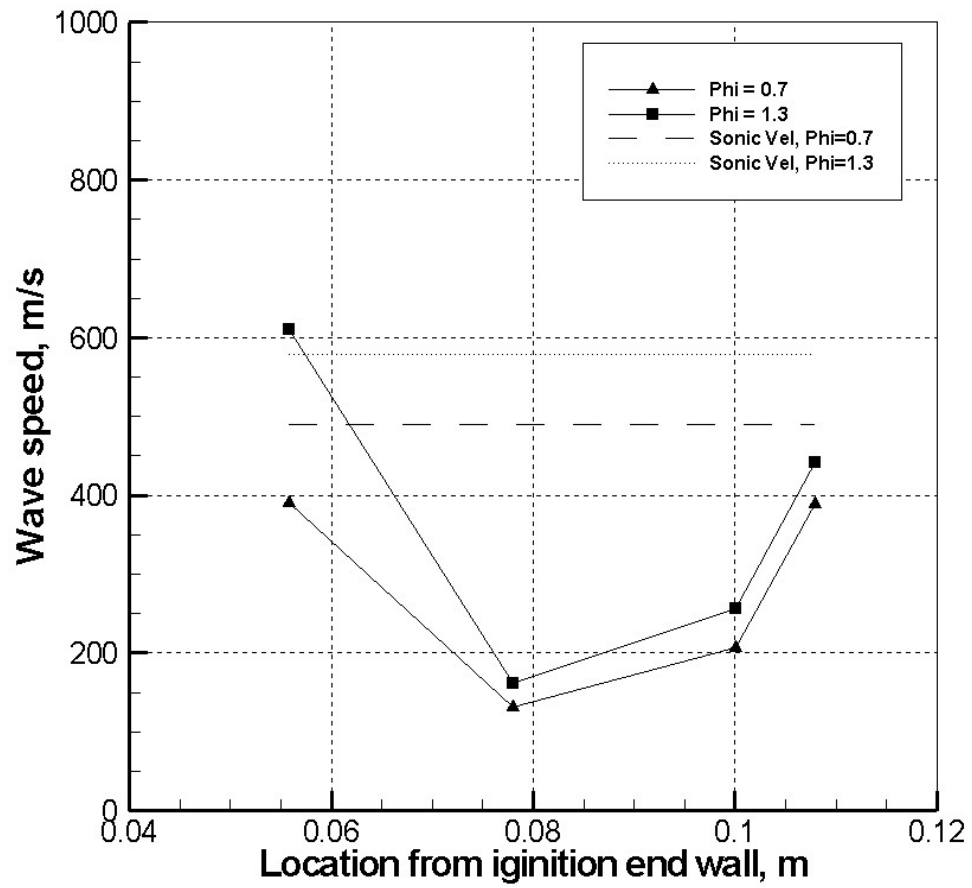
Figure 71. Wave speeds for each equivalence ratio case using actuator C.
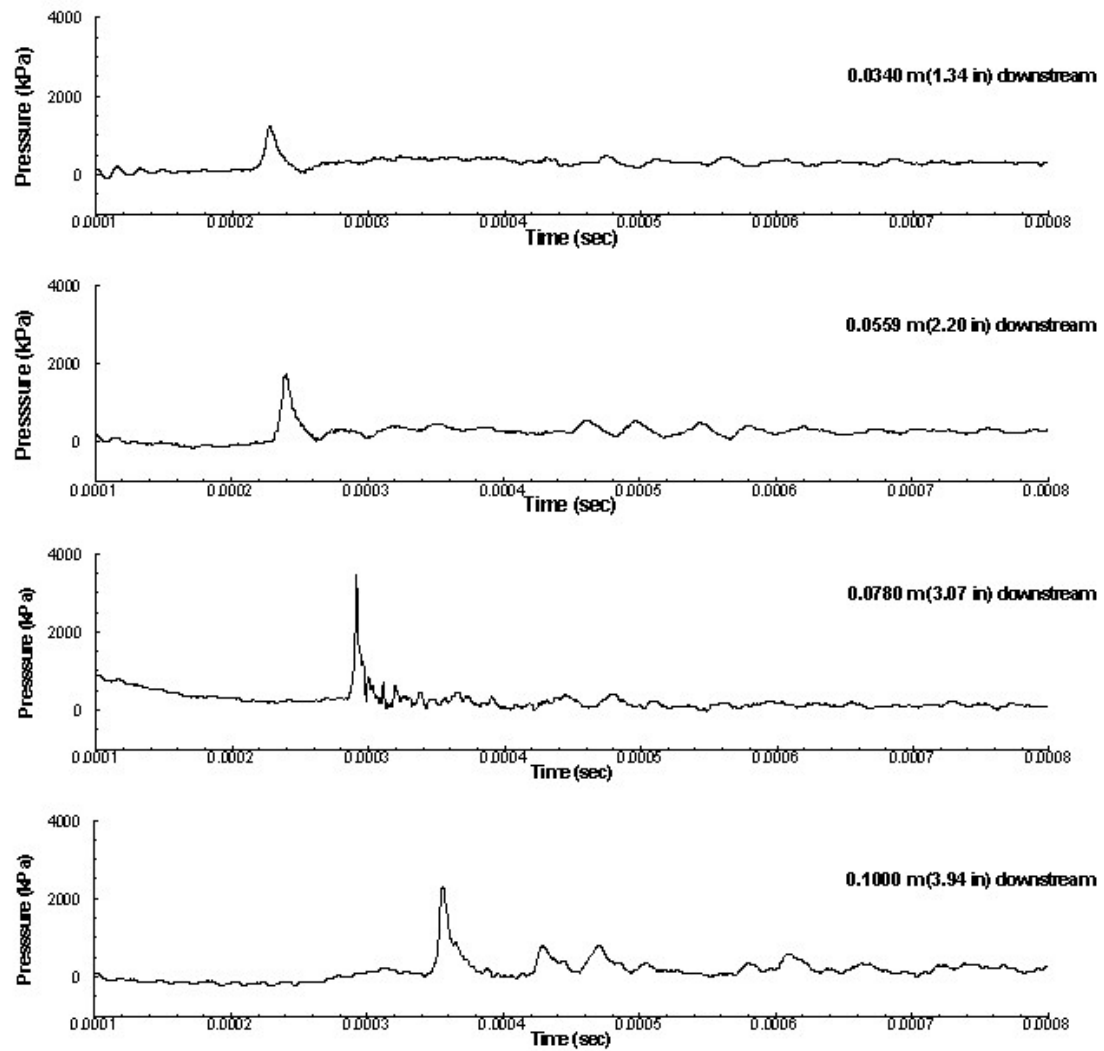
Figure 72. Pressure histories in actuator A with spiral added at 103 kPa (15 psia).
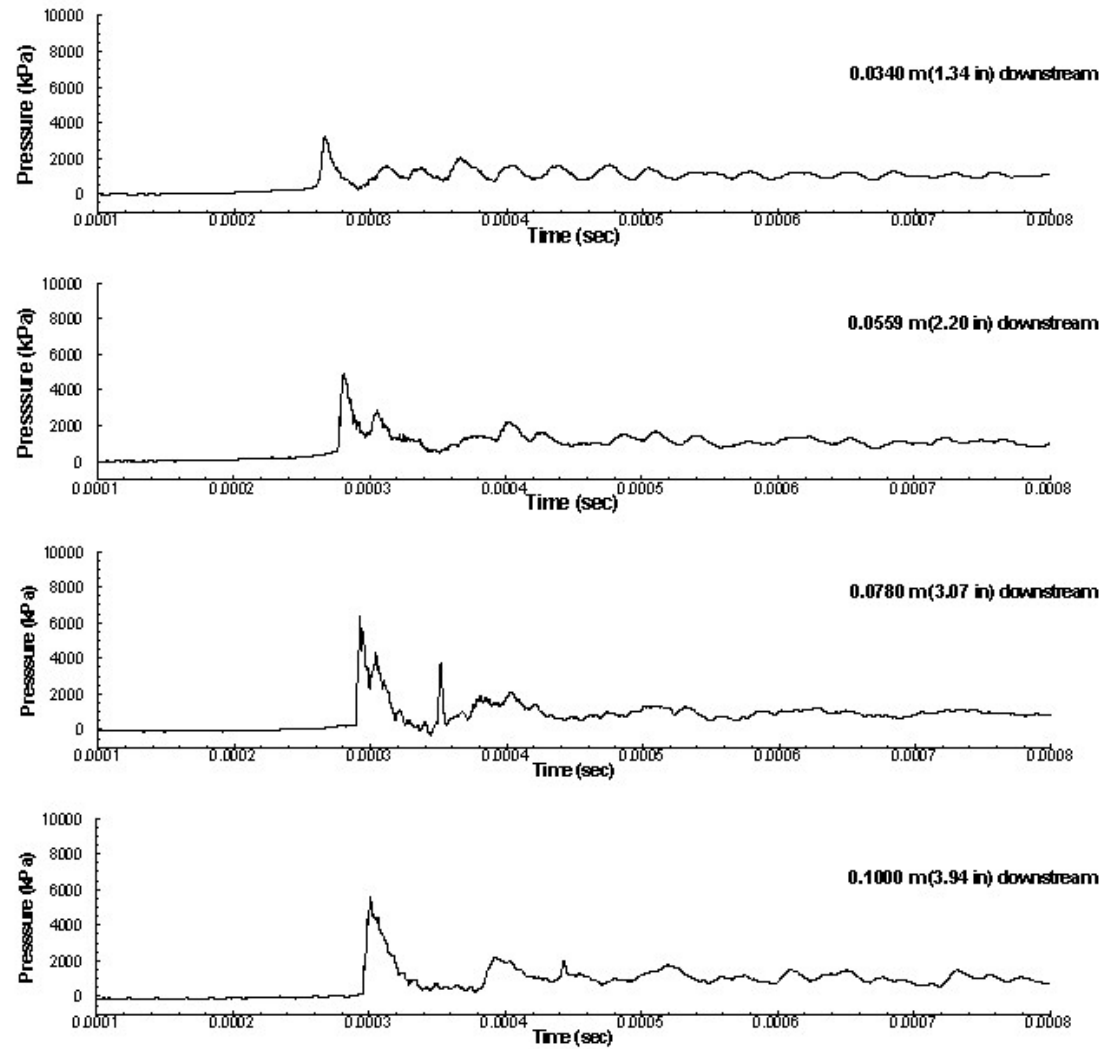
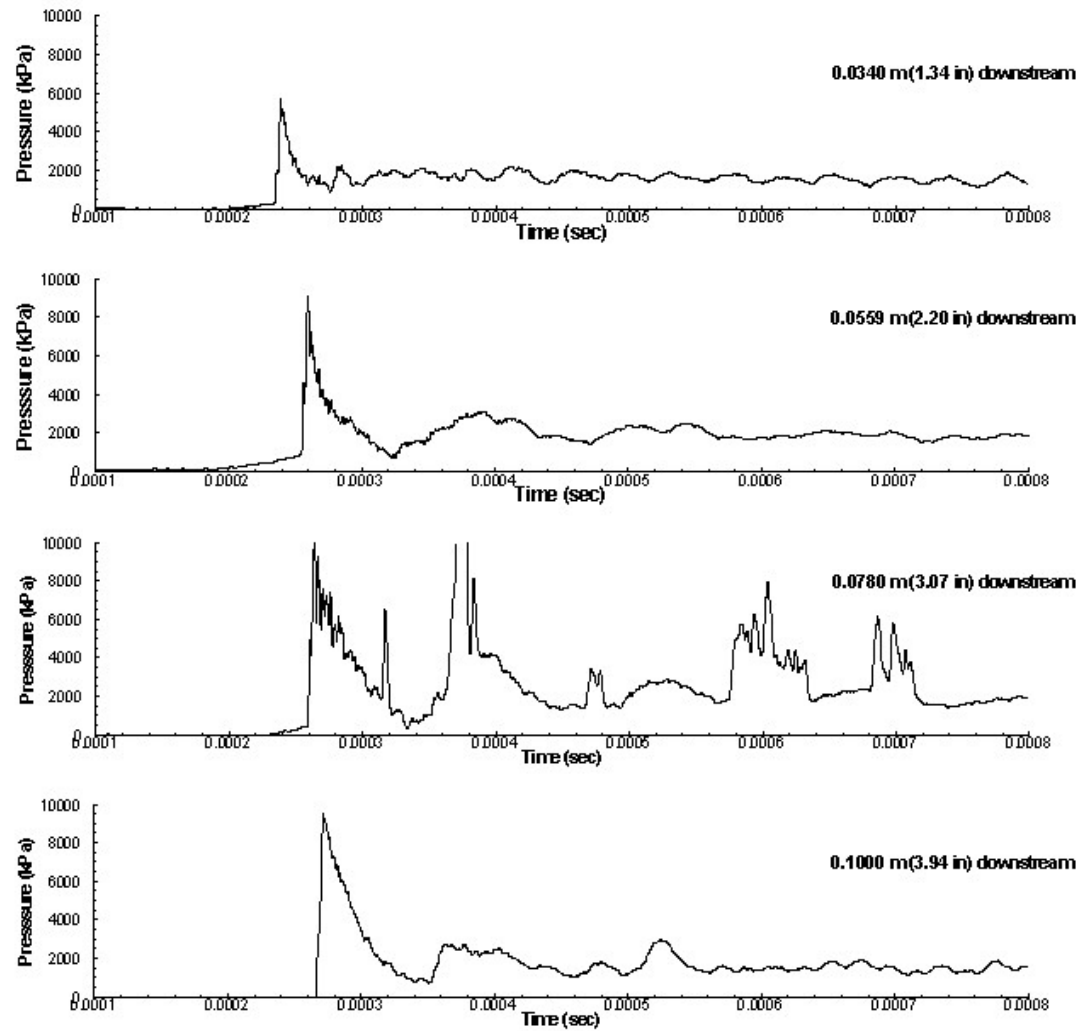Figure 73. Pressure histories in actuator A with spiral added at 207 kPa (30 psia).
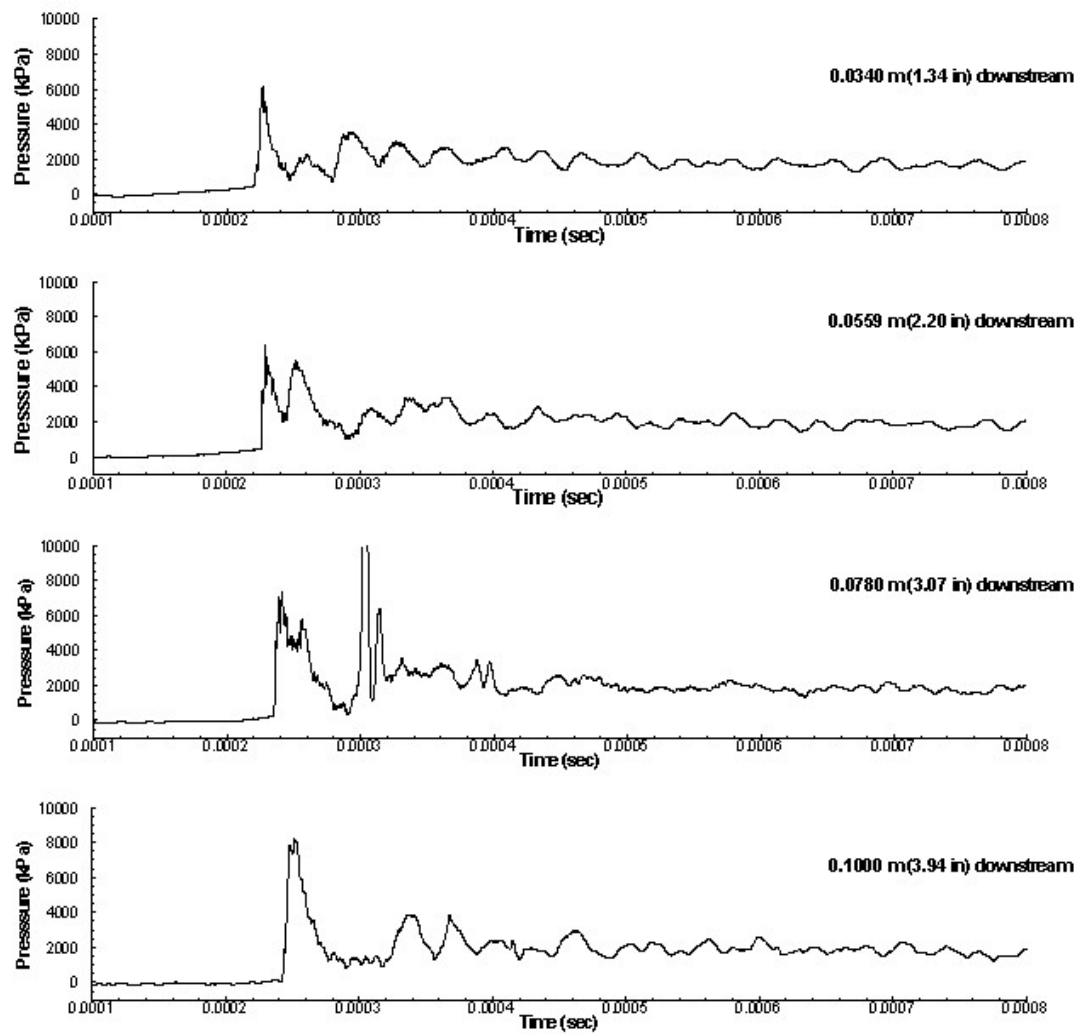
Figure 74. Pressure histories in actuator A with spiral added at 345 kPa (50 psia).
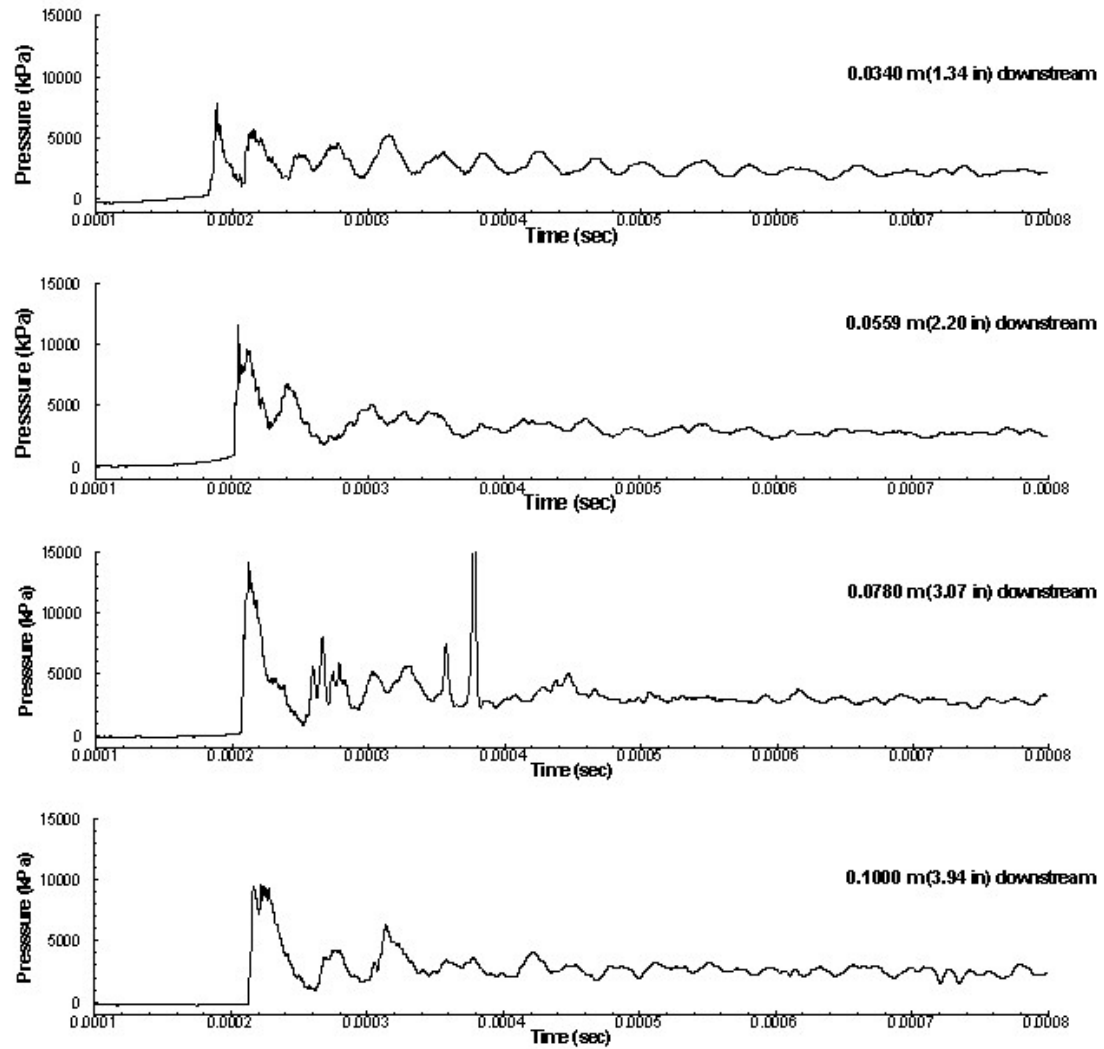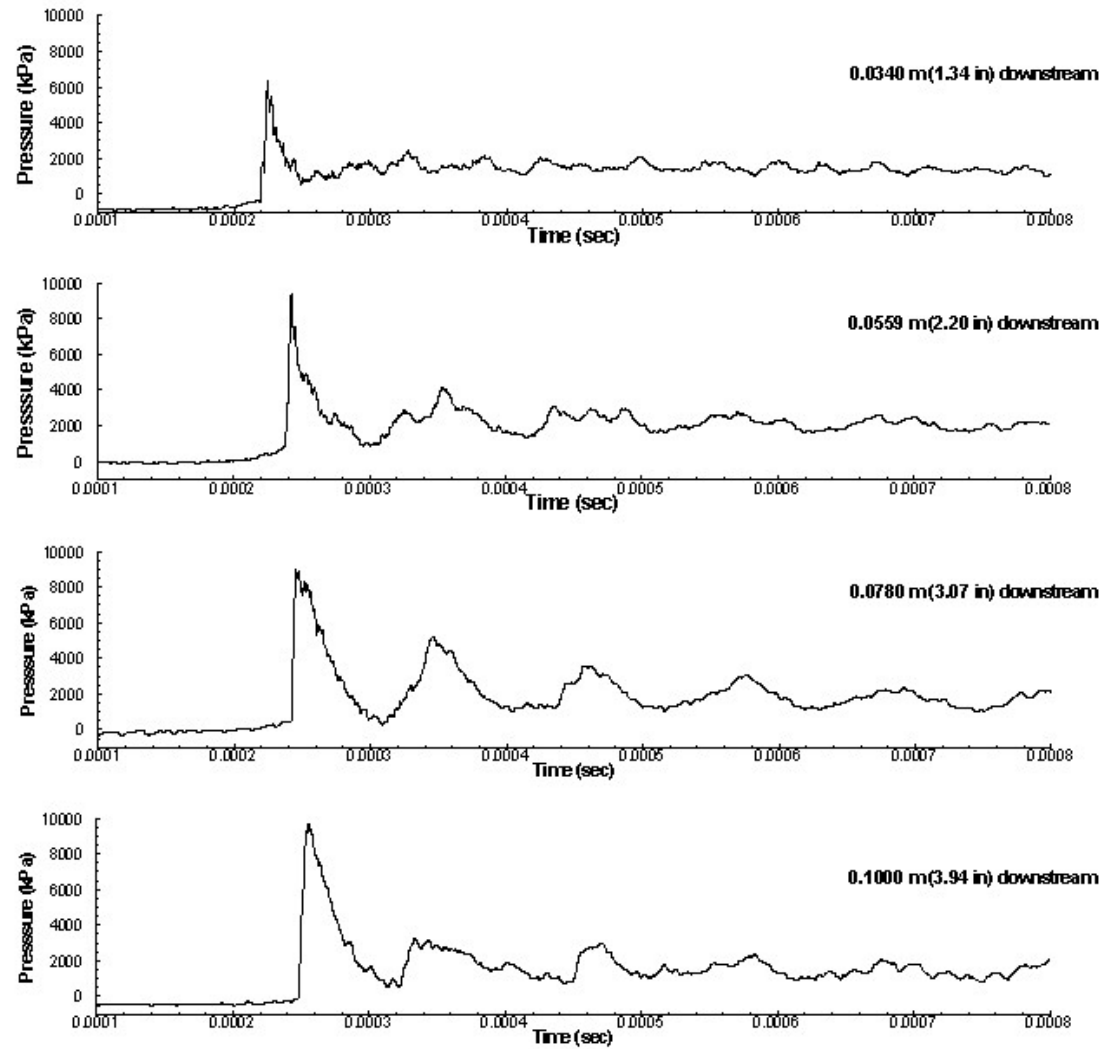
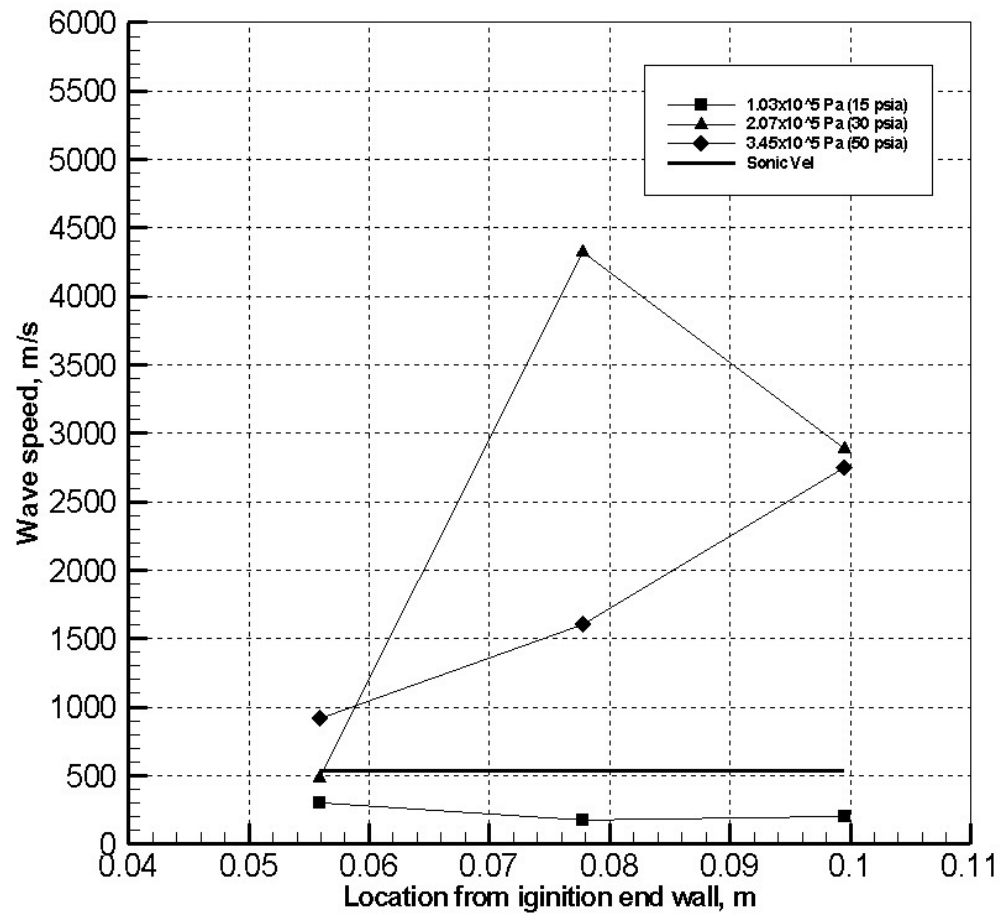Figure 75. Pressure histories in actuator A with spiral added at 483 kPa (70 psia).
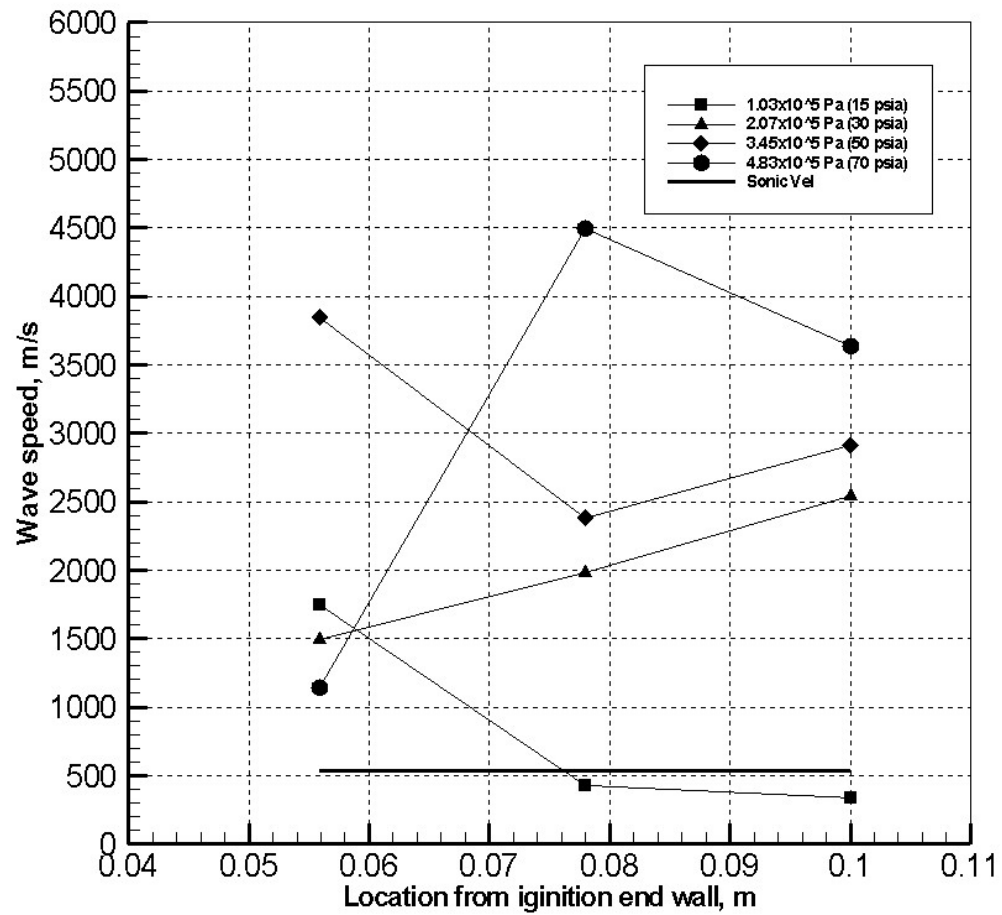
Figure 76. Wave speeds using actuator A with spiral added.
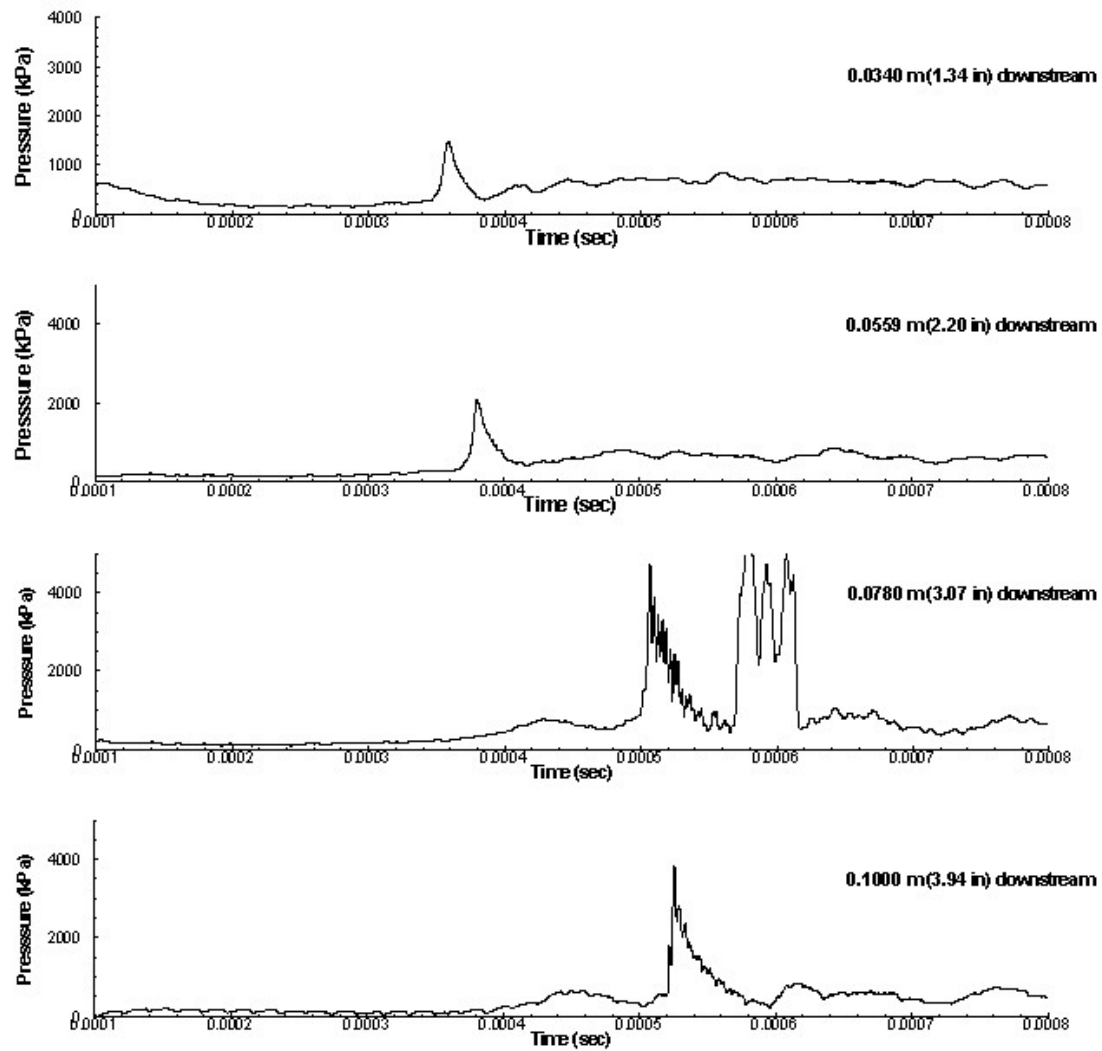
Figure 77. Pressure histories in actuator B with spiral added at 103 kPa (15 psia).
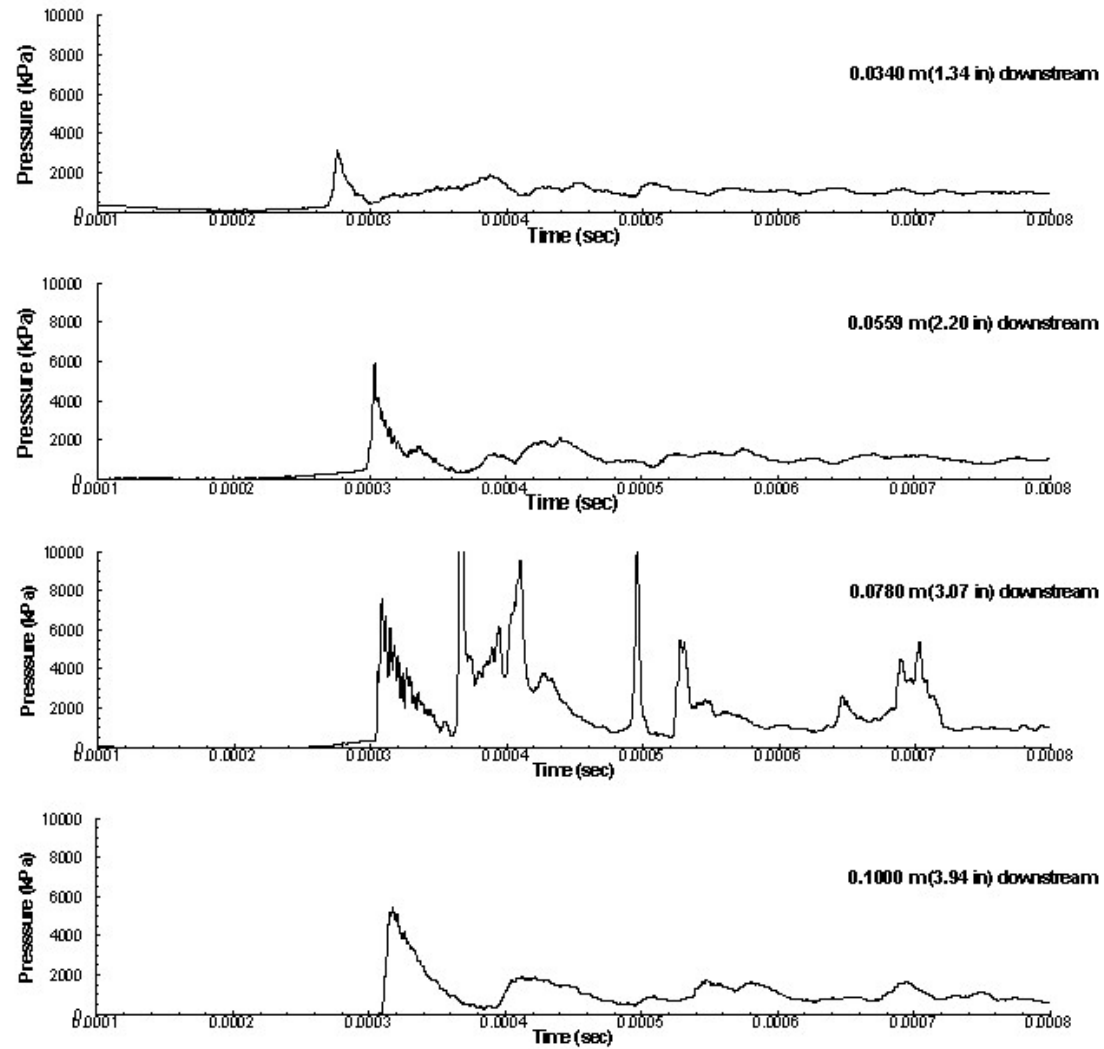
Figure 78. Pressure histories in actuator B with spiral added at 207 kPa (30 psia).

Figure 79. Pressure histories in actuator B with spiral added at 345 kPa (50 psia).

Figure 80. Pressure histories in actuator B with spiral added at 483 kPa (70 psia).

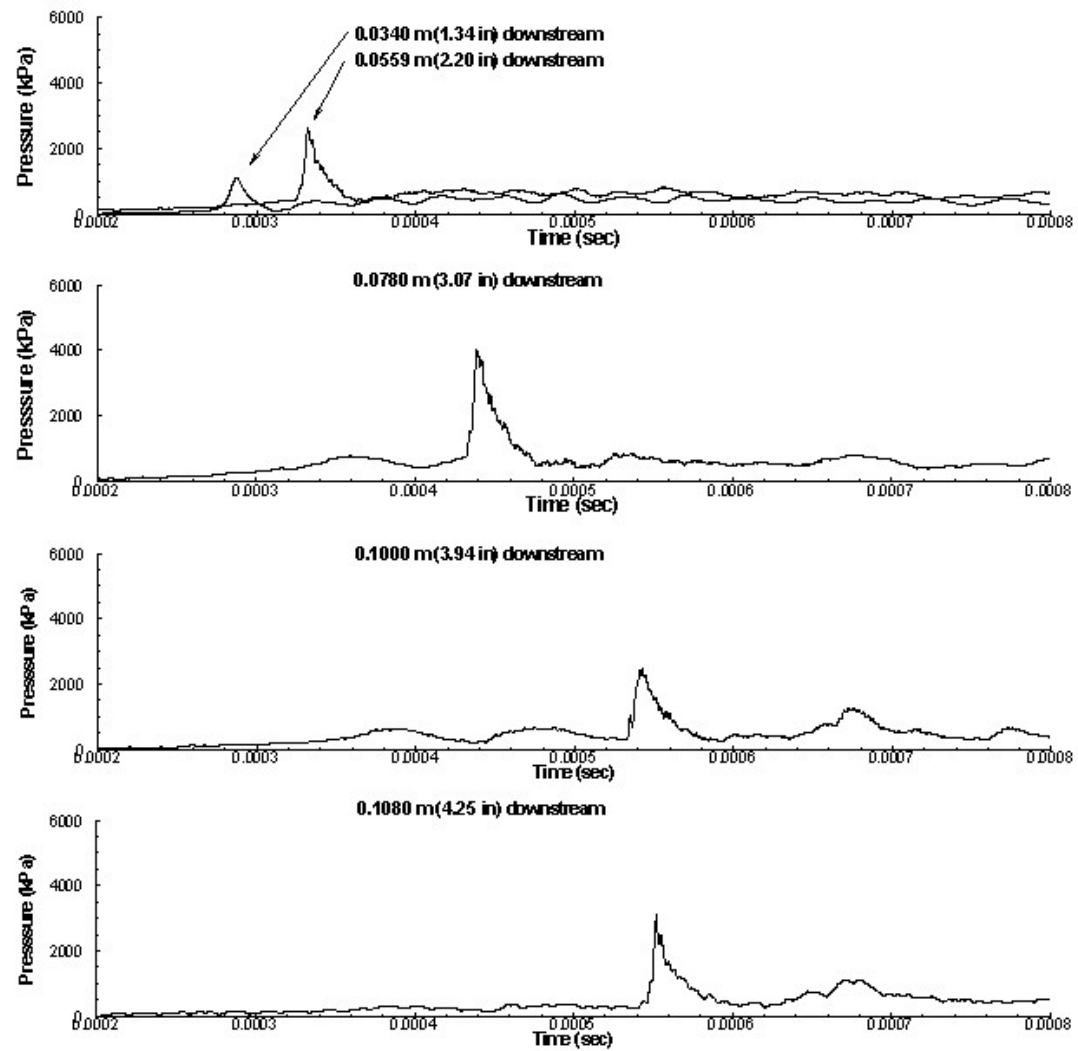Figure 81. Wave speeds using actuator B with spiral added.

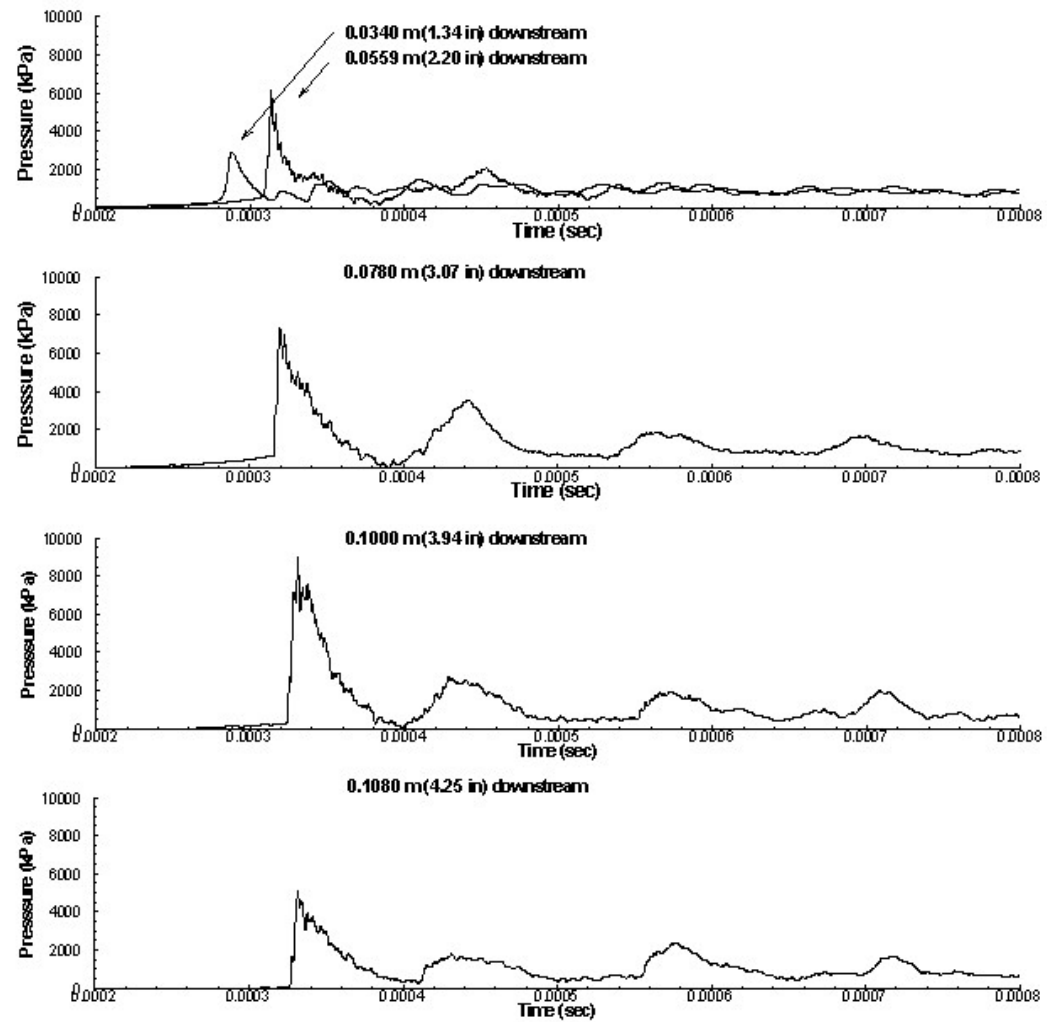Figure 82. Pressure histories in actuator C with spiral added at 103 kPa (15 psia).

Figure 83. Pressure histories in actuator C with spiral added at 207 kPa (30 psia).
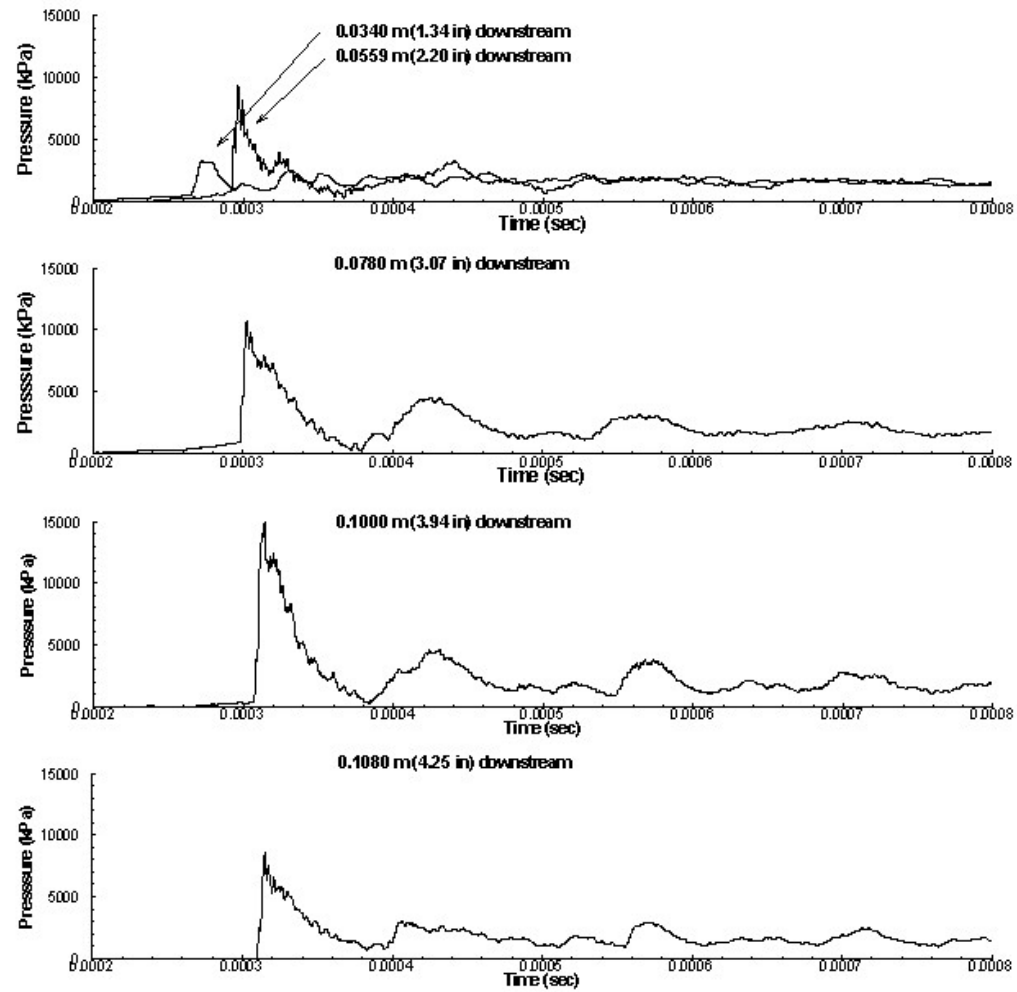
Figure 84. Pressure histories in actuator C with spiral added at 345 kPa (50 psia).
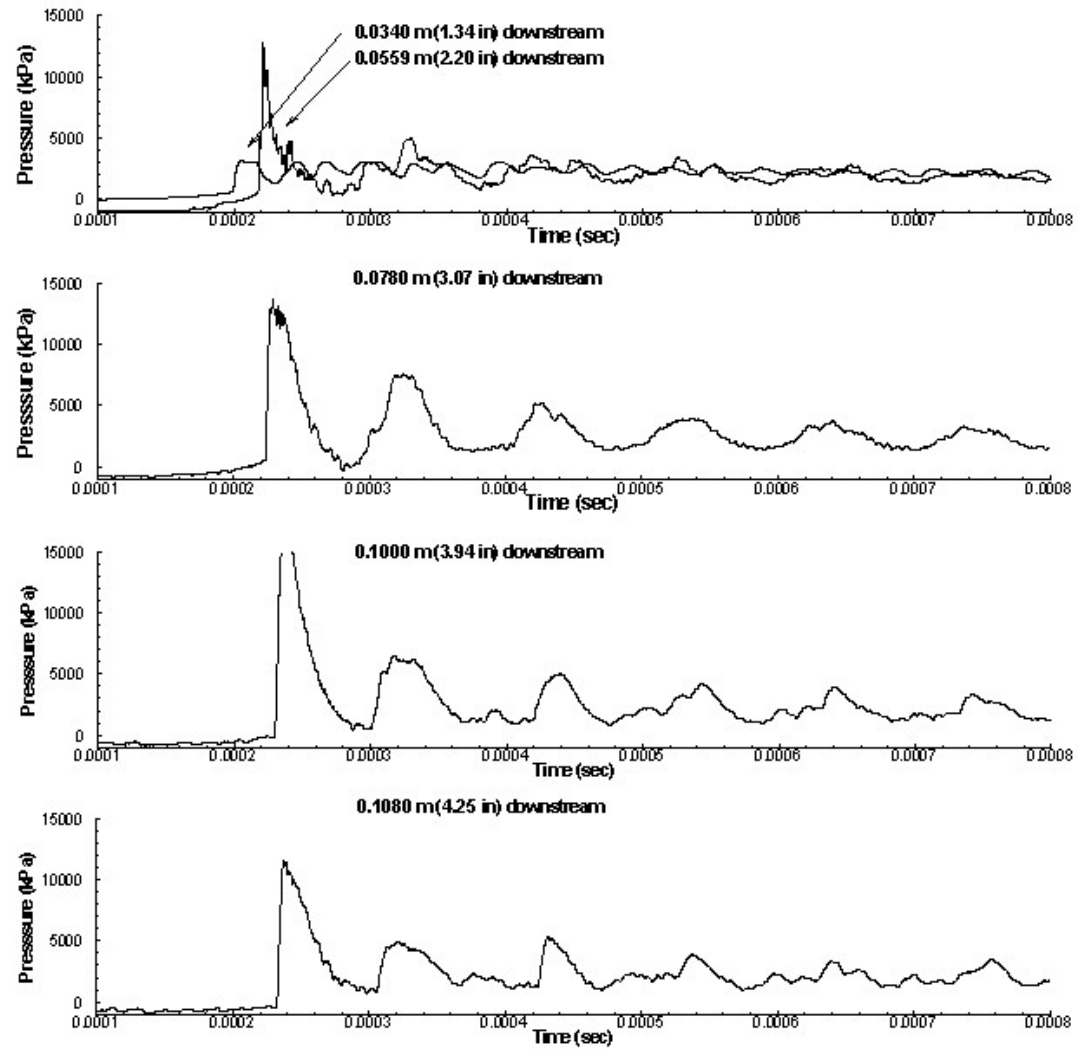
144

Figure 85. Pressure histories in actuator C with spiral added at 483 kPa (70 psia).
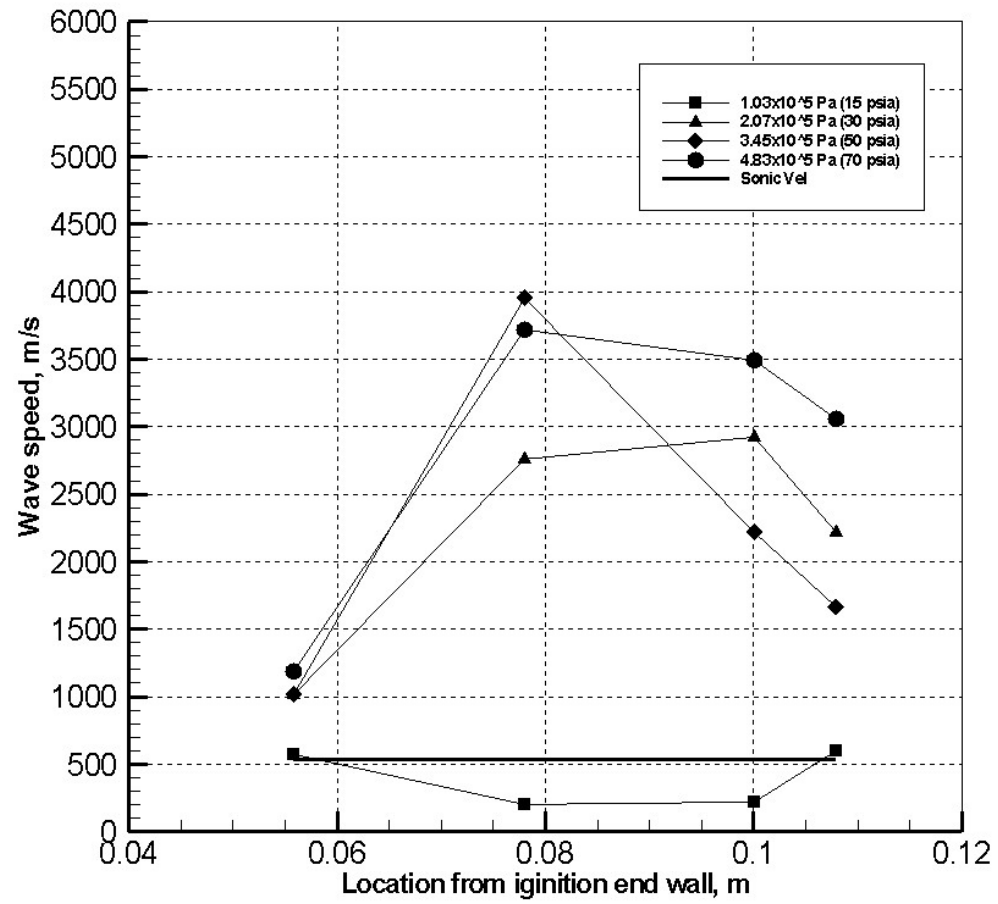
145

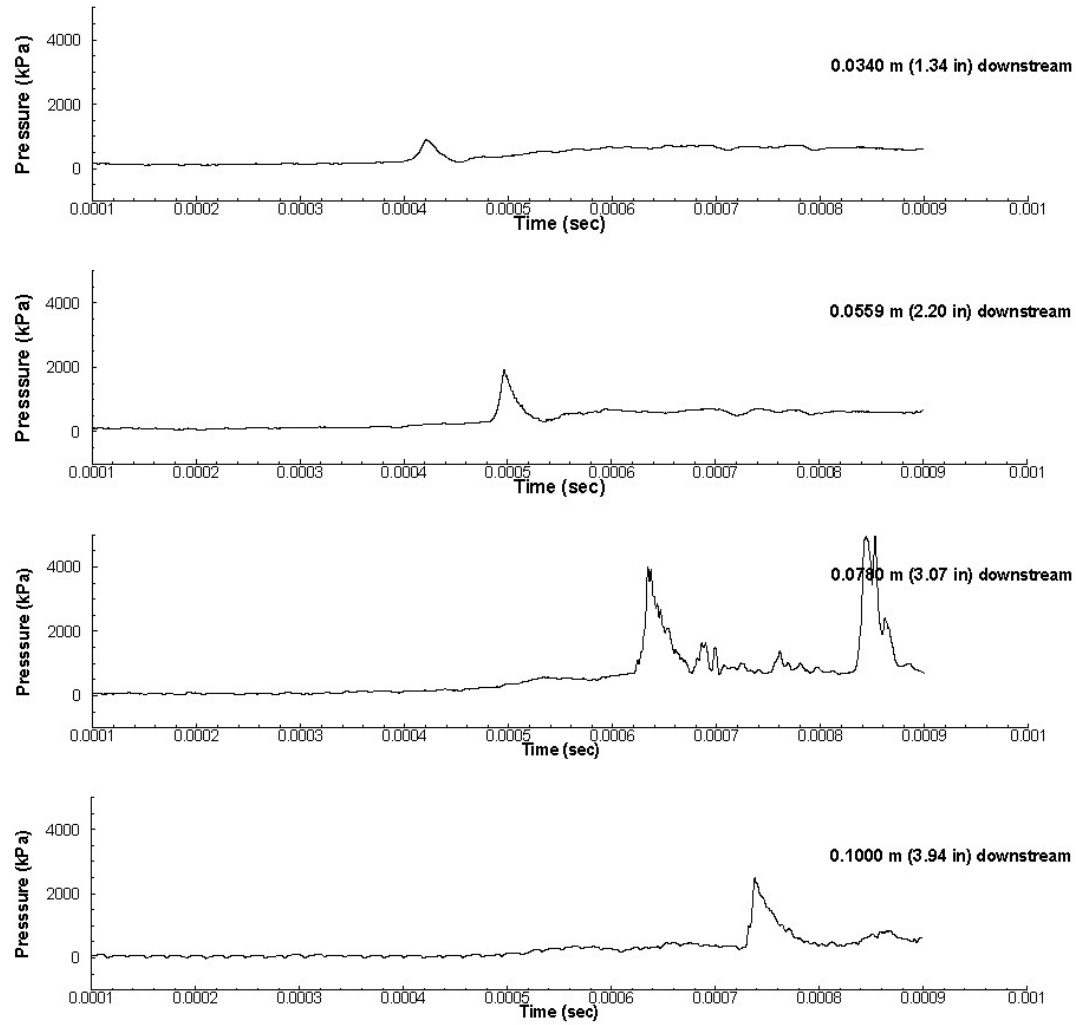Figure 86. Wave speeds using actuator C with spiral added.

Figure 87. Pressure histories with a 4.8 mm (.1875 in) spiral installed in Actuator B at 103 kPa (15 psia).
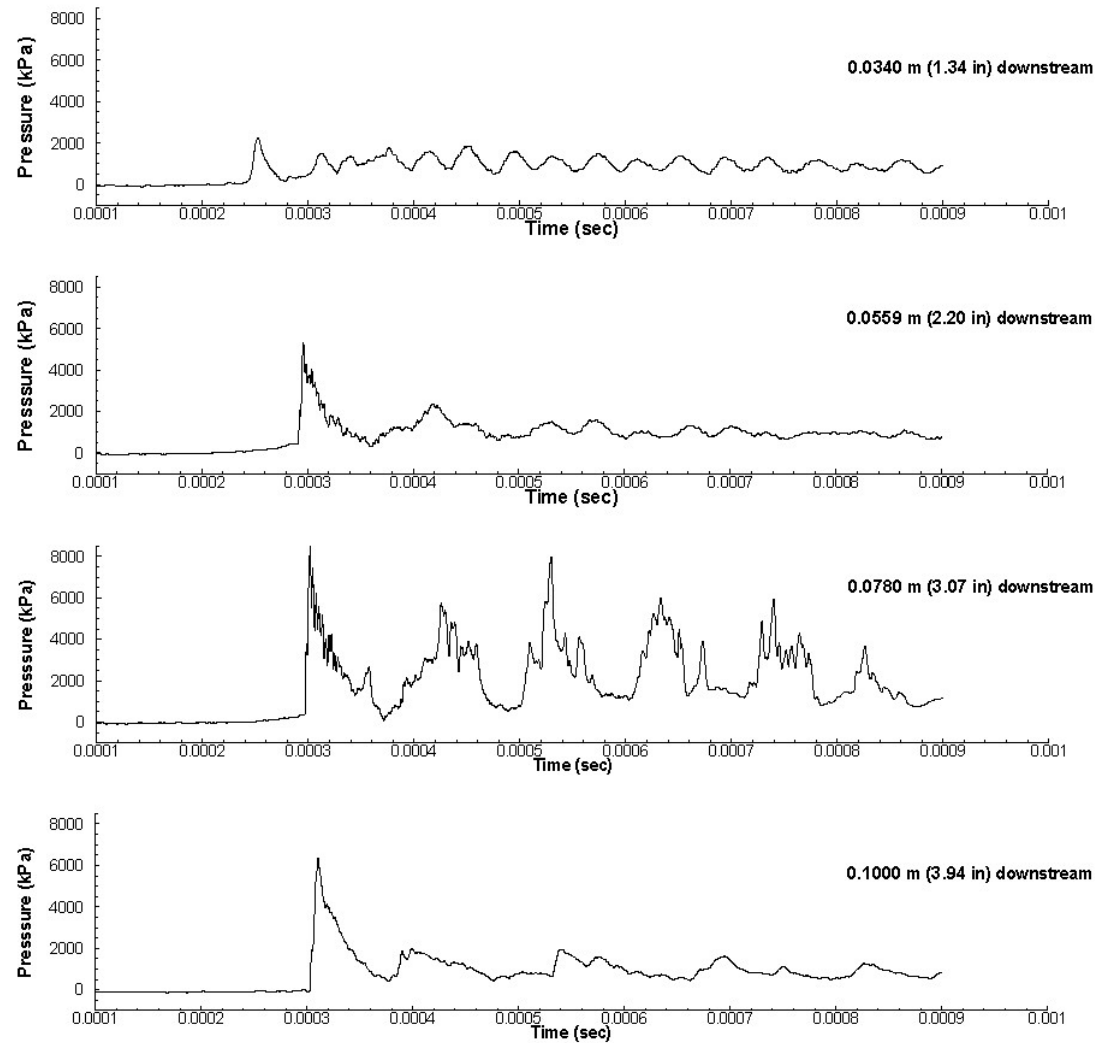
Figure 88. Pressure histories with a 4.8 mm (.1875 in) spiral installed in Actuator B at 207 kPa (30 psia).
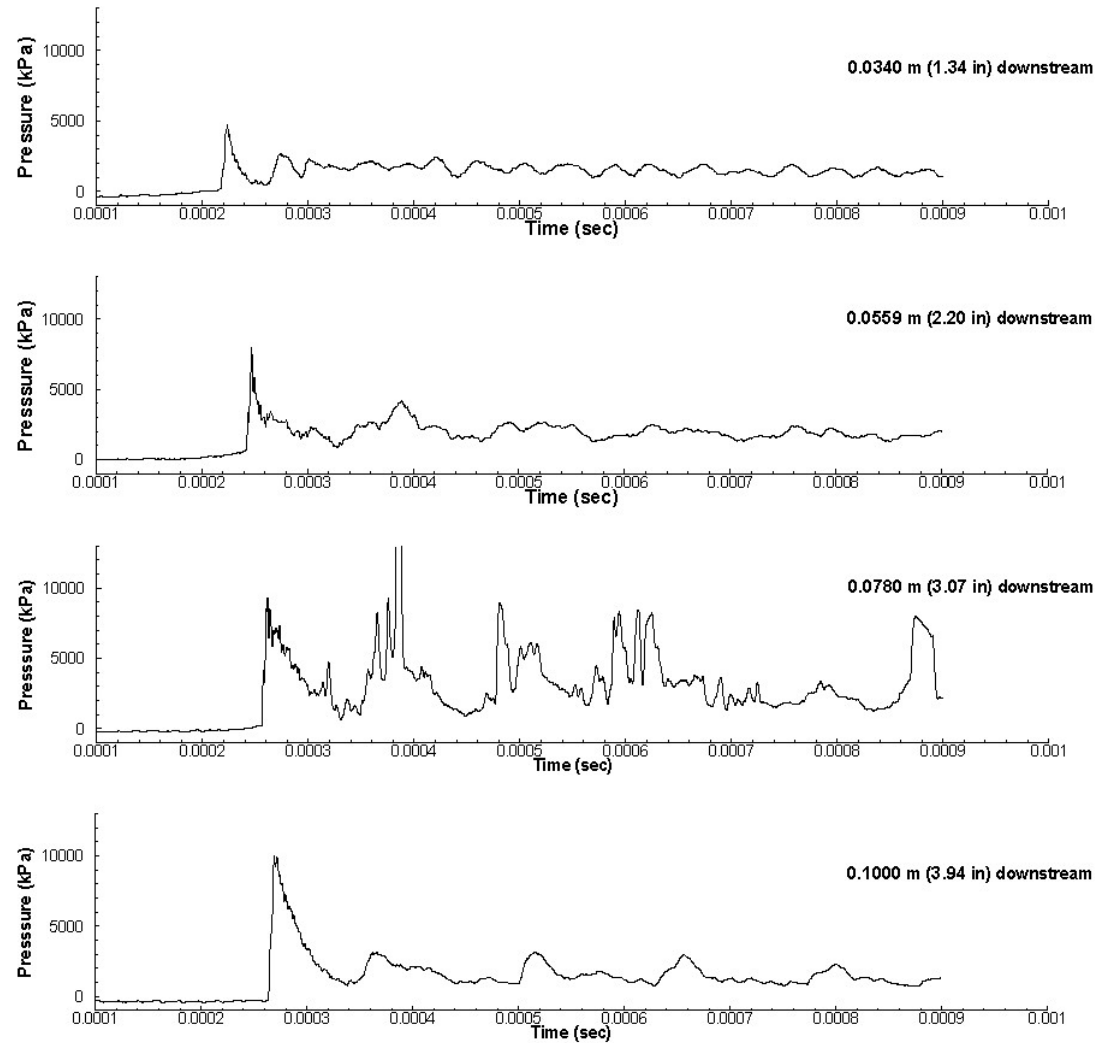
Figure 89. Pressure histories with a 4.8 mm (.1875 in) spiral installed in Actuator B at 345 kPa (50 psia).
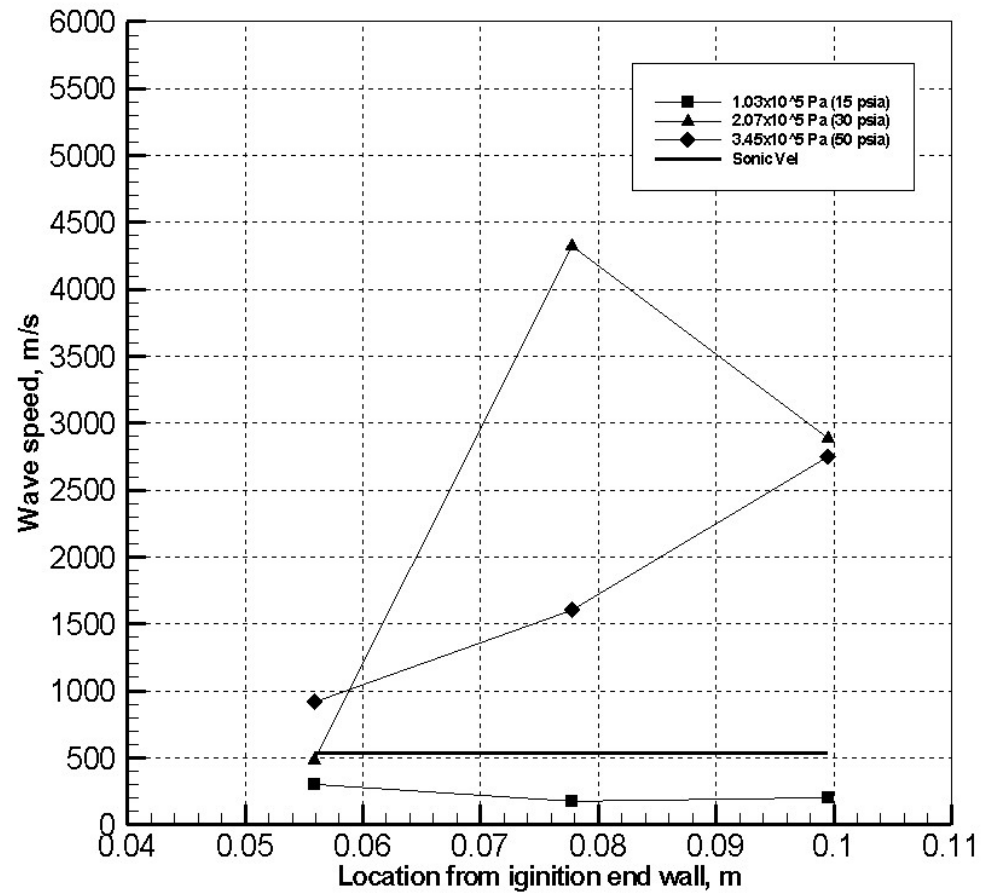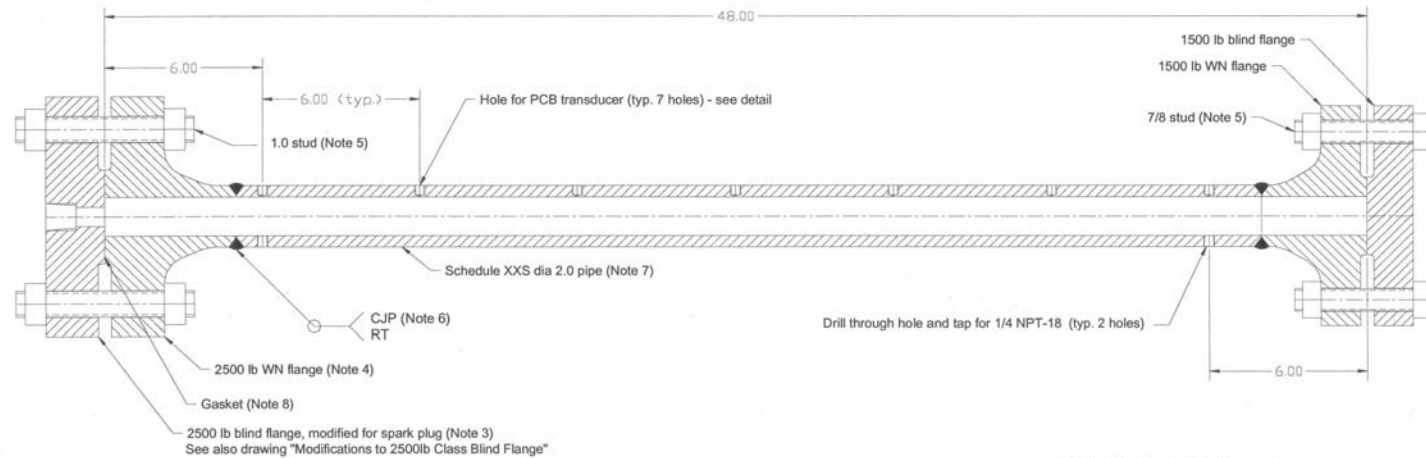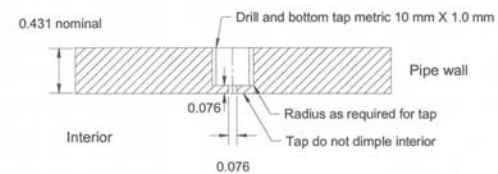
Figure 90. Wave speeds in actuator B with 4.8 mm (.1875 in) spiral installed.

.

Appendix A

Detailed Engineering Drawings

Detonation Tube - Initial Setup
Building 1221C
Andrew Cutler. April 4, 2002

48.00

6.00

6.00 (typ.)

1500 lb blind flange
1500 lb WN flange

Hole for PCB transducer (typ. 7 holes) - see detail

7/8 stud (Note 5)

1.0 stud (Note 5)

Schedule XXS dia 2.0 pipe (Note 7)

Drill through hole and tap for 1/4 NPT-18 (typ. 2 holes)

CJP (Note 6)
RT

6.00

2500 lb WN flange (Note 4)

Gasket (Note 8)

2500 lb blind flange, modified for spark plug (Note 3)
See also drawing "Modifications to 2500lb Class Blind Flange"

Detail of hole for PCB transducer

Notes:

1. Design pressure 3500 psi.
2. Design temperature ambient.
3. Blind flanges: NPS 2 inch 1500 lb / 2500 lb class, ASTM A182 type 316 stainless steel.
4. Weld neck flanges: NPS 2 inch 1500lb/2500lb class ASTM A182 type 316 stainless steel. Bore to ID 1.5003 inches to match pipe.
5. Bolts/nuts: ASTM 193 GR B7 stud and ASTM A194 2H nuts. Torque to 100 ft-lbs.
6. All welds shall be in accordance with ASME B31.3 for severe cyclic service. All welders and weld procedures shall be qualified in accordance with ASME Section IX BPV Code. All welding shall be examined by 100% Radiography in accordance with BPV Code, Section V, Article 2. Finish root of weld flush with inside diameter of pipe. Bore of flange and pipe shall be concentric.
7. Pipe 2.0 inches XXS, ASTM A312 seamless type 316 stainless steel. All piping shall be in accordance with ASME B31.3 and LaPG 1710.40.
8. Gasket material shall be Grafoil (GTB).
9. Detonation Tube configuration 1 consists of a flanged tube, blind flange, and blind flange with a single penetration with the actual operational spark plug and configuration 2 consists of a flanged tube, blind flange, and a blind flange with three electrode penetrations in a blind flange with the actual operational electrodes. Both configuratons shall be hydrostatically tested to 5250 psig in accordance with ASME B31.3 Paragraph 345.4.2. A copy of the hydrostatic test report, which includes description of test article, test pressure, date, and certification signature shall be submitted.
10. The Detonation Tube Assembly shall be a stamped pressure vessel in accordance with Boiler Pressure Code Section 8 Div. I.

0.431 nominal

Drill and bottom tap metric 10 mm X 1.0 mm

Pipe wall

0.076

Radius as required for tap

Interior

Tap do not dimple interior

0.076

Dimensions in inches unless otherwise specified

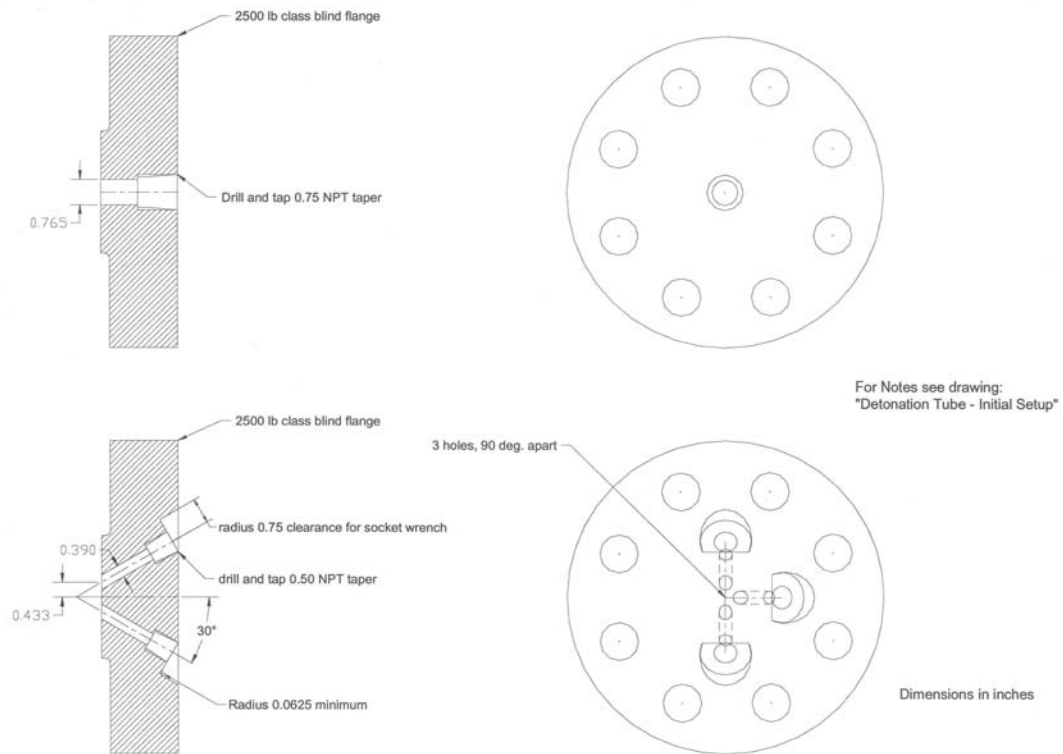Figure A1. Detailed engineering drawing of the detonation tube.

Figure A2. Detailed engineering drawing of the modifications to the ignition end blind flange.
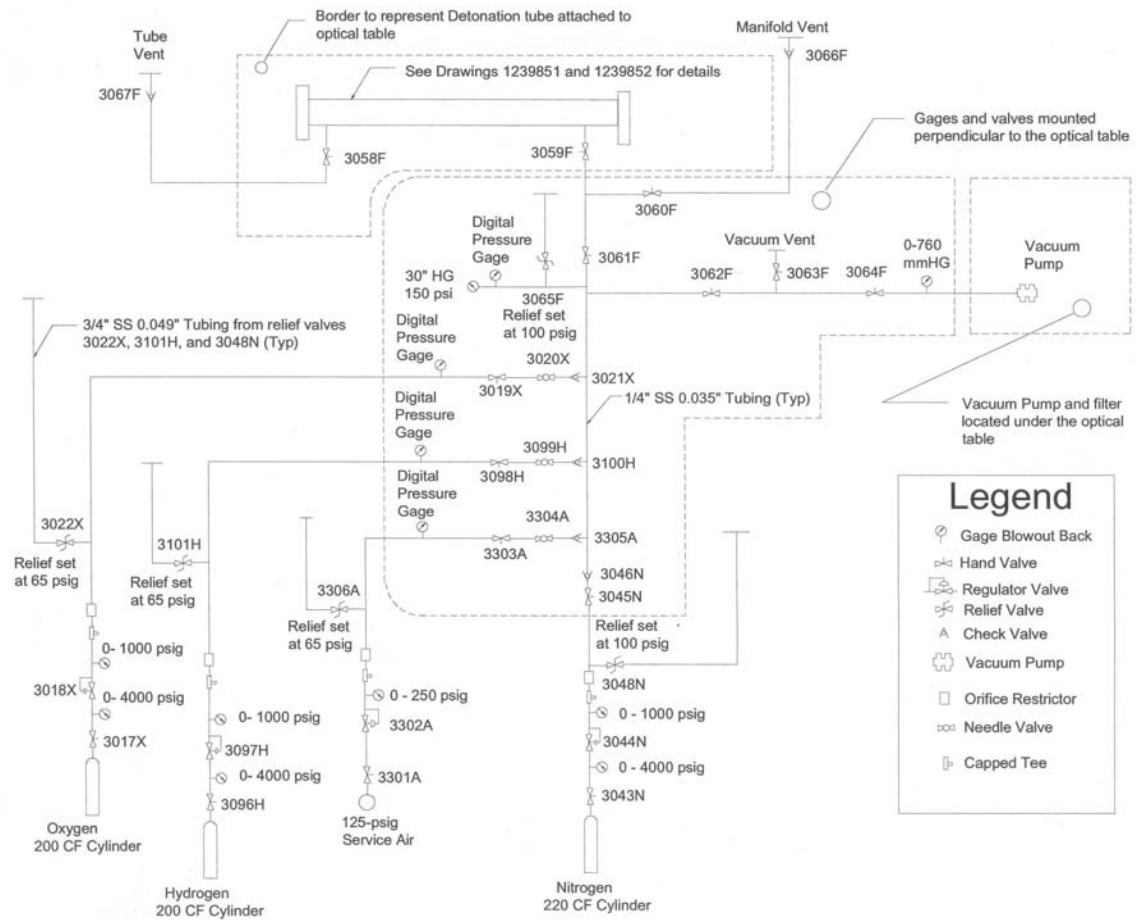
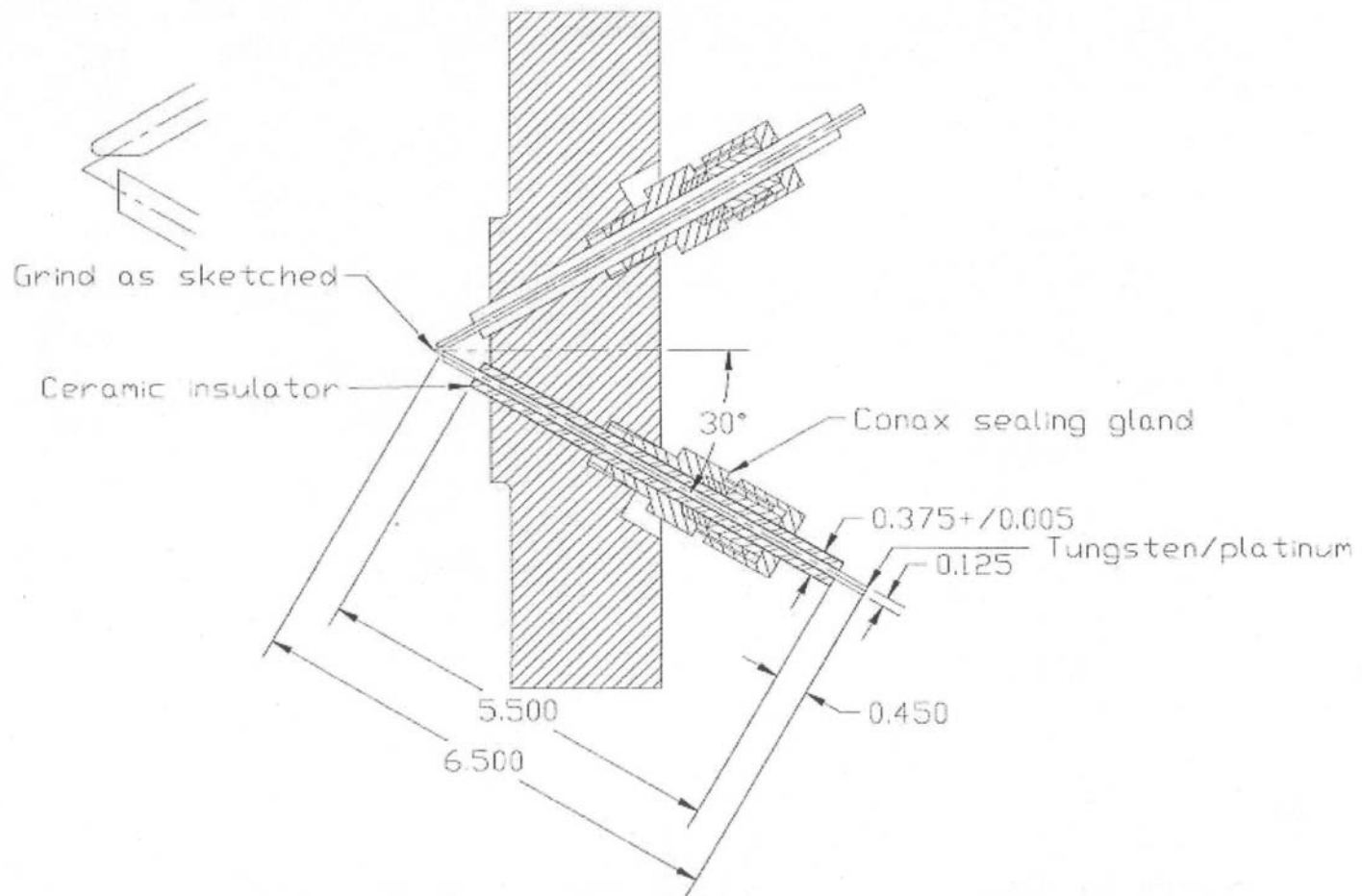Figure A3. Detailed engineering drawing of the detonation tube injection system.

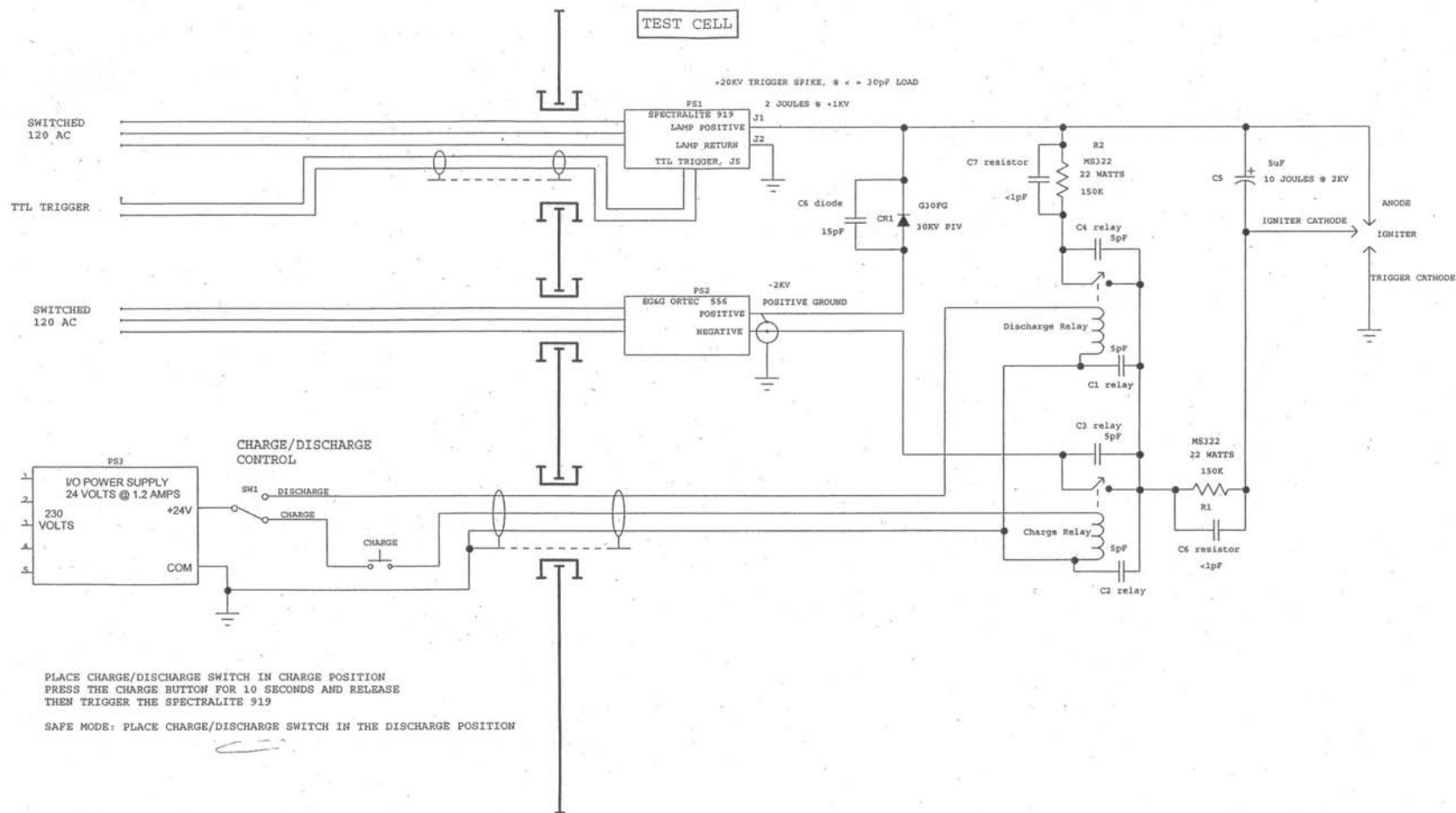Figure A4. Detailed drawing of the electrodes and installation assembly.

Figure A5. Detailed drawing of the three-electrode ignition system.

REPORT DOCUMENTATION PAGE

The public reporting burden for this collection of information is estimated to average 1 hour per response, including the time for reviewing instructions, searching existing data sources, gathering and maintaining the data needed, and completing and reviewing the collection of information. Send comments regarding this burden estimate or any other aspect of this collection of information, including suggestions for reducing this burden, to Department of Defense, Washington Headquarters Services, Directorate for Information Operations and Reports (0704-0188), 1215 Jefferson Davis Highway, Suite 1204, Arlington, VA 22202-4302. Respondents should be aware that notwithstanding any other provision of law, no person shall be subject to any penalty for failing to comply with a collection of information if it does not display a currently valid OMB control number.
PLEASE DO NOT RETURN YOUR FORM TO THE ABOVE ADDRESS.

1. REPORT DATE *(DD-MM-YYYY)*	2. REPORT TYPE	3. DATES COVERED *(From - To)*
01- 12 - 2004	Contractor Report	

4. TITLE AND SUBTITLE

Development of an Actuator for Flow Control Utilizing Detonation

5a. CONTRACT NUMBER

5b. GRANT NUMBER

5c. PROGRAM ELEMENT NUMBER

6. AUTHOR(S)

Lonneman, Patrick J.; and Cutler, Andrew D.

5d. PROJECT NUMBER

NCC1-03011

5e. TASK NUMBER

5f. WORK UNIT NUMBER

23-064-50-21

7. PERFORMING ORGANIZATION NAME(S) AND ADDRESS(ES)

NASA Langley Research Center
Hampton, VA 23681-2199

The George Washington University
Joint Institute for Advancement of
Flight Sciences
Langley Research Center, Hampton, VA 23681

8. PERFORMING ORGANIZATION REPORT NUMBER

9. SPONSORING/MONITORING AGENCY NAME(S) AND ADDRESS(ES)

National Aeronautics and Space Administration
Washington, DC 20546-0001

10. SPONSOR/MONITOR'S ACRONYM(S)

NASA

11. SPONSOR/MONITOR'S REPORT NUMBER(S)

NASA/CR-2004-213508

12. DISTRIBUTION/AVAILABILITY STATEMENT

Unclassified - Unlimited
Subject Category 01
Availability: NASA CASI (301) 621-0390

13. SUPPLEMENTARY NOTES

14. ABSTRACT

Active flow control devices including mass injection systems and zero-net-mass flux actuators (synthetic jets) have been employed to delay flow separation. These devices are capable of interacting with low-speed, subsonic flows, but situations exist where a stronger crossflow interaction is needed. Small actuators that utilize detonation of premixed fuel and oxidizer should be capable of producing supersonic exit jet velocities. An actuator producing exit velocities of this magnitude should provide a more significant interaction with transonic and supersonic crossflows. This concept would be applicable to airfoils on high-speed aircraft as well as inlet and diffuser flow control. The present work consists of the development of a detonation actuator capable of producing a detonation in a single shot (one cycle). Multiple actuator configurations, initial fill pressures, oxidizers, equivalence ratios, ignition energies, and the addition of a turbulence generating device were considered experimentally and computationally. It was found that increased initial fill pressures and the addition of a turbulence generator aided in the detonation process. The actuators successfully produced Chapman-Jouguet detonations and wave speeds on the order of 3000 m/s.

15. SUBJECT TERMS

Detonations; Nozzles; Flow control; Actuators

16. SECURITY CLASSIFICATION OF:			17. LIMITATION OF ABSTRACT	18. NUMBER OF PAGES	19a. NAME OF RESPONSIBLE PERSON
a. REPORT	b. ABSTRACT	c. THIS PAGE			STI Help Desk (email: help@sti.nasa.gov)
U	U	U	UU	175	19b. TELEPHONE NUMBER *(Include area code)* (301) 621-0390